

**Safety Margins
for Geometrical Uncertainties
in Radiotherapy**

Druk: Optima Rotterdam

**Safety Margins
for Geometrical Uncertainties
in Radiotherapy**

Veiligheidsmarges voor Geometrische Onzekerheden in de Radiotherapie

PROEFSCHRIFT

Ter verkrijging van de graad van doctor
aan de Erasmus Universiteit Rotterdam
op gezag van de rector magnificus

Prof. dr. P.W.C. Akkermans M.A.

en volgens het besluit van het College voor Promoties.

De openbare verdediging zal plaatsvinden op
donderdag 18 mei 2000 om 16⁰⁰ uur
door

Joseph Charles Stroom

geboren te Amsterdam

Promotiecommissie

Promotor: Prof. dr. P.C Levendag

Overige Leden: Dr. B.J.M. Heijmen (tevens co-promotor)
Prof. dr. Ir. C.J. Snijders
Prof. dr. B. Löwenberg
Prof. dr. Ir. J.J.W. Lagendijk

This thesis has been prepared at the Division of Clinical Physics, Department of Radiotherapy, Daniel den Hoed Cancer Center, University Hospital Rotterdam, The Netherlands.

The work in this thesis was made possible by a grant (DDHK 92-86) of the Dutch Cancer Society ("Nederlandse Kanker Bestrijding") and of the Revolving Fund of the Erasmus University (AZR 95-20). The Dutch Cancer Society also contributed to the publication of the thesis.

Address for correspondence:

J.C. Stroom, University Hospital Rotterdam, Daniel den Hoed Cancer Center, Department of Radiotherapy, Division of Clinical Physics, Groene Hilledijk 301, 3075 EA Rotterdam, The Netherlands. Phone: +31104391801. Fax: +31104391012. E-mail: stroom@kfh.azr.nl

Friedrich Nietzsche: Viel Freude haben

*Wer viel Freude hat, muß ein guter Mensch sein:
aber vielleicht ist er nicht der klügste, obwohl er gerade das erreicht,
was der Klügste mit aller seiner Klugheit erstrebt.*

Aan Mieke, Charles, Jasper en Sandra

CONTENTS

Chapter 1. General introduction	1
I. <i>Treatment of cancer</i>	1
II. <i>Radiotherapy</i>	1
III. <i>Geometrical uncertainties in radiotherapy</i>	4
IV. <i>Summary of the thesis</i>	5
Chapter 2. Automatic calculation of three-dimensional margins around treatment volumes in radiotherapy planning	9
I. <i>Abstract</i>	9
II. <i>Introduction</i>	9
III. <i>Method</i>	11
IV. <i>Results</i>	16
V. <i>Discussion</i>	19
VI. <i>Conclusions</i>	21
VII. <i>Acknowledgements</i>	21
Chapter 3. Multiple 2-dimensional versus 3-dimensional PTV definition in treatment planning for conformal radiotherapy	23
I. <i>Abstract</i>	23
II. <i>Introduction</i>	24
III. <i>Methods and materials</i>	25
IV. <i>Results</i>	27
V. <i>Discussion</i>	29
VI. <i>Acknowledgements</i>	31
Chapter 4. Inclusion of geometrical uncertainties in radiotherapy treatment planning by means of coverage probability	33
I. <i>Abstract</i>	33
II. <i>Introduction</i>	34
III. <i>Methods and materials</i>	36
IV. <i>Results</i>	46
V. <i>Discussion</i>	55
VI. <i>Conclusion</i>	59
VII. <i>Acknowledgements</i>	59
Chapter 5. Internal organ motion in prostate cancer patients treated in prone and supine treatment position	61
I. <i>Abstract</i>	61
II. <i>Introduction</i>	62
III. <i>Materials and methods</i>	64

<i>IV. Results</i>	69
<i>V. Discussion</i>	78
<i>VI. Appendices</i>	82
<i>VII. Acknowledgements</i>	85
Chapter 6. On-line set-up corrections during radiotherapy of patients with gynecological tumors	87
<i>I. Abstract</i>	87
<i>II. Introduction</i>	88
<i>III. Methods and materials</i>	89
<i>IV. Results</i>	96
<i>V. Discussion</i>	98
<i>VI. Conclusion</i>	101
<i>VII. Acknowledgements</i>	101
Chapter 7. Detection of internal organ movement in prostate cancer patients using portal images	103
<i>I. Abstract</i>	103
<i>II. Introduction</i>	104
<i>III. Methods and materials</i>	106
<i>IV. Results</i>	114
<i>V. Discussion</i>	118
<i>VI. Acknowledgments</i>	122
Chapter 8. General discussion	123
<i>I. ICRU 50 volumes</i>	123
<i>II. Automatic 3D expansion of the CTV to generate a PTV</i>	123
<i>III. Calculation and verification of 3D margins based on patient data</i>	124
<i>IV. Internal Target Volume (ITV)</i>	125
<i>V. On-line corrections</i>	127
<i>VI. Future directions</i>	128
References	133
List of publications	143
Samenvatting	145
<i>Inleiding</i>	145
<i>Automatische 3D expansie van een CTV tot een PTV</i>	146
<i>Berekening en verificatie van PTV-marges aan de hand van patiënt data</i>	147
<i>On-line corrigeren van geometrische onnauwkeurigheden</i>	148
Nawoord	149
Curriculum vitae	151

CHAPTER 1. GENERAL INTRODUCTION

I. Treatment of cancer

Cancer is the unrestricted growth of cells in an organism, which can eventually destroy organs that are needed for survival of the organism. Throughout human history, cancer has been one of the major medical causes of death. At the moment, there are about 840.000 cancer fatalities in Europe per year. It is estimated that in the western world approximately 1 in 3 people will develop some kind of tumor during their lifetime, and more than 1 in 5 will die of it. Although significant progress has been achieved in the fight against cancer in the last decades, still about half of the cancers cannot be cured.

Currently, the three main therapies for cancer are surgery (removing the tumor), radiotherapy (killing the tumor cells with radiation), and chemotherapy (the use of anti-cancer drugs). The first two are especially used for tumors that are well localized. Surgery is straightforward but cannot always be applied, for instance when the tumor is localized in or close to a vital organ. Furthermore, invisible, microscopic extensions of the tumor might be missed. In radiotherapy, those tumor extensions can be treated more easily. Moreover, this therapy may be less demanding on the patient and hospitalization is usually not necessary. When microscopic tumor cells have spread from the primary tumor site to different parts of the body, chemotherapy can be applied. The blood circulation is used to transport the drugs are transported through the body. In many cases, the different therapies are combined to improve the treatment outcome.

II. Radiotherapy

Radiotherapy is used for about half of all cancer patients. With radiotherapy, ionizing radiation in the form of high energy photons, electrons or protons is aimed at the tumor. These particles deposit some of their energy in the tumor cells, which can cause ionization of DNA or surrounding molecules. This can induce irreparable genetic damages in the tumor cells that either kill the cell directly or result in the so-called apoptosis, i.e. cellular suicide. However, since radiation may kill healthy cells

as well, one has to be careful to deliver the radiation dose in the right place. Basically, there are two ways the radiation can be delivered: by brachytherapy or by external beam radiotherapy.

In brachytherapy, small radioactive sources are placed in or close to the tumor, either by permanent implants or by inserting catheters that temporarily hold the sources. The sources must be spread evenly in the tumor to ensure a homogeneous dose distribution, so that all tumor cells are killed. Because the reach of the sources is limited, the dose can be delivered closely conform the tumor and healthy tissues can be spared quite well. Due to the invasiveness of the procedure, brachytherapy is especially used for some smaller tumors, or for boosting only a part of a tumor.

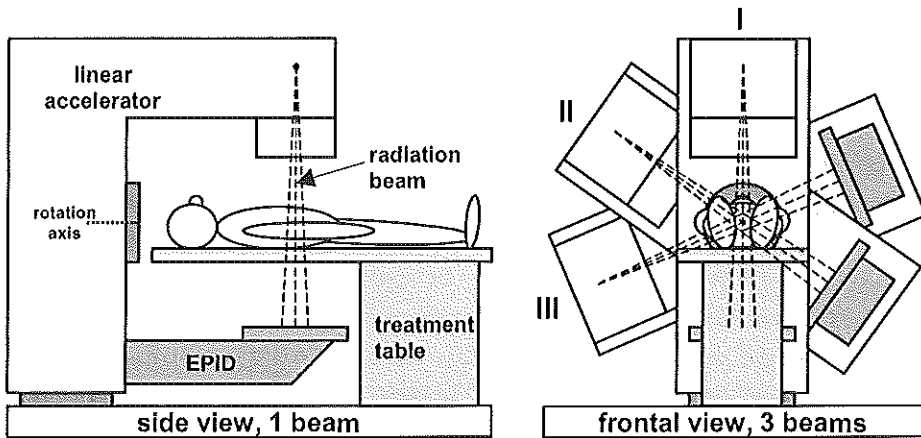


Figure 1-1 Schematic side and frontal view of external radiotherapy. A linear accelerator produces ionizing radiation which is aimed at the patient lying on the table. To make the treatment more effective, the gantry of the accelerator can be rotated to treat the patient from different directions (I,II,III). Also indicated is the electronic portal imaging device (EPID), which uses radiation that is not absorbed in the patient to make a digital radiograph of the treatment. Ideally, the patient should be in the exact same position during each fraction of the multiple-day treatment.

External radiotherapy is applied more often than brachytherapy. With external radiotherapy the dose is usually delivered by a linear accelerator, which can produce radiation beams from different angles by rotating the accelerator “arm” (i.e. the gantry). The patient is normally laid down on the treatment table in such a manner that the tumor is in or close to the rotation axis of the gantry (see Fig. 1-1). A linear accelerator can deliver a radiation beam as large as $40 \times 40 \text{ cm}^2$. However, the external

delivery of the tumor dose will inevitably cause irradiation of surrounding healthy tissues as well. In order to optimize protection of these normal tissues while obtaining a homogeneous tumor dose, several strategies are applied in clinical practice.

First, the prescribed total tumor dose is normally delivered in multiple parts by consecutive irradiation from different gantry angles (Fig. 1-1). This creates a "hot spot" at the crossing point of the beams, which is where the tumor should be positioned. The surrounding healthy tissues get a smaller dose because they are not covered by all beams. Angles which would irradiate especially sensitive structures are avoided as much as possible. Second, the irradiation fields usually closely encompass the tumor outline, i.e. the normal tissues are blocked out by thick layers of radiation absorbing material (like e.g. tungsten) in the beam. Third, the radiation intensity within a treatment field can be varied. In this manner healthy tissues may be spared and one can compensate for local variations in, for instance, patient contour. Fourth, the energy and type of irradiation can be varied. Each beam type has its own typical dose distribution in the patient for each energy. For instance, tumors close to the skin are normally irradiated with low energy beams that do not penetrate so deeply, whereas deeper lying tumors require higher energies. And finally, the total dose is not applied in one time but in multiple fractions, normally on subsequent days. If the right dose per fraction is used, the normal tissue will recover better in between the fractions than the tumor. As a consequence, a radiation treatment can consist of over 30 fractions and can last 2 months.

In most cases a computer is used to simulate and plan the treatment before the actual external radiation treatment starts. This so-called treatment planning system uses beam characteristics of the accelerator, such as the dose distribution in water. Furthermore, the patient anatomy is available, often in three dimensions (3D) in the form of a series of successive 2D images of transversal patient slices. These images are normally obtained by computed tomography (CT). The CT images should represent the patient anatomy during treatment and are used to outline the intended tumor region and critical organs. Finally, the geometry of the total treatment situation (patient and accelerator) is incorporated in the planning system as well. A dose calculation algorithm can then be used to determine an adequate treatment plan, i.e. the beam angles, field shapes, etc. are selected to yield the prescribed tumor dose while sparing the healthy organs. However, due to geometrical uncertainties, the position of the tumor with respect to the treatment beams in the simulation, can deviate from the situation during the many fractions of the actual treatment. This has to be accounted for in the planning of the treatment.

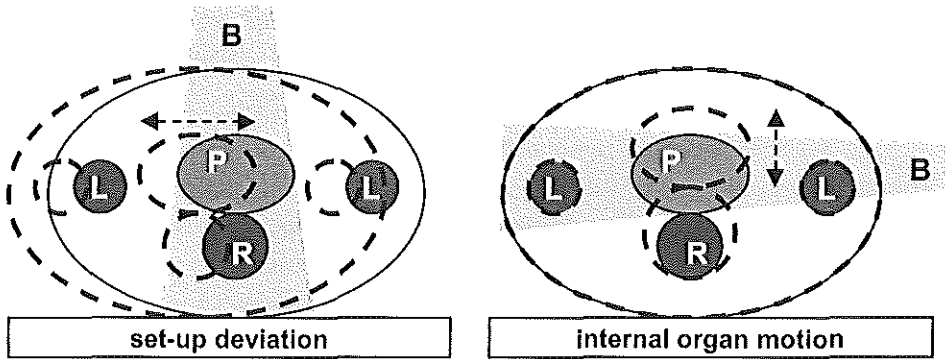


Figure 1-2 Schematic illustrations of the two types of geometrical variation using an imaginary transversal patient slice. Indicated are a prostate tumor (P), a rectum (R), and the leg bones (L). The solid lines and the beams (B) represent the intended treatment geometry. On the left, set-up errors are illustrated; the whole patient has moved (dashed lines) with respect to the planned treatment beam. On the right, internal organ motion is depicted; due to the increased rectum volume (dashed), the prostate has moved upward with respect to the intended position. It is clear that in both cases measures are needed to ensure adequate tumor coverage.

III. Geometrical uncertainties in radiotherapy

For practical reasons, the main tumor movements with respect to the treatment beams are normally separated in two types (see Fig. 1-2); the movement of the patient as a whole (the external set-up variation), and the movement of the tumor within the patient (internal variation). The set-up variations result from the daily positioning of the patient on the treatment table. Normally, external reference points on the patient skin, marked with pen or tattoo, must be aligned with fixed (laser) lines indicating the center of the treatment beams. Furthermore, several tools like arm- and leg supports can be attached to the treatment table to ensure a reproducible and stable patient position. Despite these precautions, the set-up might deviate from the planned position. Therefore, special equipment has been developed to measure the patient position with respect to the beams. Especially the use of electronic portal imaging devices (EPIDs) that can actually image the patient during treatment has been greatly increased in recent years. Portal imaging is based on the fact that the clinical photon beams that are often used for treatment, are not completely absorbed in the patient (see Fig. 1-1). Only a small part of the exit radiation is needed to display the patient anatomy, similar to a normal x-ray photo. The position of the patient during treatment as indicated by

the bony structures in the images, can then be compared to the intended position, possibly even before the bulk of the fraction dose is delivered.

The internal variations are the tumor motions with respect to the external reference marks and bony anatomy. For prostate cancer patients for instance, the variations in rectum and bladder volumes affect the position of the prostate, which is located in between these organs. Since the tumor itself is normally not visible in portal images, other techniques to determine internal organ movement are under development. It is for instance possible to implant radio-opaque markers in the tumor to allow tumor movement detection with an EPID. Moreover, other imaging modalities like ultrasound, CT or magnetic resonance imaging (MRI) can be applied without these markers. A disadvantage of CT and MRI is that the necessary equipment is normally not present in the treatment room. Studies on the extent and frequency of possible tumor movement can be performed with these machines, but correction of the tumor position prior to delivery of each treatment fraction would be very complicated.

Whatever measures are taken to minimize the organ motions and set-up variations, there will always be some uncertainty left. Therefore, safety margins must be applied around the tumor during treatment planning. The intended tumor region (i.e. the visible tumor plus microscopic spread) as delineated in the CT slices is normally called the clinical target volume (CTV). The CTV extended with the safety margins for geometrical uncertainties is called the planning target volume (PTV). The treatment is then planned in such a manner that the PTV receives the required tumor dose. In this thesis, the way to calculate these CTV-to-PTV margins, and some ways to minimize them, have been investigated.

IV. Summary of the thesis

a. Automatic 3D expansion of the CTV to generate a PTV

In Chapter 2 is described how a required CTV-to-PTV margin can be applied. The CTV, which is delineated in multiple axial CT slices by the radiation oncologist, is a 3D volume. Since geometrical variations can occur in all directions, the safety margins also have to be applied in 3D. Because it is impossible to accurately draw a 3D margin in multiple-2D CT slices manually, an algorithm has been developed for automatic 3D extension of the CTV with a prescribed CTV-to-PTV margin. The CTV contours delineated in the CT slices are used to fill a 3D calculation grid (matrix);

volume elements (voxels) that are part of the CTV are designated 1, others 0. All CTV voxels are subsequently extended with an ellipsoid with diameters equal to the margins required in the three orthogonal directions, which yields the PTV. From this PTV, 2D contours are extracted and placed back in the CT slices. This automatic procedure significantly increases the accuracy and the speed of the PTV delineation.

In Chapter 3 the clinical benefit of the 3D CTV-to-PTV expansion algorithm is studied. Since manual 3D margin drawing is impossible, the third dimension (perpendicular to the CT slices) is often ignored in clinical practice; margins are applied slice-by-slice and within the slices only (i.e., multiple 2D). For ten patients with prostate cancer, the errors made by this procedure were quantified. Depending on the shape of the CTV, it appeared that the multiple-2D approach could lead to margins being underestimated locally by more than 1 cm, which in turn could yield serious underdosages and a decrease in the expected probability of tumor control of 15%.

b. Automatic calculation and verification of 3D margins based on patient data

A more complete manner of margin calculation is proposed in Chapter 4. The size and shape of the margins for a particular patient is based on the actual knowledge of the geometrical uncertainties of a representative patient group. The CTV matrix mentioned above is convolved with the distributions of the known uncertainties, for translations as well as rotations, yielding a so-called coverage probability matrix. This matrix has voxel values between 0 and 1 that indicate the probability that a voxel is covered by the CTV. Specific “iso-probability” volumes are then chosen as the PTV. Once the dose distribution has been planned around the PTV, the same coverage probability matrices can be used to quickly calculate the *expected dose distribution in the CTV*, taking in consideration all types of uncertainties. In case of deviations from the intended dose distribution, the PTV can be adjusted by choosing a different iso-probability volume. For three different tumor sites, it appeared that the “systematic variations” (i.e., deviations from the planning situation that occur every treatment fraction) are about three times more important for the CTV-to-PTV margin than the “random variations” (i.e., deviations that vary from fraction to fraction).

In Chapter 5 two treatment positions for patients with prostate cancer were compared with respect to the required CTV-to-PTV margins. One half of a group of 30 patients was treated in prone treatment position, the other half in supine position. Internal as well as external geometrical uncertainties were measured. Internal varia-

tions were determined by making 4 CT scans of the patients during the 7 week treatment period. The delineated CTVs were subsequently registered using a fully automatic 3D matching technique, which yielded the translations and rotations of the CTV. External set-up variations were measured from portal images and combined with the internal variations to determine the CTV-to-PTV margins. Although at first glance the prone position seemed superior, adequate separation of systematic and random variations resulted in about equal CTV-to-PTV margins for both groups.

c. On-line correction of geometrical uncertainties

In Chapter 6 the feasibility of on-line corrections of external set-up deviations was investigated for a group of 14 patients with gynecological tumors. These patients are prone to relatively large set-up errors, even when a (routine) off-line correction protocol is applied. Off-line corrections reduce the *systematic* deviation of a patient by determination of the average deviation for the first fractions, followed by corrections for all subsequent fractions. With on-line corrections, the patient position during each fraction is assessed from a portal image acquired using only a small part of the total fraction dose. If necessary, corrections are applied before the bulk of the fraction dose is given. In this manner *systematic* as well as *random* deviations are minimized. It appeared that at the cost of some extra treatment time, the set-up deviations for gynecological patients could be reduced to very low values. Application of on-line corrections would therefore justify a significant CTV-to-PTV margin reduction.

The possibility of detecting internal organ motion with routine portal images is examined in Chapter 7. Apart from bony structures, gas pockets in the rectum are also clearly visible in portal images of patients irradiated in the pelvic region. The idea is that gas pockets visible in the lateral images, can be used to determine the anterior rectum wall and, since the prostate rests on the rectum, the prostate position. The CT data sets for the 15 supine patients from Chapter 5 were used to simulate this. Portal images were digitally reconstructed from the CT data sets and the movement of the rectal wall was estimated from the ventral edge of gas pockets in the images. These movements were correlated with the “real” rectal wall shifts, as obtained from delineations in the CT scans, and with the prostate movements determined from 3D matching. Especially the rectum wall shifts could be accurately derived from the portal images, which might therefore be used for online adjustment of the treatment geometry.

CHAPTER 2. AUTOMATIC CALCULATION OF THREE-DIMENSIONAL MARGINS AROUND TREATMENT VOLUMES IN RADIOTHERAPY PLANNING

J.C. Stroom and P.R.M. Storchi

Phys. Med. Biol. **42**, 745-755, 1997

I. Abstract

Following the publication of the ICRU-50 report, the concepts of GTV (gross tumor volume), CTV (clinical target volume) and PTV (planning target volume) are being used in radiotherapy planning with increasing frequency. In 3D planning, the GTV (or CTV) is normally outlined by the clinician in CT- or MRI-slices. The PTV is determined by adding margins to these volumes. Since manual drawing of an accurate 3D margin in a set of 2D slices is extremely time consuming, software has been developed to automate this step in the planning. The target volume is represented in a 3D matrix grid with voxel values 1 inside and 0 outside the target volume. It is expanded by centering an ellipsoid at every matrix element within the volume. The shape of the ellipsoid reflects the size of the margins in the three main orthogonal directions. Finally, the PTV contours are determined from the 50% iso-value lines of the expanded volume. The software tool has been in clinical use since the end of 1994 and has mostly been applied to the planning of prostate irradiations. The accuracy is better than can be achieved manually and the workload has been reduced considerably (from 4 hours manually to ca. 1 minute automatically).

II. Introduction

Radiotherapeutic treatment of cancer is most effective if a high and homogeneous dose is given to the tumor while surrounding normal tissues are maximally spared. In conformal radiotherapy the radiation beams are shaped conform to the target volume. Accurate determination of the (smallest possible) volume to be irradiated is therefore essential. To avoid ambiguity in the definition of the radiotherapy target volumes, the

International Commission on Radiation Units and Measurements (ICRU) has defined a number of treatment volumes for use in radiotherapy planning [54]. The gross tumor volume (GTV) is the gross palpable or visible malignant growth, which is normally outlined by hand in CT- or MRI-slices. The clinical target volume (CTV) is the GTV plus a volume containing subclinical malignant disease, and the planning target volume (PTV) is the CTV plus a margin taking into consideration all possible geometrical variations of the CTV during treatment, such as internal organ motion and patient positioning errors during subsequent fractions.

Many authors have described alternatives ways of incorporating geometrical inaccuracies in RT planning [38,43,63,67,74,98,107] and/or have discussed the required size of the margins [7,13,25,42,69,114,119]. However, to our knowledge the problem of actually implementing margins, once their size has been established, has not yet been discussed in detail. Although the ICRU concepts are clear, their application can cause some problems. In most cases the PTV is also outlined manually by adding a margin in three dimensions around the GTV (or CTV). It is however all but impossible to accurately draw 3D margins in 2D slices, especially if the shape of the GTV varies significantly from slice to slice. It would even be difficult to draw 2D margins in a slice if the margin in the lateral direction must be different from that in the ventro-dorsal direction.

A frequently applied method to avoid the drawing of 3D margins is by using beams eye view (BEV) projections which are available in most commercial planning systems nowadays. The 2D beam shape is directly determined from the back projection of the GTV to the accelerator head, with margins added for subclinical disease, geometrical inaccuracies and beam penumbra. However, this is not so obvious in case of anisotropic margins and oblique fields. In addition, the BEV procedure does not define a 3D PTV. It will then be difficult to evaluate and compare dose distributions using dose volume histograms. It is therefore more convenient to use all ICRU planning volumes and determine the 3D PTV from GTV and/or CTV and use it for subsequent planning.

Hence, a computer program has been written to increase the accuracy and speed of this step in radiotherapy planning. The program, which has been called CTV2PTV, is able to expand 3D target volumes in three dimensions. Different margins can be added in the three main directions (lateral, cranio-caudal and ventro-dorsal), generally within one minute.

III. Method

The program can be divided into four steps. (i) The input volume to be expanded (GTV or CTV) is originally represented as a set of slices with contour points which are obtained from the planning system. For each slice a rectangular 2D coverage matrix is determined with values equal to the fraction (0 to 1) of the pixel area that is inside the input contour. The 2D coverage matrices are then combined to yield a 3D matrix representation of the selected volume. (ii) The margins are represented by an ellipsoid which is also imbedded in a 3D calculation grid. Voxel values are 1 if the voxel center is inside the ellipsoid. If not, voxel values decrease to 0 with increasing distance of the voxel center to the ellipsoid. The shape of the ellipsoid is determined by the size of the margins in the three main directions. (iii) A margin is added to the input volume by scanning the ellipsoid within the 3D coverage matrix. If an input voxel value is larger than 0, it is expanded by the ellipsoid centered at that voxel. Hence a 3D margin is added and an output coverage matrix (PTV), also containing values from 0 to 1, is created. The method will be referred to as the ellipsoid expansion algorithm. (iv) The output contours are obtained from the output matrix by applying a 0.5 isovalue search algorithm to all slices. The resulting contour points are transmitted to the planning system.

In the following paragraphs the operation of the program will be explained in more detail.

a. The calculation of a 3D coverage matrix

For each slice containing an input contour, a 2D $n \times m$ coverage matrix M is determined with values equal to the fraction of the pixel that is inside the contour. The pixel size of M is equal to the CT-pixel size $\delta_x \times \delta_y$. The slice distance is defined as δ_z . M is calculated by combining two intersection matrices, A_x and A_y , which represent the intersection points of the (closed) contour with the horizontal and vertical matrix grid lines. The dimensions of A_x and A_y are $n \times (m+1)$ and $(n+1) \times m$ respectively. The algorithm for the determination of A_x is given in a Nassi-Shneiderman diagram [82] in figure 2-1. First all horizontal matrix lines are scanned for intersection points with all segments of the contour (see figure 2-2). Line by line the sorted intersection points on the current line are used to fill the intersection matrix A_x . The first intersection pixel on a line is given a value equal to the distance in pixel units of the intersection point to the grid line (i.e. between 0 and 1). Subsequent pixels on the line are filled with values

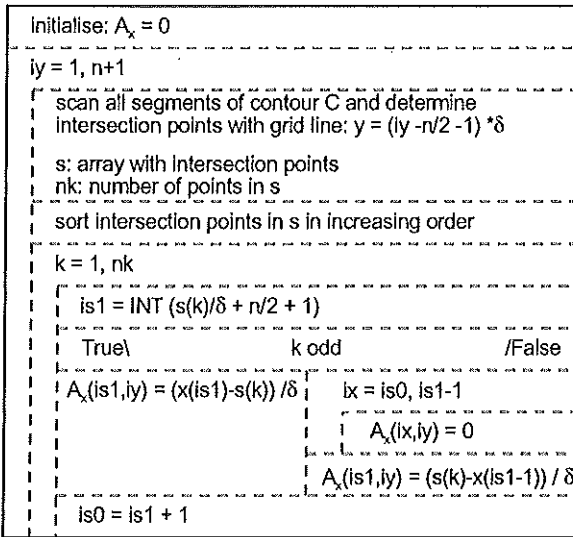


Figure 2-1 A Nassi-Shneiderman diagram of the algorithm used for the determination of the intersection matrix A_x in a 2D plane. Matrix A_y is computed in a similar way. A Nassi-Shneiderman (or box) diagram is a graphical design tool to represent computer algorithms in a clear and well defined manner.

1 until another edge pixel is encountered. This is repeated until all intersection points on the line are done. Necessarily there must be an even number of intersection points per line because the contour must fit completely within the calculation grid. Intersection matrix A_y is calculated similarly.

The intersection matrices are subsequently used to determine the coverage matrix M . For each surface element M_{ij} , the area covered by the contour can be calculated from the intersection values of its four sides. The element may be covered in several ways, three of which

are shown in figure 2-2. It is clear that a contour line right through the middle of a pixel results in a pixel value of 0.5, so a 0.5 isovalue search algorithm applied to the 2D coverage matrix will closely regenerate the original contour line. A 3D matrix of the input volume is obtained by stacking the 2D coverage matrices in the correct order. The voxel size of the matrix is then equal to the slice distance δ_z times the CT pixel size. The matrix size depends on the size of the input volume and of the margins to be applied.

b. The calculation of a 3D ellipsoid matrix

The ellipsoid which represents the margins in the three main directions (m_x, m_y, m_z) is contained in a 3D calculation matrix E with a voxel size equal to that of matrix M . The voxels are also 1 inside and 0 outside the ellipsoid. The edge values are however not equal to the coverage but depend on the minimal distance D_{\min} of a matrix grid

point to the ellipsoid. D_{\min} can be determined by minimization of the following function:

$$\Phi(x_e, y_e, z_e, \lambda) = (x - x_e)^2 + (y - y_e)^2 + (z - z_e)^2 + \lambda \left(\frac{x_e^2}{m_x^2} + \frac{y_e^2}{m_y^2} + \frac{z_e^2}{m_z^2} - 1 \right) \quad 2-1$$

where $(x-x_e)^2 + (y-y_e)^2 + (z-z_e)^2$ is the square distance of a grid point (x,y,z) outside the ellipsoid to a point (x_e,y_e,z_e) on the ellipsoid and

$$\frac{x_e^2}{m_x^2} + \frac{y_e^2}{m_y^2} + \frac{z_e^2}{m_z^2} = 1 \quad 2-2$$

is the equation for an ellipsoid. λ is the so-called Lagrange parameter. Minimizing the

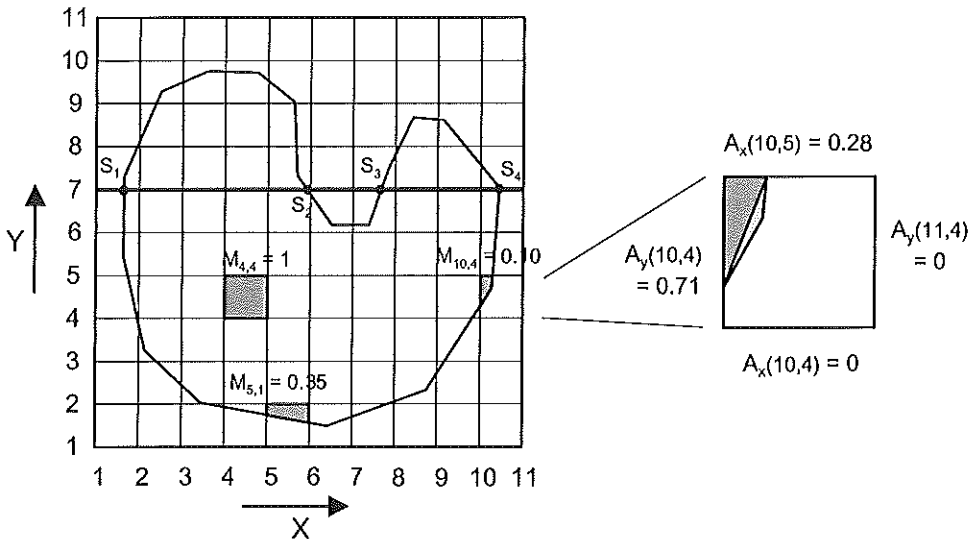


Figure 2-2 Illustration of a closed contour on a 10x10 coverage matrix M . The values of the elements M_{ij} are assigned to the center of the surface elements. The intersection points (S_1, \dots, S_4) on one horizontal grid line ($y = 6\delta$) in matrix A_x are shown by circles. Furthermore three of the possible cases the algorithm considers, when filling a surface element intersected by a contour line, are shown. The shadowed regions show the part of the element that is inside the contour. One of the elements is magnified to indicate how the intersection matrices A_x and A_y are used to determine the coverage, which is in this case $M_{10,4} = 0.5 \cdot A_x(10,5) \cdot A_y(10,4)$. Note that the calculated area is a little too small because of the presence of a contour point in this element.

cost function (numerically) for $\lambda < 0$ yields the closest point on the ellipsoid (x_e, y_e, z_e) and hence D_{\min} . The value of D_{\min} is used to fill the matrix E for every element $e(x, y, z)$ as follows:

if e is inside the ellipsoid: $E(e) = 1$

$$\text{if } D_{\min}(e) < \delta_{\text{norm}} : E(e) = (1 - F) \cdot \left(1 - \frac{D_{\min}(e)}{\delta_{\text{norm}}}\right) + F \cdot \sqrt{1 - \frac{D_{\min}(e)}{\delta_{\text{norm}}}} \quad 2-3$$

if $D_{\min}(e) \geq \delta_{\text{norm}} : E(e) = 0$

with δ_{norm} being the grid size normalized along the line through the grid point (x, y, z) and the ellipsoid center $(0, 0, 0)$

$$\delta_{\text{norm}} = \frac{\sqrt{x^2 + y^2 + z^2}}{\sqrt{\frac{x^2}{\delta_x^2} + \frac{y^2}{\delta_y^2} + \frac{z^2}{\delta_z^2}}} \quad 2-4$$

Equation 2-3 and the F -factor ($0 \leq F \leq 1$) in that equation have been determined by trial and error to give the most accurate results in the ellipsoid expansion and output contour acquisition (see next section). If only the linear term in equation 2-3 is used ($F = 0$), the calculated margins are on average slightly too small while just the square root term ($F = 1$) results in too large margins.

c. The 3D ellipsoid expansion algorithm

The ellipsoid matrix E is combined with the input volume matrix M_{in} to yield an output matrix M_{out} which contains the input matrix plus a 3D margin. The method is similar to a convolution. Firstly, all voxels in the output matrix are given the value 0. Secondly, for all voxels in the input volume larger than 0, the ellipsoid matrix is multiplied by the input voxel value and centered at the position of that voxel. If an ellipsoid voxel value at a certain position is higher than the current local voxel value at that position in the output volume, the ellipsoid value replaces the value in the output voxel, i.e.

FOREACH v : $M_{\text{out}}(v) = 0$

FOREACH v :

IF $M_{\text{in}}(v) > 0$:

FOREACH e : $M_{\text{out}}(v + e) = \text{MAX}(M_{\text{out}}(v + e), M_{\text{in}}(v) \cdot E(e))$

2-5

with ν and e being the three-dimensional indices for volume- and ellipsoid voxels respectively. The result is an expansion of the input volume with a 3D margin. The output matrix also consists of values 1 inside the new volume, 0 outside, and values between 0 and 1 at the boundary.

d. Calculation of output contours

The contour points of the output volume are obtained by applying a standard search algorithm, for 0.5 isovalue curves, to all 2D slices of the 3D output matrix. The algorithm is similar to those used in the determination of isodose contours from 2D dose matrices and is able to handle more complicated situations as contours consisting of multiple segments or contours crossing the borders of the matrix. The intersection points of the isovalue curves with the horizontal and vertical grid lines are determined by linear interpolation. Usually the number of output contour points is much larger than the number of input points. To avoid problems with the storage of the contours, a number of points may be deleted by a reduction algorithm.

e. Extra options of the model

The representation of volumes and margins in 3D matrices allows for handling of more complicated problems as well. If the GTV (or CTV) consists of several separate targets, separate coverage matrices are calculated for each target. They are combined into one 3D input matrix and the program continues with steps (ii) to (iv) to generate one PTV. In addition, it is possible to vary margins by altering the shape of the ellipsoid. Different margins for positive and negative directions can be entered and each octant of the ellipsoid is then created separately. The use of an asymmetrical ellipsoid with, for instance, different size in positive and negative y-direction, will yield output volumes with different margins in corresponding ventral and dorsal directions. Asymmetrical margins can also be acquired by a translation of an output volume calculated with symmetrical margins. A translation might actually reflect the clinical reason for the asymmetry; in case of organ motion for instance, asymmetrical margins are required if the organ position during planning CT scan is on average systematically shifted from the position during treatment. Furthermore, the margin can be adjusted locally, for instance in the neighborhood of a critical organ. The organ can also be represented in a 3D matrix and a second ellipsoid can be generated for

margins close to it. During the volume expansion the appropriate ellipsoid can be selected depending on whether a voxel in the input volume is inside or outside the organ at risk. Finally, margins can be subtracted if the voxels in the input volume are inverted before the ellipsoid expansion, i.e. $M_{in,new}(x,y,z) = 1 - M_{in,old}(x,y,z)$. After the expansion of the input volume, the output volume should also be inverted to get the final result.

IV. Results

In figure 2-3 results of two dimensional calculations are shown to illustrate the accuracy of the program. An irregular shape has been contoured with and without the addition of a margin. The 2D margin was 8 mm in the horizontal and 4 mm in the vertical direction. The program is accurate in all situations, except at sharp corners; if a pixel in the coverage matrix contains a contour edge point, the calculation of the area tends to yield values which are too small (or too large) because of a rounding of the corner (see also figure 2-2). The zero-margin curve clearly shows this effect which will generally yield margins which are too small. However, in clinical practice this is not a significant problem because anatomical organs with sharp edges do not exist.

There are a couple of other inaccuracies in the ellipsoid expansion algorithm. Firstly, the CT slice distance is often significantly larger (5 - 10 mm) than the pixel size (ca. 2 mm), so the voxels will be stretched. Despite the use of the normalization factor δ_{nom} in

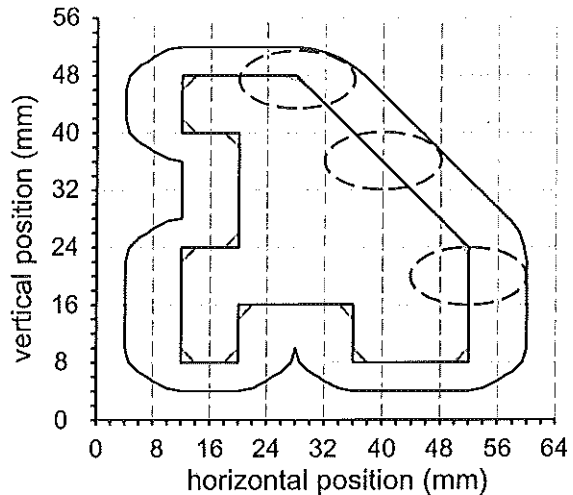


Figure 2-3 Illustration of a 2D margin, 8 mm horizontally and 4 mm vertically, applied to a simple geometrical shape (inner thick contour). The zero-margin contour is also calculated and shown by the inner thin contour. Note the rounding at the edges of the zero-contour by the approximation shown in figure 2. For clarity three ellipsoids are shown.

equation 2-3, the accuracy in the cranio-caudal direction is smaller than the accuracy within the slices. The problem can be circumvented by decreasing the slice distance of the input volume; extra slices can be generated by interpolation. Secondly, as described in the method-section, the ellipsoid expansion algorithm is not exact, but has been determined semi-empirically. The position of the edge after the addition of the margin and determination of the 0.5 isovalue curves can differ a little from what would be expected. By changing the F -factor in equation 2-3, the shape of the ellipsoid is somewhat changed and hence the outcome of the expansion. From one-dimensional computer simulations for 10,000 different combinations of edge position and margin size, the best value for F appeared to be 0.5. This yielded an average error of 0.00 ± 0.12 pixel (1 SD).

Figure 2-4 illustrates the problems with the determination of a 3D margin in a normal clinical situation. A sagittal cut through a 3D geometrical volume is shown. The margin added by the program was 6 mm in all directions. Also indicated is the margin added in the transversal slices only, that is in 2D. The latter situation is how one tends to add a 6 mm margin manually, i.e. slice by slice and without taking into account neighboring slices. However, if input contours in neighboring slices vary in size or shape, one slice will influence the margin in the other. Ignoring this will result in margins that are too narrow. They appear

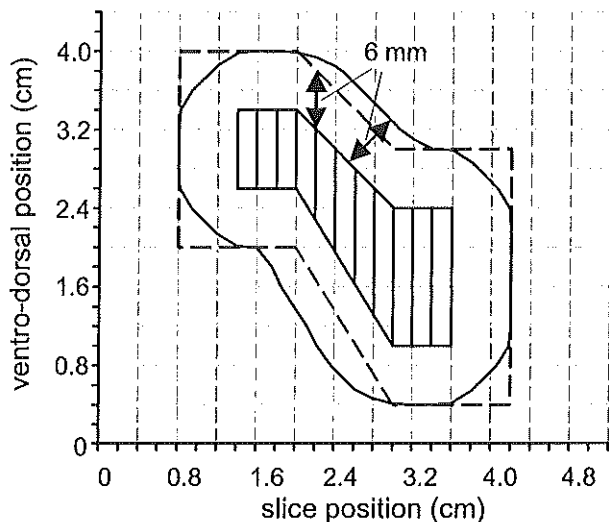


Figure 2-4 Illustration of a logical error made when drawing margins manually without taking the 3D aspect of the problem into account. A sagittal cut through a 3D geometrical shape is shown. Margins of 6 mm in all directions are required. Visible are the 3D margin as calculated by the program (solid line) and the margin as would likely be drawn by hand in 2D slices (dotted line). The manually determined margins are too small in the diagonal sections and too large at the cranial and caudal edges of the volume.

correct within a slice but are too small perpendicular to the surface of the 3D input object. This is clearly visible in the diagonal sections of the object in figure 2-4. Furthermore, when drawing margins manually in transversal slices one is inclined to forget the natural rounding at the cranial and caudal edges of the object; to get a cranio-caudal margin the outer slices with input contour are simply copied further outward. This generally yields excessive contours in the outermost slices.

In figure 2-5 clinical results are shown for a prostate planning. A 3D margin of 1 cm is applied to the GTV which has been determined manually by the clinician. In figure 2-5 (a, b and c) transversal slices through the prostate at different cranial-caudal

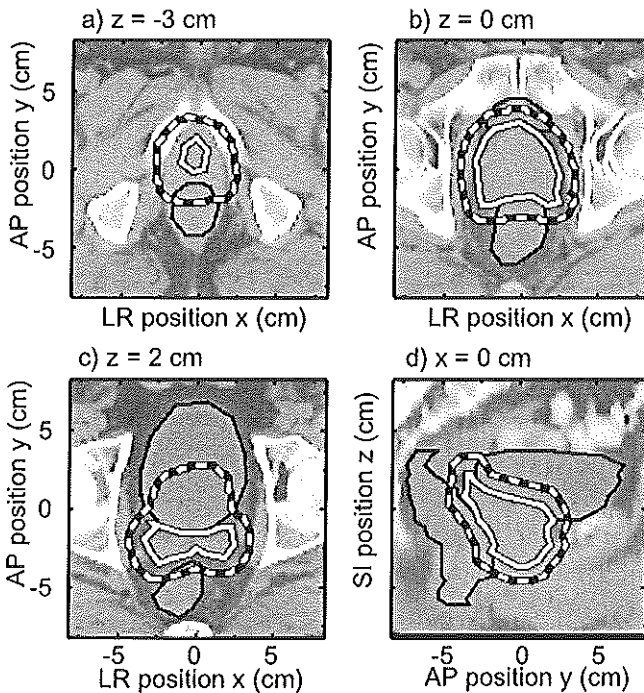


Figure 2-5 Illustration of a clinical example of the program. A 3D margin is applied to a prostate GTV which is shown in three transversal slices (a, b, and c) and a sagittal slice (d). The transversal slices are respectively a caudal, central, and cranial slice. The GTV (white), bladder (black), and rectum (black) are drawn by the clinician, the PTV (dashed) is calculated by the program. Note the apparently too large margin in (a) and (c).

z-positions are shown.

The GTV, bladder, and rectum are drawn by a clinician, while the PTV is calculated by the algorithm. The pixel size is 2 mm and the slice distance 5 mm. It is clearly visible that the margin is always equal to or larger than 1 cm.

The large deviation from 1 cm at the ventral side of the GTV in figure 2-5c is caused by the completely different shape of the prostate in neighboring slices (5b) to that of the vesiculae in this slice. This makes it sometimes difficult to interpret the results in 2D slices; margins may be judged to be unacceptably large but are really a result of taking into account the third

dimension. Figure 2-5d shows a sagittal cut through the middle of the prostate which indicates that the margin is equal to 1 cm in all dimensions.

Finally, in figure 2-6 a 3D representation of a more complex cervix CTV with a 1 cm margin is depicted. The CTV consists of the primary tumor region, the iliacal nodes, and the para aortic nodes. The pixel size was ca. 2 mm and the slice distance originally 1 cm. In the calculations, the resolution in the cranio-caudal direction has been doubled by use of extra interpolated slices. The figure clearly shows the 3D effect of the tool; the margin is constant in all directions all around the various parts of the CTV.

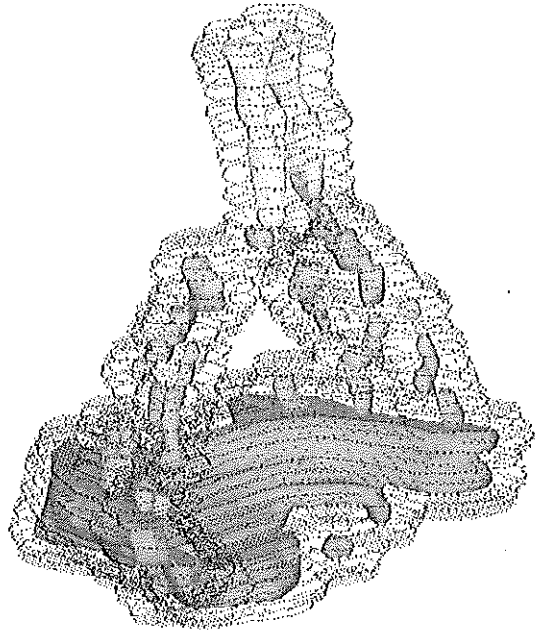


Figure 2-6 Representation of a cervix CTV with a 1 cm margin in 3 dimensions. The CTV consists of the primary tumor region (dark grey), the iliacal nodes (grey), and the para aortic nodes (light grey). The margin (black) is constant all around the CTV.

V. Discussion

The largest benefit of the program is a decrease in time necessary for patient planning. A completely manual outlining of a prostate PTV by adding 3D margins to the GTV took on average four hours. Using CTV2PTV, this step is performed within one minute for standard prostate targets on a HP 9000/715 Unix work station. An apparently more complex problem does not necessarily require more time; the calculation of the cervix PTV as shown in figure 2-6 was almost as fast as the prostate PTV in figure 2-5. The computation time depends mainly on the actual expanding of the volume (formula 2-5). CT-scans for prostate patients are normally acquired with a 5 mm slice distance and ca. 2 mm pixel size. To apply a 1 cm margin, the size of volume matrices in CTV2PTV are typically $60 \times 60 \times 25$ (in- and output matrix) and $15 \times 15 \times 7$ (ellipsoid matrix), so about $1.4 \cdot 10^8$ voxels have to be scanned in formula 2-5. Time may be gained by excluding the voxels in the bulk of the input volume from the

calculations and only computing the voxels near the edge. Bulk voxels can for instance be marked during calculation of the coverage matrix.

Two other important advantages of the program are the accuracy, which is generally within half a pixel, and the reproducibility of the results. These cannot be attained manually for a 3D margin. Even in 2D (within one transversal slice), already considerable effort would be demanded to draw a margin which is different in the horizontal and vertical directions. See for instance figure 2-3; especially in the region of the diagonal, drawing the transition from horizontal to vertical margin would be rather complicated. As mentioned before, it is difficult to assess the accuracy of the calculations by analyzing the results in 2D slices; apparently excessive margins can appear. It gets even more complicated if variable margins in combination with critical organs are calculated. In those cases sagittal and frontal reconstructions, beams eye view plots or 3D displayed volumes are necessary to judge the outcome of CTV2PTV.

Until now it has been assumed that the margins are required in directions along the main axes of the CT coordinate system. The studies to determine those margins are normally performed using either the CT coordinate system (in case of multiple CT scans to determine organ motion) or AP and lateral simulation photo's (in case of portal imaging to determine set-up errors). Although the CT coordinate system is the most convenient, margins in an arbitrary direction might incidentally be necessary in the future, for instance in case of margins for set-up deviations determined from portal images made under oblique gantry angles. The currently described algorithm will have to be extended slightly to enable this possibility. The obvious way is by a straightforward coordinate transformation of the input volume M_{in} to the required coordinate system. The required margin can then be added in the normal way. The output volume M_{out} must be transformed back to the original coordinate system before the output contours are obtained.

In our institute 3D conformal radiotherapy is increasingly being used, especially since the Racetrack Microtron MM-50 was commissioned at the beginning of 1994. The demand for accurate 3D planning and planning volumes increased likewise. The program CTV2PTV has been in clinical use for the last two years, mainly for the planning of prostate patients. To account for subclinical disease and geometrical uncertainties a constant 1.5 cm margin has been applied to the GTV in all three dimensions. In practice the input to CTV2PTV has been half a CT-pixel larger (1.6 cm) because the clinicians wanted at all costs to avoid smaller margins, which might

occur due to rounding errors near the corner points of the contour. At the moment the program is beginning to be applied more frequently, for instance in the case of gynecological tumors.

The program interface is especially designed for the CadPlan planning system.¹ A simplified version of the algorithm (without the extra options described in the method section) has been incorporated in the latest version of the system. In principle the software will be made available as shareware. It has been set up in a modular way so it should be relatively easy to modify for other planning systems. For information, the authors can be reached at their E-mail or regular address.

VI. Conclusions

A computer program has been developed to automatically add margins in three dimensions to treatment volumes. The input volumes are represented in 3D calculation matrices and expanded by centering an ellipsoid at every voxel in the volume. The program has proven to be a useful tool in our institute. The accuracy is a fraction of a CT-pixel which is generally more than sufficient and better than can be achieved manually. Apart from straightforward 3D margins around a simple volume, also more complicated cases with multiple input volumes and variable margins can be handled. The tool has been in clinical use for two years now, mainly to calculate prostate PTV's from GTV's. The workload for the planning technicians has been reduced enormously; from several hours manual contouring to one minute automatically.

VII. Acknowledgements

The work described in this paper has been supported by the Dutch Cancer Society (NKB-project 92-86). The authors would like to thank Hans de Boer and Andries Visser for their valuable input during the discussions and their careful reading of the manuscript. Henk Huizenga, Ben Heijmen and Peter Koper are thanked for their stimulating support. Finally Gert Korevaar, John van Sörnsen de Koste, Sandra Quint,

¹ Varian-Dosetek

Merik Seven, Marjolein van Os and the other users of the program in its immature state, are thanked for testing the program.

CHAPTER 3. MULTIPLE 2-DIMENSIONAL VERSUS 3-DIMENSIONAL PTV DEFINITION IN TREATMENT PLANNING FOR CONFORMAL RADIOTHERAPY

J.C. Stroom, G.A. Korevaar, P.C.M. Koper, A.G. Visser, B.J.M. Heijmen

Radiother. Oncol. 47, 297-302, 1998

I. Abstract

Purpose: To demonstrate the need for a fully 3-dimensional (3D), computerized expansion of the gross tumor volume (GTV) or clinical target volume (CTV), as delineated by the radiation oncologist on CT-slices, to obtain the proper planning target volume (PTV) for treatment planning according to the ICRU-50 recommendations. *Methods and materials:* For ten prostate cancer patients two PTVs have been determined by expansion of the GTV with a 1.5 cm margin, a 3D PTV and a multiple 2D PTV. The former was obtained by automatically adding the margin while accounting in 3D for GTV contour differences in neighboring slices. The latter was generated by automatically adding the 1.5 cm margin to the GTV in each CT-slice separately; the resulting PTV is a computer simulation of the PTV that a radiation oncologist would obtain with (the still common) manual contouring in CT-slices. For each patient, the two PTVs were compared to assess the deviations of the multiple 2D PTV from the 3D PTV. For both PTVs conformal plans were designed using a three field technique with fixed block margins. For each patient, dose volume histograms and tumor control probabilities (TCPs) of the (correct) 3D PTV were calculated, both for the plan designed for this PTV and for the treatment plan based on the (deviating) 2D PTV. *Results:* Depending on the shape of the GTV, multiple 2D PTV generation could locally result in a 1 cm underestimation of the GTV-to-PTV margin. The deviations occurred predominantly in the cranio-caudal direction at locations where the GTV contour shape varies significantly from slice to slice. This could lead to serious underdosage and to a TCP decrease of up to 15%. *Conclusions:* A full 3D GTV-to-PTV expansion should be applied in conformal radiotherapy to avoid underdosage.

II. Introduction

To ensure a correct dose delivery to the tumor in radiotherapy treatment, the ICRU has suggested a scheme for the determination of the planning target volume (PTV) that should be used for treatment planning [54]. Initially, the gross tumor volume (GTV), which is the visible and/or palpable volume of malignant growth, should be outlined in the diagnostic images. This volume is then extended to the clinical target volume (CTV) which contains GTV plus areas of suspected subclinical microscopic disease. Finally a margin is added to take into account geometrical uncertainties like patient and organ movement, resulting in the PTV.

Although the ICRU concepts for definition of a PTV are clear, their application can be problematic. The nature of the problem is demonstrated in figure 3-1. In figure 3-1a, a transversal CT slice through a prostate GTV is depicted. An isotropic 1.5 cm margin has been added in 2D around the GTV contour to get the PTV. The same has been done in all other slices, i.e. a "multiple 2D" PTV has been generated which reflects a normal manual outlining procedure. However, due to GTV contour differences in neighboring slices this would yield too small margins in the cranial direction, as is indicated in a sagittal CT reconstruction through the prostate (figure 3-1b). In

Figure 3-1 Illustration of the problem discussed in this paper. Multiple 2D margins (dotted curves) around a prostate GTV (solid curves) in a transversal CT slice (a) may yield too narrow margins in the cranio-caudal directions as shown in a sagittal reconstruction (b). The 3D margins (dashed curves) may appear too large in a transversal CT slice (c) but are actually correct (d). The arrows in the sagittal reconstructions indicate the position of the transversal CT slice.

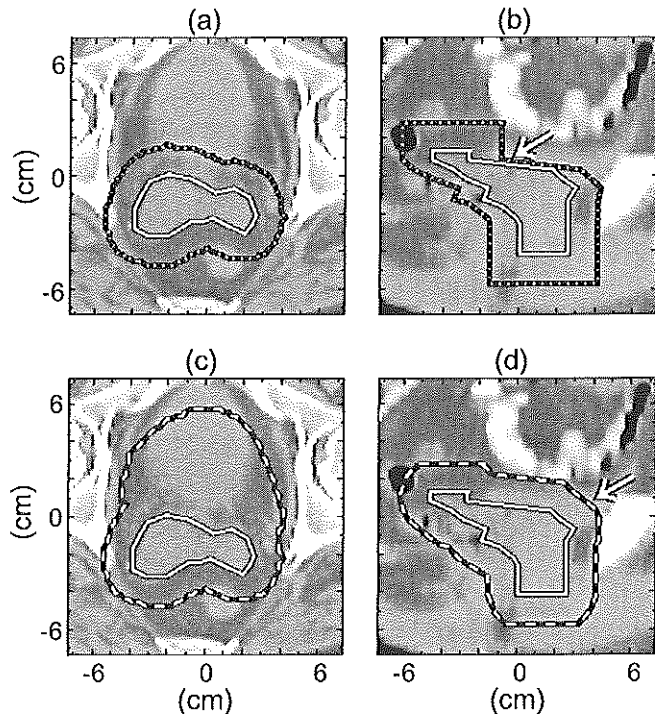


figure 3-1c, the correct 3D PTV has been generated by automatic expansion in all three dimensions. In the anterior part of the PTV the margin is clearly larger than 1.5 cm but the sagittal reconstruction (figure 3-1d) shows that this margin is correct. It is obviously all but impossible to accurately draw a 3D margin in 2D CT slices without the aid of software tools. Consequently, several groups have pointed out the importance of automatic 3D margin delineation [5,15,106].

In this paper we want to explore the geometrical and dosimetrical consequences of the still common but incorrect multiple 2D PTV generation, by comparison with the correct 3D PTV calculation for a group of prostate cancer patients. In the following "3D PTV" will stand for the full 3D PTV and "2D PTV" will refer to the multiple 2D PTV.

III. Methods and materials

Ten prostate cancer patients were selected for this study. Three of the patients had stage T1 tumors, the others had T2 tumors for whom the vesiculae seminalis were part of the GTV. All patients were routinely CT-scanned in the supine treatment position with 5 mm slice distance. The GTV was outlined in all relevant slices by a radiation oncologist. The position of the apex of the prostate was verified by the use of sagittal reconstructions through the prostate. The GTV-to-PTV margin for subclinical disease and geometrical uncertainties was at the time of the study taken to be 1.5 cm. For all patients 3D and 2D PTVs were automatically determined.

The algorithm for automatic margin generation has been described in a separate paper [106] and roughly works as follows. The GTV is represented in a 3D matrix grid with voxel values equal to the fraction of the voxel volume that is inside the GTV contours (i.e. in between 0 and 1). It is expanded in three dimensions by centering an ellipsoid at every matrix element within the volume. The shape of the ellipsoid reflects the size of the margins in the three main directions. The PTV is subsequently obtained by extracting the 0.5 iso-value surface from the expanded volume. Depending on margin and volume size, the whole operation is generally performed within one minute.

The 3D PTV was generated by applying an isotropic margin to the GTV in all three dimensions, i.e. the ellipsoid in the expansion algorithm actually was a sphere with 1.5 cm radius. The 2D PTV was calculated by expanding each GTV voxel by a circle with 1.5 cm radius and orientation parallel to the CT slices. This procedure

simulates the manual slice-by-slice contouring of the PTV (without taking the GTV shape in neighboring slices into account). For the 2D PTV, the GTV extension in cranial and caudal directions was obtained by copying the PTV contours at both ends of the GTV to the next three slices without GTV. The geometrical differences between the 3D PTV and corresponding 2D PTV were assessed from sagittal and frontal CT reconstructions through the PTV and by comparison of the volumes.

For each patient our standard isocentric three-field treatment plan with conformal blocks was designed for both PTVs. It consisted of one anterior-posterior beam and two lateral-oblique beams. The lateral beams were partly delivered with a 60° degrees motor wedge and were slightly tilted posteriorly in order to minimize rectum irradiation. Beam weights were such that each field contributes equally to the dose at isocenter. For all plans, the orientation dependent block margins between the beam's-eye-view (BEV) PTV-projection and conformal blocks were at the time of the study: 5 mm in the lateral direction of the AP fields, 9 mm in the ventro-dorsal direction of the lateral fields, and 15 mm in the cranial caudal-direction of all fields [32]. All plans were made for the 25 MV photon beam of a Racetrack Microtron MM50 (Scanditronix) and complied with the ICRU recommendation for dose homogeneity in the PTV, i.e. the variation of the dose in the PTV is kept within +7% and -5% of the prescribed dose [54].

To analyse the consequences of the use of the 2D PTV in treatment planning, the dose distribution as resulting from the beam shapes determined for that PTV was assumed to have been delivered to the (correct) 3D PTV. Differences in dose volume histograms (DVHs) and tumor control probabilities (TCPs) with the treatment plan that was designed for the 3D PTV were calculated. The model that was used for TCP calculations is described by Munzenrider *et al.* [81]. The parameters for the TCP calculations were $TCP_{66} = 70\%$ (based on data of our own institute), $\gamma_{pop} = 1$, and $\gamma_{ind} = 8$ [70]. Since the TCP values are mainly determined by the average dose, all plans were normalized so that the average dose in the original PTV became 66 Gy.

All treatment planning was performed on HP 9000/7xx work stations using the CadPlan planning system (Varian-Dosetek). The software for 3D extension of planning volumes delineated in CT slices was developed to run with CadPlan and is now routinely used for most patients that are 3D planned. Part of the software has been integrated in the latest CadPlan version (2.7.7).

IV. Results

In figures 3-2a and 3-2b sagittal and frontal reconstructions through the center of the prostate in a plane near the isocenter are shown for all patients, and the GTV, 2D

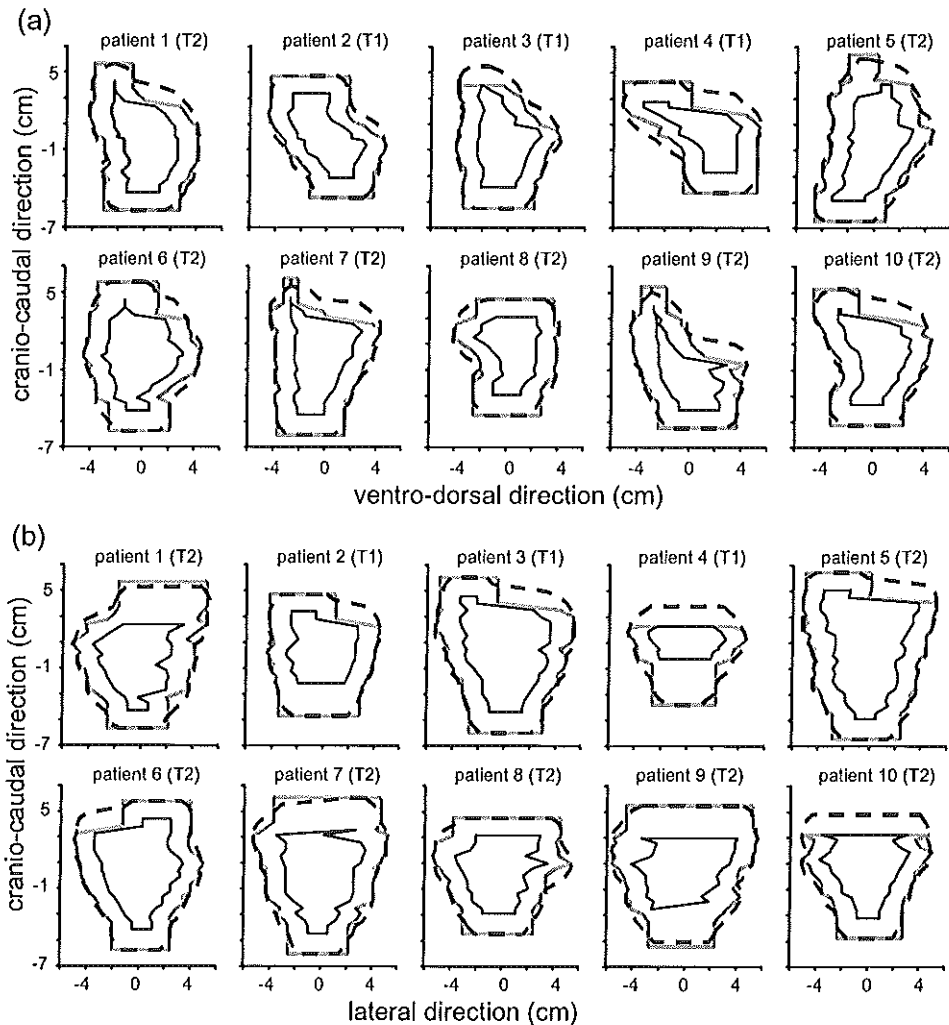


Figure 3-2 Sagittal (A) and frontal (B) reconstructions through the centre of the prostate for ten patients. The GTVs are indicated by the black curves, the 2D PTVs by the grey curves, and the 3D PTVs by the dashed black curves. Large differences between 2D and 3D PTVs occur in areas with large GTV contour differences between neighbouring CT-slices.

PTV, and 3D PTV are depicted. As expected, the 2D PTV generally follows the GTV at exactly 1.5 cm in lateral and ventro-dorsal directions. The seemingly larger margins that sometimes occur (especially near the seminal vesicles) are due to the data being presented as reconstructions in 2D planes; certain parts of the GTV responsible for a GTV-to-PTV extension as seen in the reconstruction may in itself be invisible in that reconstruction. However, figures 3-2a and 3-2b clearly show that for some patients the multiple 2D extension of the GTV results in extremely narrow margins between GTV and 2D PTV in the cranio-caudal direction, see for example patients 4, 7, and 10 in figure 3-2a. These deviations occur in areas with large GTV contour differences in neighboring slices. The 3D PTV does not suffer at all from this problem due to the full 3D extension of the GTV. The spikes that are visible in the cranial part of some of the contours (see for instance figure 3-2a, patient 7) are due to a graphical artifact of the planning system. If the volume of interest divides into more than one branch (like the vesiculae), the planning system requires that the separate GTV contours that are delineated in one slice are connected with a line. These lines can appear as spikes in sagittal or frontal reconstructions but contain no volume and are subsequently ignored.

The average volume of the 3D PTV is 519 ± 59 (1 SD) cc whereas the average 2D PTV is 456 ± 54 (1 SD) cc, i.e. there is a mean difference of 62 ± 10 (1 SD) cc (see Table 3-1). This implies that on average at least 12% of the 3D PTV volume is not included in the 2D PTV. Actually this percentage is slightly larger because the copying of the outer PTV slices of the 2D PTV somewhat overestimates the margin, and hence the volume, at the cranio-caudal edges.

In figure 3-3 two BEV plots of the 3D PTV of patient 4 are shown together

patient	stage	ΔV (cc)	ΔTCP (%)
1	T2	68	4
2	T1	55	11
3	T1	72	13
4	T1	68	15
5	T2	81	13
6	T2	57	8
7	T2	56	10
8	T2	58	4
9	T2	50	3
10	T2	67	7
Mean(SD)	-	62(10)	9(4)

Table 3-1 Volume and TCP reduction for the ten prostate patients described in this study. ΔV is the volume difference between the 3D PTV and the 2D PTV. ΔTCP is defined as the TCP for the 3D PTV resulting from the plan designed for the 3D PTV, minus the TCP for the 3D PTV resulting from the plan designed for the 2D PTV.

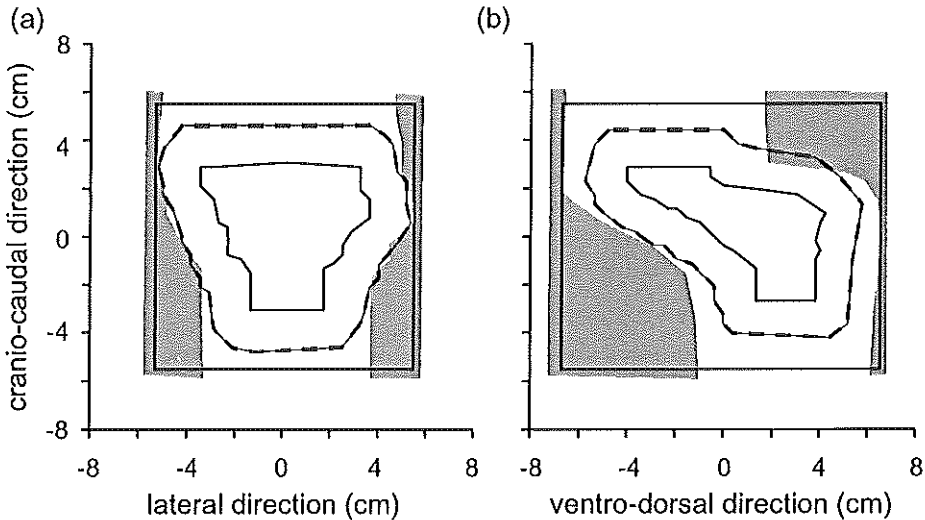


Figure 3-3 AP (A) and lateral (B) beam's eye view plots of the 3D PTV (dashed lines) with conformal blocks designed for the 2D PTV for patient 4. The solid lines are the BEV projection of the GTV. Over large areas the block margins are too narrow to account for the beam penumbra. In some areas the blocks even overlap the PTV.

with the conformal blocks designed for irradiation of the 2D PTV. In large areas the blocks overlap or fit too tight around the 3D PTV, leaving too little room to account for the beam penumbra. Applying these blocks will therefore result in underdosage of the 3D PTV. This is further illustrated in figure 3-4 by the average DVHs for the 3D PTV resulting from the treatment plans designed for the 2D and 3D PTV respectively. The average minimum dose in the 3D PTV decreases from about 62 Gy for the plan designed for the 3D PTV to about 51 Gy for the plan designed for the 2D PTV. The average TCP difference between the correct plan and the plan designed for irradiation of the 2D PTV was 9 ± 4 (1 SD)% (see Table 3-1).

V. Discussion

The magnitude of the observed TCP reduction when the PTV margins were assumed to be two-dimensional, depended mainly on the shape of the GTV. There appeared to be a relation with the tumor stage; all patients with stage T1 tumors had TCP reductions of over 10% whereas only one of seven T2 tumors showed this phenomenon. One would expect large variations in GTV delineation especially with T2 tumors,

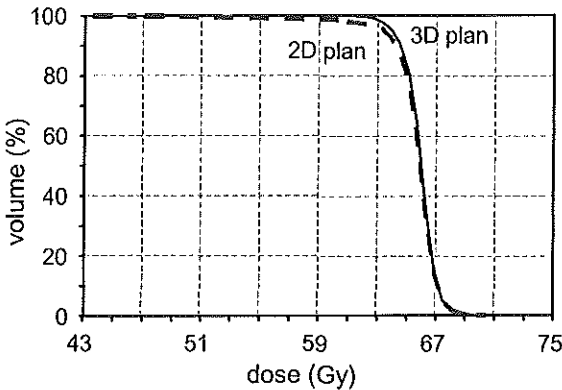


Figure 3-4 Cumulative DVHs for the 3D PTV, averaged over the ten patients. The dashed curve represents the averaged DVH of the plans designed for the 2D PTV, the solid curve is the averaged DVH designed for the 3D PTV. There is a systematic underdosage of the 3D PTV when planned with the beams designed for the 2D PTV.

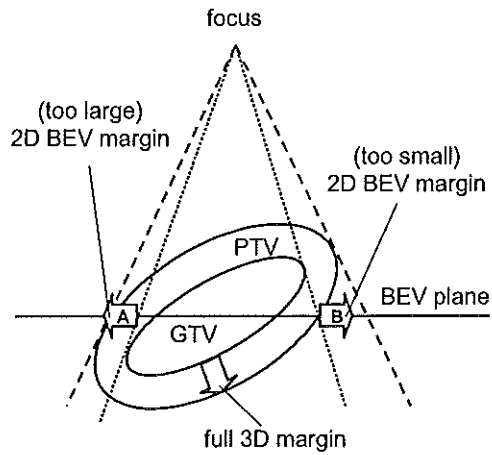
three-field technique and, for instance, a four-field technique with similar block types will therefore be small. However, if rectangular fields would have been used instead of conformally shaped fields, the multiple 2D procedure would not result in underdosage. The rectangular field size is normally determined by the outermost tumor extensions and these are the same for the 2D PTV and the 3D PTV. If the beams would have been shaped by multi-leaf collimators, the block margins around the PTV would on average be larger than for conformal blocks and hence the errors due to 2D PTV determination would be smaller.

A possible 2D alternative for treatment planning based on a 3D PTV is beam's eye view planning [87]. Using this technique, the PTV- and block margins around the BEV projection of the GTV are automatically calculated in 2D in the BEV plane. Consequently, the BEV technique does not result in a 3D PTV. Straightforward evaluation of the dose distribution in the PTV, as recommended by the ICRU [54], is therefore not possible. Moreover, the projection of the GTV volume to one plane may yield over- or underestimation of the margin if the outermost extensions of the GTV are not at the level of the BEV plane, as is demonstrated in figure 3-5 for a hypothetical tumor. Due to the divergence of the treatment beams, the magnitude of the required 3D margins is altered when projected to the BEV plane. This effect is not taken into account by the BEV method. In normal clinical situations (with the BEV

where the seminal vesicles are part of the GTV. However, also in all T1 cases the most cranial GTV contours were significantly smaller than the ones in neighboring slices.

Obviously, the TCP reductions depend on the dose distribution and hence on the treatment technique. The more conform the 95% isodose volume encloses the PTVs, the larger the errors will be when 2D PTVs are used instead of 3D PTVs. The difference between our

Figure 3-5 Illustration of a drawback of 2D BEV planning (based on a BEV projection of the GTV) compared to planning based on a full 3D PTV. The GTV-to-PTV margins are indicated by the arrows and the dotted and dashed lines indicate the projection to the BEV plane of the GTV and 3D PTV respectively. Due to the divergence of the beam, two-dimensional extension of the GTV in the BEV plane may yield too large (A) or too small (B) margins compared to the (correct) margins that result from projections of the 3D PTV.



plane through the GTV, a GTV "diameter" of about 10 cm, and a focus-BEV plane distance of about 100 cm) the errors are relatively small (maximally 1 mm). A final objection to the BEV method is that it is quite impractical in case of anisotropic margins and/or oblique fields, especially when the direction of the margins is not perpendicular to the field.

In conclusion, for ten prostate cancer patients we have shown that multiple 2D calculation of PTV margins instead of full 3D calculations can lead to serious underdosage and TCP reductions of up to 15%. The same conclusion holds, of course, for other than prostate tumors. Delineated GTV- or CTV contours normally vary from slice to slice and hence full 3D PTV margin calculation is required when conformal radiotherapy is used.

VI. Acknowledgements

The authors want to thank the Dutch Cancer Society (NKB-project 92-86) and the Revolving Fund of the University Hospital Rotterdam for sponsoring the research described in this paper. Furthermore, the support of John van Sörnsen de Koste during the various treatment planning sessions and the useful suggestions of Filicity Yorke during the writing of the paper are greatly appreciated.

CHAPTER 4. INCLUSION OF GEOMETRICAL UNCERTAINTIES IN RADIOTHERAPY TREATMENT PLANNING BY MEANS OF COVERAGE PROBABILITY

J.C. Stroom, J.C.J. de Boer, H. Huizenga, and A.G. Visser.

Int. J. Radiat. Oncol. Biol. Phys. 43, 905-919, 1999.

I. Abstract

Purpose: Following the ICRU-50 recommendations, geometrical uncertainties in tumor position during radiotherapy treatments are generally included in the treatment planning by adding a margin to the clinical target volume (CTV) to yield the planning target volume (PTV). We have developed a method for automatic calculation of this margin. *Methods and materials:* Geometrical uncertainties of a specific patient group can normally be characterized by the standard deviation of the distribution of systematic deviations in the patient group (Σ) and by the average standard deviation of the distribution of random deviations (σ). The CTV of a patient to be planned can be represented in a 3D matrix in the treatment room coordinate system with voxel values one inside and zero outside the CTV. Convolution of this matrix with the appropriate probability distributions for translations and rotations yields a matrix with coverage probabilities (CPs) which is defined as the probability for each point to be covered by the CTV. The PTV can then be chosen as a volume corresponding to a certain iso-probability level. Separate calculations are performed for systematic and random deviations. Iso-probability volumes are selected in such a way that a high percentage of the CTV volume (on average > 99%) receives a high dose (> 95%). The consequences of systematic deviations on the dose distribution in the CTV can be estimated by calculation of dose histograms of the CP matrix for systematic deviations, resulting in a so-called dose probability histogram (DPH). A DPH represents the average dose volume histogram for all systematic deviations in the patient group. The consequences of random deviations can be calculated by convolution of the dose distribution with the probability distributions for random deviations. Using the convolved dose matrix in the DPH-calculation yields full information about the influence of geometrical

uncertainties on the dose in the CTV. *Results:* The model is demonstrated to be fast and accurate for a prostate, cervix, and lung cancer case. A CTV-to-PTV margin size which ensures at least 95% dose to (on average) 99% of the CTV, appears to be equal to about $2\Sigma+0.7\sigma$ for three all cases. Because rotational deviations are included the resulting margins can be anisotropic, as shown for the prostate cancer case. *Conclusion:* A method has been developed for calculation of CTV-to-PTV margins based on the assumption that the CTV should be adequately irradiated with a high probability.

II. Introduction

Geometrical uncertainties in radiotherapy treatments cause differences between intended and actually delivered dose distribution in the clinical target volume (CTV), as defined by the ICRU [54]. The uncertainties primarily consist of external set-up deviations and internal organ movement. Both deviations consist of a systematic component, i.e. the same for each fraction of the treatment, as well as a random component, i.e. varying from day to day. The size of the patient set-up deviations can be assessed by comparison of images acquired during the treatment (with megavoltage portal films or electronic portal imaging devices) with those of the intended treatment (simulator radiographs or digitally reconstructed radiographs generated by the planning system). By imaging several patients of a specific patient group regularly, the typical size of the systematic and the random positioning deviations for that group can be determined [11,25], which may indirectly lead to improved set-up techniques and/or equipment. In principle, systematic deviations of an individual patient can be estimated during the first few fractions and couch corrections can be applied for subsequent irradiations [12,14,126]. This so-called "off-line protocol" reduces systematic deviations while random deviations remain unchanged. Both systematic and random set-up deviations can be reduced to negligible values if on-line corrections are applied [31,105]. In this case, the patient position is verified at each fraction using a small number of monitor units. If necessary, the couch position is adjusted before the remaining dose is given. At the moment however, on-line correction procedures are too time consuming to be routinely used in clinical practice.

Internal organ motion is the movement of an organ relative to the bony structures. For instance, the prostate can move due to variations in bladder- and rectum filling. These movements can not be assessed directly by portal imaging since the tumor is generally not visible. By implantation of radio-opaque markers in or near the

CTV the internal organ motion can be visualized which enables on-line positioning corrections [7,28]. In other clinical studies repeated CT-scans have been acquired to get an indication of internal prostate movements [95,119]. Intra-fraction movement of the tumor will add to the random deviation. Due to breathing and cardiac motion a tumor in thorax or abdomen can vary significantly in position in a matter of seconds [97]. Complex techniques like real-time couch movement, respiration gated irradiation or breathing control might limit the consequences of this variation [62,79,124].

Whatever is done to minimize the geometrical uncertainties, to some extent inaccuracies are unavoidable. Once the typical values for a specific group of patients are known they should be included in the treatment planning for individual patients from that group. Patient set-up deviations not only affect the dose in the tumor region, but in neighboring, possibly critical, organs as well. For random deviations, the effect of this deviation can be simulated by a convolution of the dose distributions with the distribution of movements in three dimensions. Several groups have implemented this for translational deviations [52,98]. Systematic deviations are more of a problem since they are a priori not known for a specific patient and only the distribution of systematic deviations for the patient group can be determined. The effect of systematic deviations on the dose distribution is more significant than that of random deviations, hence relatively small systematic deviations should not be ignored. One possible way to deal with systematic deviations has been proposed by Goitein [43]. He suggested three parallel planning calculations, one with nominal set-up deviations and the others with extreme values, and allow only those plans for which all three dose distributions are acceptable in terms of tumor coverage and critical organ sparing. Recently this idea has been further developed by Mageras and colleagues, especially to include internal organ motion in radiotherapy planning [74]. Killoran and colleagues simulate systematic and random uncertainties simultaneously by multiple Monte Carlo simulations which result in multiple dose volume histograms (DVHs) that are used for evaluation of the treatment plan [60].

The above techniques operate directly on the CTV and are more sophisticated than the conventional approach as proposed by the ICRU [54], i.e. using a planning target volume (PTV) which is defined as the CTV plus margins for all geometrical uncertainties. However, the practical application of the concept of PTV is not always clear. First of all, it is rather cumbersome to manually draw margins in three dimensions around an irregularly shaped tumor volume [104]. Therefore several groups have developed algorithms for automatic margin calculation, either multiple 2D [5] or fully 3D [15,106]. Furthermore, the geometrical uncertainties can originate from

rotations as well as translations. Rotational deviations will yield anisotropic margins, i.e. the size of the margin will vary depending on the position with respect to the axis of rotation. None of the aforementioned algorithms have incorporated this. Finally the exact margin size necessary to ascertain adequate coverage of the CTV depends on the kind of deviation (systematic or random) and on the dose distribution. How this must be taken into account has up till now not been specified.

We have developed a model that calculates the CTV-to-PTV margins step by step, based on clinically measured CTV position deviations and on the requirement that the dose distribution delivered to the CTV will satisfy the ICRU recommendations for dose homogeneity with a high probability. Internal organ motion as well as external set-up deviations, translations as well as rotations, and systematic as well as random deviations are included in the model. Once the dose distribution has been planned around the resulting PTV, the same algorithms can be used to calculate the influence of all geometrical uncertainties on the dose in the CTV and hence to verify the planned dose distribution. The use of the model will be demonstrated for a prostate, cervix, and lung cancer planning.

III. Methods and materials

a. Parameters required

Since the geometrical uncertainties of an individual patient which is to be planned are not known, measured data of a group of similar patients must be used. Clinical studies performed in our department and elsewhere have shown that translational deviations in patient positioning of a specific group can be approximated by normal distributions of systematic and random deviations in the three main directions, e.g. [11,25]. For each patient in the study the average set-up deviation and the standard deviation (SD) of the distribution around that average is determined. The random variation σ characterizing a certain patient group is then defined as the SD of the day-to-day set-up positions, averaged over all patients in the group. The systematic variation Σ is defined as the SD of the distribution of average set-up deviations per patient in the group of patients. The overall mean deviation M is the average value over all fractions and all patients. If the reference set-up (during simulation) can be considered as a sample from the random distribution, M will be close to zero and Σ will be close to σ . Rotational deviations around the three main axes can in principle be described

similarly. The study of internal organ motion can yield random and systematic deviations for translations and rotations as well. Hence a set of twelve (x/y/z * rot/trans * int/ext) standard deviations Σ and σ and six rotation axes are necessary to describe all geometrical uncertainties of a specific patient group. These values are the input parameters of our method and do not only depend on the tumor sites, but also on set-up techniques and treatment protocols (and possibly even on more specific variables like tumor stage, patient weight, accelerator etc.).

The parameters are used to calculate margins around a CTV which is initially represented by a set of input contours as outlined in 2D CT-slices. The contour data points are used to determine a 3D volume in a cubic calculation grid in the treatment room (i.e. CT) coordinate system. The algorithm has been described before [106] and can be summarized as follows. For each slice, intersection points of contour lines with 2D grid lines are calculated to fill a 2D matrix with values equal to the fraction of the grid element that is enclosed by the contour. The slices are stacked with increasing slice position so that a 3D matrix $M_{CTV}(x,y,z)$ is created with values 1 inside the volume and 0 outside the volume (and between 0 and 1 at the edge). This matrix is used for subsequent calculations.

b. Coverage probability calculation using convolutions

Two separate, equivalent methods have been developed to calculate a matrix with coverage probabilities (CPs) which is defined as the probability for each point to be covered by the CTV and which will be used for PTV margin determination. They will be designated as the convolution method and the Monte Carlo method. The *convolution method* uses a straightforward convolution of the CTV matrix with normal distributions describing the geometrical uncertainties. The effect of translational and rotational deviations is calculated separately. The normal distribution of mutually independent deviations in translations is given by:

$$N(x, y, z) = \frac{e^{-\frac{1}{2} \cdot \left(\left(\frac{x}{sd_x} \right)^2 + \left(\frac{y}{sd_y} \right)^2 + \left(\frac{z}{sd_z} \right)^2 \right)}}{\sqrt{8 \pi^3} \cdot sd_x \cdot sd_y \cdot sd_z} \tag{4-1}$$

with sd_x , sd_y , and sd_z the standard deviations of the distributions in the three main directions. The input matrix $M_{CTV}(x,y,z)$ is convolved numerically with the probability distribution:

$$M_{CP}(x,y,z) = \sum_{x'} \sum_{y'} \sum_{z'} M_{CTV}(x',y',z') N(x-x',y-y',z-z') \Delta x \Delta y \Delta z \quad 4-2$$

with $\Delta x \Delta y \Delta z$ the voxel size. In the output matrix $M_{CP}(x,y,z)$ the original contents of the voxels is spread out according to the distribution of translations. The value in each voxel of this "coverage probability" matrix represents the probability of the voxel being covered by the CTV.

Inclusion of rotational positioning deviations is cumbersome in the orthogonal coordinate system. To be able to handle rotations around axes in the three main directions, an input matrix $M_{CTV}(x,y,z)$ is transformed to cylindrical coordinates $M_{CTV}(r,\theta,a)$ using bilinear interpolations, where a is x , y or z for rotations about x -, y -, or z -axis respectively. The center of the new matrix ($r = 0$) is taken to be at the (user-defined) position of the rotation axis. A one-dimensional distribution matrix $N(\theta)$ is defined similar to $N(x,y,z)$ and the convolution is performed:

$$M_{CP}(r,\theta,a) = \sum_{\theta'} M_{CTV}(r,\theta',a) N(\theta-\theta') \Delta \theta \quad 4-3$$

with $\Delta \theta$ the bin size. Subsequently the output matrix $M_{CP}(r,\theta,a)$ is transformed back to orthogonal coordinates $M_{CP}(x,y,z)$. The transformation to a different coordinate system and back, on a discrete grid, will already smooth the CTV matrix, even without convolutions. To limit this effect, the pixel size in the cylindrical coordinate system is kept four times smaller than in the original. To minimize the number of cylindrical matrix elements and keep the element size approximately equal for all values of r , the number of angles θ increases with r , i.e. the (r,θ) -calculation grid is not rectangular but rather triangular in shape.

In case more than one rotational deviation is present, the above procedure is performed again using the output matrix of the first calculation as input for the second, etc. The order is arbitrary for distributions that are mutually independent and for the small rotational deviations ($< 10^\circ$) that are usual in patient set-up and organ move-

ment (as will be justified later on, see figure 4-4). In case both rotational and translational deviations must be considered, the rotations should be performed first.

c. Coverage probability calculation using a Monte Carlo approach

The *Monte Carlo method* simulates the fractionated radiotherapy treatment more directly by sampling the translations t_x, t_y, t_z and rotations r_x, r_y, r_z from their respective distributions. Subsequently all points in the CTV matrix (x,y,z) are moved to a new position (x',y',z') according to:

$$\begin{aligned}
 x' &= x + t_x + x_{r,y} (\cos(r_y) - 1) + x_{r,z} (\cos(r_z) - 1) - y_{r,z} \sin(r_z) + z_{r,y} \sin(r_y) \\
 y' &= y + t_y + y_{r,z} (\cos(r_z) - 1) + y_{r,x} (\cos(r_x) - 1) - z_{r,x} \sin(r_x) + x_{r,z} \sin(r_z) \\
 z' &= z + t_z + z_{r,x} (\cos(r_x) - 1) + z_{r,y} (\cos(r_y) - 1) - x_{r,y} \sin(r_y) + y_{r,x} \sin(r_x)
 \end{aligned}
 \tag{4-4}$$

where $x_{r,y} = (x-R_{x,y}), x_{r,z} = (x-R_{x,z}),$ etc. the coordinates of the matrix point with respect to the x-, y-, and z-axes of rotation, respectively $(R_{y,x},R_{z,x}), (R_{x,y},R_{z,y}), (R_{x,z},R_{y,z}).$ The input value at point (x,y,z) can be assigned to the eight grid points nearest to (x',y',z') using trilinear interpolations or assigned completely to the one nearest point which is faster but less accurate. Hence a new matrix $M_n(x,y,z)$ is calculated with n being the sample number. The procedure is repeated many times (> 1000) and the resulting matrices $M_n(x,y,z)$ are averaged over the number of samples to yield the final result $M_{CP}(x,y,z).$

A difference between Monte Carlo and convolution method is the way in which rotational deviations are incorporated. The Monte Carlo method handles all rotations at once. The voxel displacement resulting from each rotation is calculated assuming the same starting position for all rotations, i.e. the input voxel position for the second rotation is not the output from the first. The computation of translations is similar for both methods; all three directions are handled simultaneously. Comparison of the methods will give an indication of their accuracy.

d. Interpretation of coverage probability

As mentioned before, the elements in the CP matrix M_{CP} (of which the values vary from 0 to 1) represent the probability of a fixed point in space to be actually covered

by the CTV. For sufficiently large volumes (larger in diameter than about 2 SD of the distribution of deviations), the CP value of a certain voxel also represents the probability that the volume border lies outside that voxel; i.e. if a point is covered by some part of the CTV, the CTV border must lie outside of that point (or exactly on it). Iso-coverage probability volumes are therefore logical candidates to define the PTV. Considering translational deviations in one dimension and given a selected coverage probability CP_s smaller than 0.5, the probability (P_o) that any point of the CTV volume is outside the PTV will then be equal to $2 CP_s$. For translations in more dimensions and for rotations the relationship between CP_s , or the margin size and P_o becomes less straightforward. A special case may however serve as an estimate for the general case.

That special case is a spherical CTV with an isotropic margin m to represent the PTV. The probability P_o that any point of a CTV with normally distributed translational deviations sd in all three dimensions will be outside the PTV can be calculated analytically:

$$P_o = \frac{2}{\sqrt{2\pi}} \int_{r>m/sd} r^2 e^{-\frac{1}{2}r^2} dr \quad 4-5$$

with r being equal to $\sqrt{(x^2 + y^2 + z^2)}$. The integral can be solved using partial integration. For deviations in two dimensions a similar expression can be derived. In figure

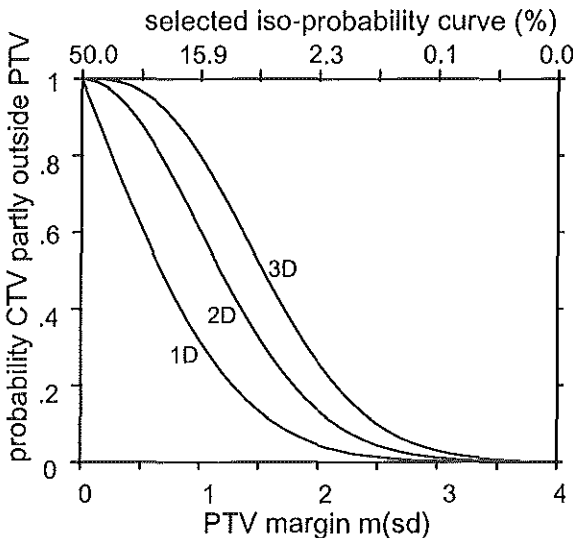


Figure 4-1 Theoretical curves for a spherical CTV with variations in translations with standard deviations sd . Rotational variations are zero. Indicated is the probability that the CTV is partly outside the PTV (P_o) for variations in one, two, and three dimensions with varying CTV-to-PTV margin size in units of sd . The corresponding selected iso-probability values (CP_s) are indicated on the upper horizontal axis.

4-1 P_o is displayed as a function of the margin in units of sd , for the one-, two-, and three-dimensional case. The coverage probability values CP_s that should be selected to obtain a margin $m(sd)$ are displayed along the upper horizontal axis. The relation between CP_s and $m(sd)$ is normally independent of CTV shape as long as the volume is sufficiently large ($> 2 sd$, as indicated before). For 3D translational deviations, the probability of the CTV being partly outside the PTV is considerably higher than for 1D deviations. For instance, a PTV margin of 1 sd (or $CP_s = 16\%$) has a P_o -value of 32% for deviations in one dimension as opposed to 80% when deviations in all three dimensions are considered. However, not only the probability of CTV miss but also the extent of that miss is important. Even for large P_o -values, the fraction of the CTV outside the PTV is small and the dosimetrical consequences are limited.

e. Influence of systematic deviations on the CTV dose: dose probability histograms

To investigate the effect of the geometrical uncertainties on the dose distribution in the CTV, different approaches for systematic and random deviations are required. Systematic geometrical misses will cause underdosage of the same part of the CTV for every fraction of the treatment, whereas random deviations will cause underdosage in different parts of the CTV for each fraction. For *systematic* deviations, the CP matrix can be used to estimate the influence of systematic deviations on the DVH of the CTV. A normal cumulative DVH is constructed by summation of all CTV voxels that receive more than a certain dose, for all dose values D :

$$\begin{aligned}
 V(D) &= \sum_{\vec{r} \in CTV} S_D(D'(\vec{r})) \Delta V = \Delta V \sum_{\vec{r} \in \mathfrak{R}_3} S_D(D'(\vec{r})) M_{CTV}(\vec{r}) \\
 \text{with } S_D(D'(\vec{r})) &= \begin{cases} 1 & \text{for } D'(\vec{r}) \geq D \\ 0 & \text{for } D'(\vec{r}) < D \end{cases}
 \end{aligned}
 \tag{4-6}$$

with $D'(\vec{r})$ the dose value at position \vec{r} , ΔV the voxel volume, and $M_{CTV}(\vec{r})$ the previously defined CTV matrix. $\vec{r} \in CTV$ and $\vec{r} \in \mathfrak{R}_3$ are those positions which are member of the CTV and the whole 3D space, respectively. At the time of planning the systematical deviations in CTV position are unknown for a specific patient but the probability of the CTV being systematically at a different position is determined by the systematic variations Σ of translations and rotations for the patient group. The

average DVH, taking all systematic deviations of the CTV position with respect to the dose distribution into account, can then be determined to be:

$$\begin{aligned}
 \langle V(D) \rangle &= \Delta V \sum_{\vec{i} \in \mathfrak{R}_6} N(\vec{i}) \sum_{\vec{r} \in \mathfrak{R}_3} S_D(D'(\vec{r})) M_{\vec{i}(CTV)}(\vec{r}) \\
 &= \Delta V \sum_{\vec{r} \in \mathfrak{R}_3} S_D(D'(\vec{r})) \sum_{\vec{i} \in \mathfrak{R}_6} N(\vec{i}) M_{\vec{i}(CTV)}(\vec{r}) \\
 &= \Delta V \sum_{\vec{r} \in \mathfrak{R}_3} S_D(D'(\vec{r})) M_{CP}(\vec{r})
 \end{aligned} \tag{4-7}$$

with \vec{i} being a transformation (translations and rotations), $N(\vec{i})$ the probability for a certain transformation \vec{i} (see Eq. 1), and $M_{\vec{i}(CTV)}$ the transformed CTV. In the last step of the derivation Eq. 2 is used. Hence instead of counting voxels receiving a dose $\geq D$, as for a normal DVH, the average of the DVH for all systematic deviations of the CTV is obtained by summation of the coverage probability values for each dose $\geq D$. Therefore the results of those calculations will be denoted as dose probability histograms (DPHs). It should be emphasized that the CP matrix M_{CP} in Eq. 7 is calculated using the *systematic* variations Σ . A dose histogram of a CP matrix for random (day-to-day) variations of one patient has no physical meaning since DVHs of different fractions should not be added; information about the position of the dose, which is essential when adding dose distributions of different days, is lost in a DVH.

In figure 4-2 a clinical example of DPH calculations is shown. For an arbitrary prostate cancer patient planned according to the ICRU dose specification rules (i.e. block margins are such that the 95% isodose volume encloses the PTV), DPHs of CTV have been calculated for six different 3D translational variations Σ . Naturally, the probability of CTV underdosage increases with increasing variations. Since the ICRU suggested a maximal tumor underdosage of 5% [54], an additional dashed line is drawn to indicate the 95% dose. The DPH curves for the CTV now immediately indicate that the 95% isodose will enclose on average a large part of the CTV ($>$ about 99%) as long as the CTV-PTV margin is at least 2Σ . This implies a high probability of the 95% isodose enclosing the whole of the PTV. For smaller margins there will be an increasing probability of underdosage of the CTV. The DPH as an average of the DVHs for all systematic deviations seems therefore a reliable tool to determine the margin size required to cover for these deviations for a specific treatment plan. Also indicated in figure 4-2 are similar curves for variation in rectum position. The same

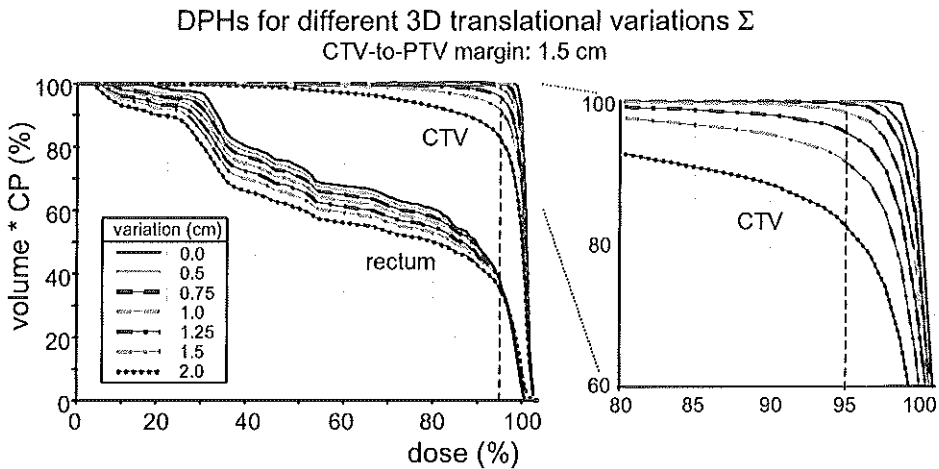


Figure 4-2 Example of dose probability histograms for six different systematic variations in translation (Σ) for a prostate case planned to conform to ICRU recommendations with a 1.5 cm CTV-to-PTV margin. With increasing variation in CTV position there will be a higher probability of underdosage. The rectum will on average also receive less dose as the variations increase, although the maximum dose increases. On the right the CTV curves near the 95% dose are magnified.

variations are assumed without any change in rectum shape. As expected, the maximum dose of the DPH increases as the variations increase; the probability that the rectum will be part of the higher dose regions will be higher. At the same time however, the lower dose volumes decrease with increasing variations. This is due to the fact that for isotropic movements in all directions, the probability of the rectum moving toward the higher dose regions is lower than for moving away from them.

f. Influence of random deviations on the CTV dose

The *random* deviations displace the CTV with respect to the dose distribution differently for each fraction of the treatment. This can be simulated by convolution of the dose distribution matrix with the probability distributions, as has been described before [13,52,98,107]. The same algorithms as for the CP calculations can be applied. If the input file in Eq. 2 (M_{CTV}) is a dose distribution instead of the CTV, the output will be a dose distribution which is spread out locally as a result of random deviations. This distribution is the best estimate of the actually delivered distribution during the radiotherapy treatment. In general the higher iso-dose regions will decrease in size,

while the lower iso-dose regions will increase. The extent of shrinkage of the 95% iso-dose volumes should give an indication for the size of the required margin [13]. If only the random *set-up* deviations are considered, one calculation will be sufficient to determine its effect on CTV and critical organs simultaneously. If the internal random deviations of the critical organs are different for different organs, separate convolutions of the combined distributions of random set-up and organ movement should be performed with the local dose matrix surrounding each organ. Compared to CP calculations, dose modifications are more accurate because gradients in dose matrices are considerably flatter than those in CTV matrices.

g. PTV margin determination

The goal of a PTV is to create a volume around which the 95% dose can be planned so that the CTV is adequately irradiated, which can be verified using DPHs (see next section). In principle one might find the correct PTV by trial and error but CP calculations can also be used to calculate a good PTV to start with. Because of the different effect of the systematic and random deviations on the CTV dose (Σ and σ cannot be added), the PTV is calculated in two steps.

For *systematic* geometrical uncertainties a high irradiation probability is obtained by choosing the margin according to a low iso-probability volume. From figure 4-2 a margin equal to about 2Σ would seem reasonable and from the upper horizontal axis in figure 4-1 can be deduced that this corresponds to iso-probability curves of about 2.5%. Hence the first step in the PTV calculation (PTV1) is the determination of the 2.5% iso-probability volume of the CTV (i.e. the volume bounded by voxels having a CP equal to 2.5%), using the systematic variations Σ as input to the model. From figure 4-1 this implies that for a spherically symmetric situation and deviations in all directions, there still is at least a 28% chance of the a part of the CTV is outside PTV1 for all fractions. In other words, there is maximally a 72% probability of complete enclosure of the CTV by the PTV1 during the radiotherapy treatment. However, the DPH curves of the example in figure 4-2 indicate that the 95% isodose will enclose the CTV in practically all cases. The internal and external deviations can be handled simultaneously by adding the respective standard deviations in quadrature.

To cover for the remaining *random* deviations only a moderate increase in the margin will be necessary. The total random variation equals the quadratic sum of in- and external random variations. The procedure is similar to that for the systematic

deviations, this time using PTV1 instead of the CTV as input volume. The difference is that random deviations do not affect the dose distribution in the tumor as much as systematic deviations. Therefore the margins can be smaller and the selected iso-probability volume can be higher. Bel *et al.* studied the dosimetric consequences of random translational variations σ for their prostate patients and concluded that a 0.7σ margin would be sufficient to keep the minimal CTV dose above 95% [13]. Based on those results we considered the 25% iso-probability volume appropriate for random deviations. This means that PTV1 will be partly outside the PTV in over 90% of the fractions (see figure 4-1). Once this final margin is added to PTV1, the calculation of the PTV is complete. Naturally, the choice of the iso-probability volume for either PTV1 or PTV margins is to some extent arbitrary and can be varied according to the individual preferences of the clinician. Eventually it should be based on quantitative models for the tumor control probability.

h. PTV margin verification

Normally, the patient will be planned with certain block margins around the PTV to account for the penumbra of the beam. The concepts described can be applied to evaluate and judge the effect of geometrical uncertainties on the dose distribution in the CTV. Firstly, to calculate the expected dose distribution actually delivered during the treatment series, the dose matrix is convolved with the distribution of random deviations. The 95% isodose volume will shrink but should still enclose the PTV1 volume. Secondly the systematic deviations are used to determine the DPH of the CTV (and possibly critical organs), using the dose modified for random deviations. This DPH indicates whether the dose distribution is adequate to irradiate the CTV, given the systematic and random deviations. If the patient has been planned correctly, the average CTV volume receiving > 95% dose must be high (e.g. > 99%). In case the probability of underdosage is too high, the 95% isodose volume is too tight around the CTV and either the PTV margin or the block margin is too small. The plan can be recalculated using lower iso-probability contours as PTV margin or larger block margins. In case the DPH is practically equal to the original DVH (i.e. systematic deviations have no influence on the dose in the CTV), the PTV margins might be too large and the plan should be recalculated using higher iso-probability values as PTV margins (or smaller block margins). In this iterative manner the size of the block-to-CTV margins is directly optimized for irradiation of a specific CTV and DPHs of CTV instead of DVHs of PTV are used to evaluate the planning.

i. Hardware

The method has been implemented using the C programming language on a HP 9000/712 (100 MHz) workstation. It runs as a separate application next to the CadPlan planning system² and hence uses CadPlan contour and dose files as input. The results are written back to CadPlan files for visualization and further planning. At the moment, the voxel sizes in the calculations are equal to those used in the planning system, which vary in practice from about 2 mm for CT pixel size to maximally 10 mm for the slice distances. The dose matrices normally have a resolution of 2.5 or 5 mm. Geometrical uncertainties smaller than about 1 mm (1 SD) are consequently not reflected in the calculations.

IV. Results*a. Accuracy of the methods*

To get an indication of the accuracy of the convolution and Monte Carlo method, results of the two methods are compared for a schematic example. Figure 4-3a depicts a 2D geometrical object which represents a target volume. The simulated random translational variations are different in horizontal and vertical direction and the coverage probabilities are calculated for both methods. The number of runs in the Monte Carlo method was 1500. The iso-probability contours of the different methods coincide well, only the 1% iso-probability curves deviate slightly. In figure 4-3b an additional variation in rotation is simulated. As expected, the area within the higher probability curves decreases while that in the lower increases. Due to the rotations the distance from one curve to the next becomes anisotropic. Near the upper right part of the object the lower iso-probability curves actually shrink compared to the curves in figure 4-3a; because of the rotations there is a lower probability that voxels in that area are enclosed by the object. The differences between the two methods become slightly larger, especially near the low probability curves. This is attributed to the limited number of runs of the Monte Carlo method which yields poor statistics in those regions.

² Varian-Dosetek

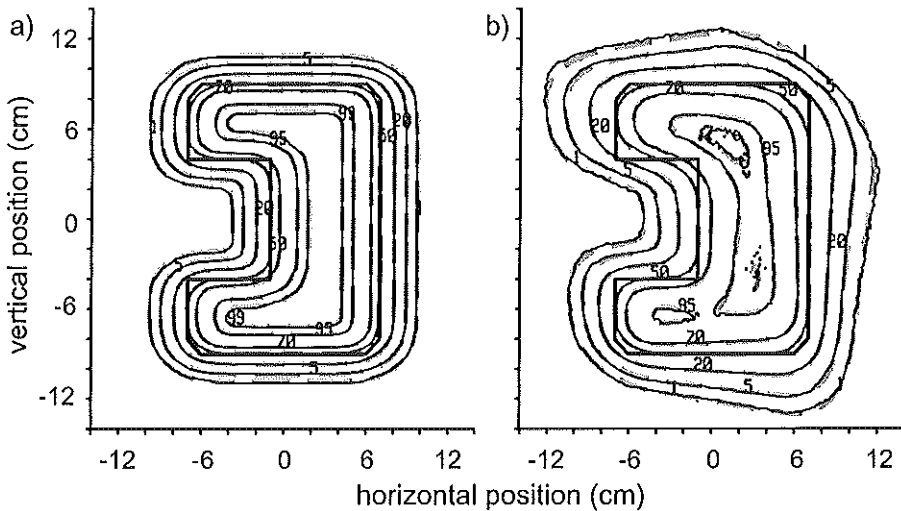


Figure 4-3 Comparison of convolution and Monte Carlo method. The schematic 2D CTV is the object outlined by the thick solid contour, the pixel size is 2 by 2 mm. A) A horizontal 12 mm (1 SD) and vertical 8 mm variation in translation has been simulated. The 1, 5, 20, 50, 70, 95, and 99% iso-probability curves of both methods are shown; the thin black lines represent the result of the Monte Carlo method (1500 runs), the thick grey dashes the convolution method. B) A 5 degrees (1 SD) variation in rotation is added. The rotation axis is at the lower left corner of the figure (-12, -12 cm). The iso-probability curves of the two methods still coincide well.

The largest differences between the two CP calculation methods are expected for coverage probability calculations with large rotational deviations. Hence an exaggerated (and unrealistic) variation in rotations around the three orthogonal axes through a point in the lower left and cranial corner of the input matrix is calculated for a lung tumor CTV in the upper thorax. Figure 4-4 shows the 5% iso-probability curves for both methods in a transversal, sagittal, and frontal slice near the center of the CTV. The two contours do not overlap in all areas but the differences are small: maximally 2 mm (1 CT pixel) while the margin is on average 2 cm. In slices near the edges of the volume the maximum differences that are found are 4 mm which is adequate considering the irregularity of the Monte Carlo contours. The difference between the two 5% iso-probability volumes is 4 cc (1%). In clinical practice rotational deviations of extreme values are rare and the occurrence of more than one deviation simultaneously is unlikely. Consequently, this close agreement may serve as assurance that the calculation of rotational deviations is reliable for both methods.

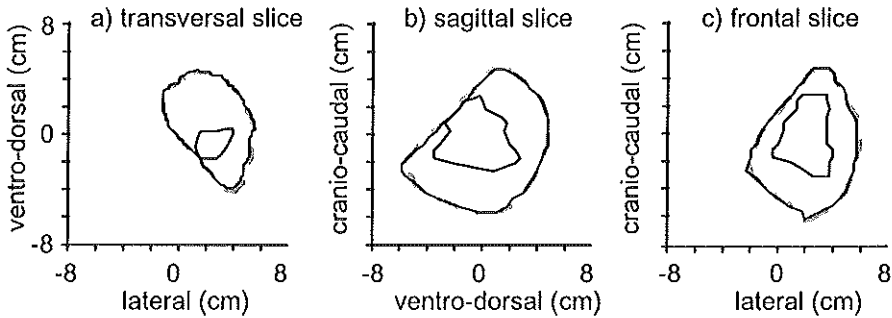


Figure 4-4 Comparison of the two methods for an extreme case of rotational deviations. A lung CTV (thick black lines) has been modified with rotational deviations of 10, 8, and 6 degrees (1 SD) around the three major axes in a point about 8 cm left, cranial, and below the CTV center. The 5% iso-probability curves for the convolution (thick grey dashes) and Monte Carlo method (thin black lines) are displayed in a transversal (a), sagittal (b), and frontal cut (c) through the CTV. Although the two methods handle the effect of rotational deviations differently, the results are quite similar.

Although Eq. 5 was derived for a spherically symmetric case, the results are a reasonable approximation for more general clinical situations. For translational deviations, computer simulations for a prostate CTV indicate that, even if the margins become anisotropic, the deviations from the values in figure 4-1 are small ($< 5\%$). A restriction is that the CTV volume should be devoid of sharp edges, which is usually satisfied. Another limitation is that rotational deviations are not included in the calculations, hence Eq. 5 underestimates the P_o -value if rotations are present.

b. Clinical examples

In three clinical examples the stepwise PTV calculation and the verification procedure will be illustrated. The values for the geometrical uncertainties are taken from literature or have been measured in our institute. In all cases it is assumed that the application of an off-line protocol (as mentioned in the introduction) halves the systematic translational set-up deviations [12]. The values used are summarized in Table 4-1. All calculations are done with the convolution method and all rotation axes are through the center of the CTV unless specifically stated otherwise. CT slice distances are 5 mm and CT pixel size are about 2×2 mm. The grid size of the dose matrices is in all cases 2.5 mm in the plane of the CT slices and equal to the CT slice

distance in the direction perpendicular to the CT planes. All three patients were planned with multi-leaf collimators. Block margins were such that the 95% isodose closely fitted the PTV and the dose homogeneity in the PTV satisfied the ICRU 50 recommendations (i.e. dose variation of maximally 95% - 107%).

c. Prostate cancer case

Due to variations in rectum and bladder filling, the range of the internal prostate movements is considerable. The values that are used in our calculations have been estimated from several studies available in the literature [7,28,119]. The lateral rotation axis was taken to be near the apex of

the prostate as suggested by van Herk *et al.* [119]. The values for external set-up deviations are taken from routine portal imaging data of 228 patients treated at our clinic. The final PTV is constructed in several steps as shown in transversal and sagittal slices through the tumor (figure 4-5). The CTV has been outlined manually by a radiation oncologist. This volume is expanded with a margin to cover all systematic deviations; a CP matrix is calculated using the quadratically summed internal and external systematic variations (Table 4-1). PTV1 is taken to be the volume enclosed by the 2.5% iso-probability contours. To get the final PTV a subsequent margin is added to PTV1 from the calculated 25% iso-probability volume with the quadratically

variation direction	translation (mm, 1 SD)			rotation (degrees, 1 SD)/axis		
	LR	CC	AP	LR	CC	AP
Prostate						
σ_{ext}	2.0	2.0	2.0	1	1	1
Σ_{ext}	1.2	1.2	1.4	1	1	1
σ_{int}	1	2	2	4*	2	1
Σ_{int}	1	2	2	4*	2	1
Cervix						
σ_{ext}	3.5	4.0	3.5	3	1.5	2
Σ_{ext}	2.0	2.5	2.0	2	1	1
σ_{int}	1	1	1	1	1	1
Σ_{int}	1	1	1	1	1	1
Lung						
σ_{ext}	3.0	3.0	3.0	2	2	2
Σ_{ext}	2.0	2.0	2.0	1	1	1
σ_{int}	4	5	5	2	2	2
Σ_{int}	2	3	3	1	1	1

*Table 4-1: Overview of geometrical uncertainties used as input for the model for three different tumor sites. Systematical (Σ) and random (σ) variations are indicated for translations as well as rotations and internal organ movement (int) as well as external set-up deviations (ext). All rotation axes are assumed to be at the center of the CTV except for those indicated by * which are assumed to be at the caudal apex of the CTV.*

summed random variations as input for the CP calculations. The random deviations add only an extra 1 - 2 mm (which is close to the pixel size). In total, the margin around the CTV varies from minimally 6 mm in the caudal to maximally 13 mm in the cranial region of the PTV. The anisotropy is due to the significant rotation around the apex of the prostate.

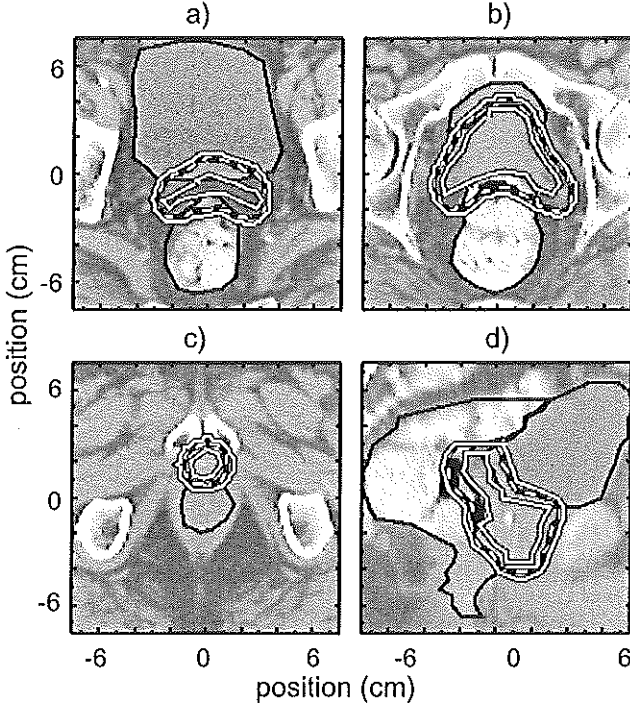


Figure 4-5 Prostate planning example of the stepwise PTV calculation in a cranial transversal slice (a), an isocentric slice (b), a caudal slice (c), and a sagittal reconstruction (d). The geometrical uncertainties are from Table 4-1. The CTV (grey curve) is extended with a margin to cover for the systematic deviations by selection of the 2.5% isoprobability volume of the CP matrix (PTV1, dashed curve). The final PTV (white curve) results from the 25% isoprobability volume of the CP matrix of random deviations applied to the PTV1. Especially in the sagittal slice the influence of the rotations around the apex is clear; the PTV margin in the caudal part is significantly smaller than that in the cranial part of the prostate. The critical organs (bladder and rectum) are depicted by the thin black curves.

apex of the prostate.

The interpretation of the contours in the two-dimensional slices is sometimes misleading due to the 3D aspect of the margins; they may appear too large in one slice due to the influence of a differently shaped tumor contour in the next slice as, is especially apparent in the (cranial) transversal slice. This effect is also visible in the cervix and lung cancer case that follow.

A three field technique was applied to plan the patient. To verify the dose distribution in CTV, rectum, and bladder, DVHs have been calculated for each volume and are shown in figure 4-6. Subsequently, the dose distributions around the volumes of interest have been convolved with the

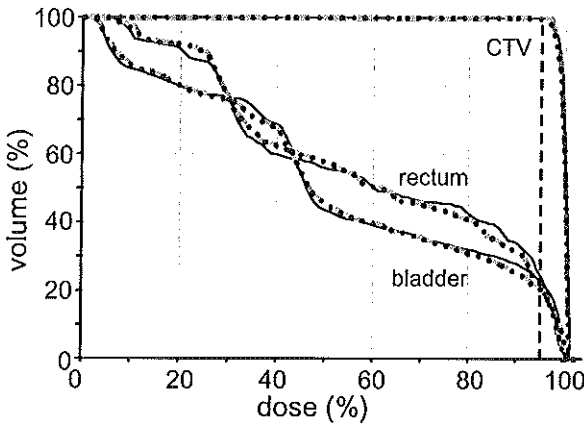


Figure 4-6 DVHs and DPHs for the prostate cancer patient in figure 4-5. The original DVHs of CTV, bladder and rectum are indicated by the thin black lines. DVHs for the dose distributions adjusted for random deviations are represented by the dashed grey curves. The effect of random deviations on the CTV dose is negligible, whereas the bladder and rectum high dose volumes decrease. The DPHs (dotted curves) for the systematic deviations have been determined using the dose distributions modified for random uncertainties. There is only a noticeable effect on the CTV but the curve does not intersect the 95% dose line (dashed) so the probability of underdosage of the CTV is negligible.

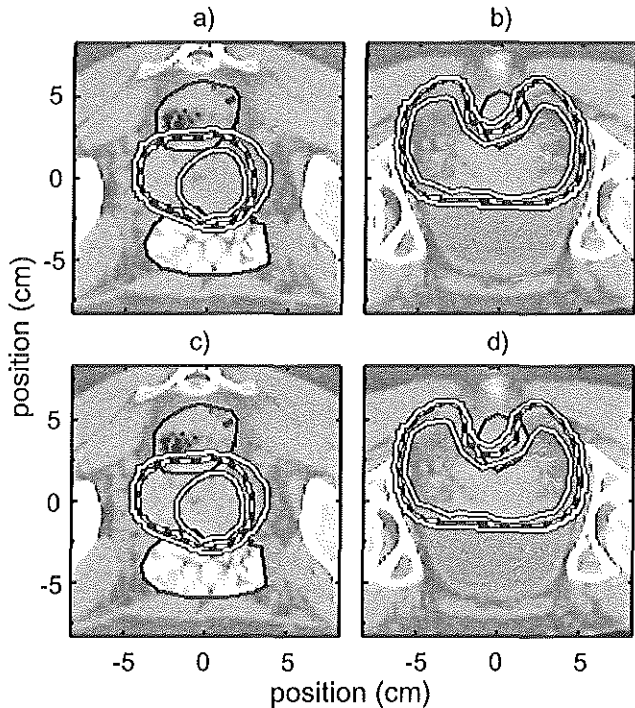
distributions of random deviations. For the CTV the values are directly obtained from Table 4-1, for bladder and rectum the internal random motion was estimated to be equal to that of the prostate without the rotation. Bladder and rectum volumes were assumed to be constant. Resulting DVHs show that the effect of random deviations on the CTV dose is negligible, whereas the bladder and rectum high dose volumes are somewhat reduced. Finally, the DPHs for the systematic deviations have been determined using the dose distributions modified for random uncertainties. Standard deviations are taken from

Table 4-1 similar to the random deviations. The DPH of the CTV is different from the original DVH but the DPH-curve does not quite intersect the 95% dose line, i.e. the probability of underdosage of the CTV is negligible. The DPHs for the critical organs do not deviate from the DVHs.

d. Cervix cancer case

Compared to prostate cancer patients, external set-up deviations play a major role in the planning of (post-operative) gynecological cancer patients. Positioning accuracies of cervix cancer patients are also determined by studies in our own institute, one of which is described by Creutzberg *et al.* [25]. Also in contrast with the prostate case, the internal organ movement is expected to be relatively small considering the

Figure 4-7 Example of the PTV calculation for a cervix cancer plan. The geometrical uncertainties are from Table 4-1. The same procedure and line styles as for the prostate case (figure 4-5) are used except for the small bowel that is depicted instead of the bladder. Three transversal (a,b,c) and a sagittal slice (d) through the PTV are shown. The overall CTV-to-PTV margin becomes about 1 cm.



involved anatomy. In figure 4-7 four slices through the initially drawn CTV are depicted. The PTV1 margins due to systematic deviations are calculated similar to the prostate case and vary from 6 to 9 mm. They are mainly caused by the external deviations. The addition of a margin for random deviations completes the PTV calculation. The final CTV-to-PTV margin is then about 1 cm. An additional feature of margin calculation using coverage probabilities is the smoothness of the PTV surface. This especially manifests itself in the sagittal view in figure 4-7d; the inconsistencies in the CTV delineation disappear in the PTV.

The patient was planned in prone position with a three field technique. The relatively large random positioning deviations are solely responsible for the random deviations. DVHs and DPHs for CTV, small bowel, and rectum have been calculated similar to the prostate case. The results are shown in figure 4-8. The effect of the random uncertainties on the rectum and small bowel is again a noticeable reduction of the high dose volume. The original DVH of the CTV indicates a less homogeneous dose distribution than for the prostate case. It is however hardly influenced by the systematic or random deviations and the final DPH proves that adequate margins have been applied.

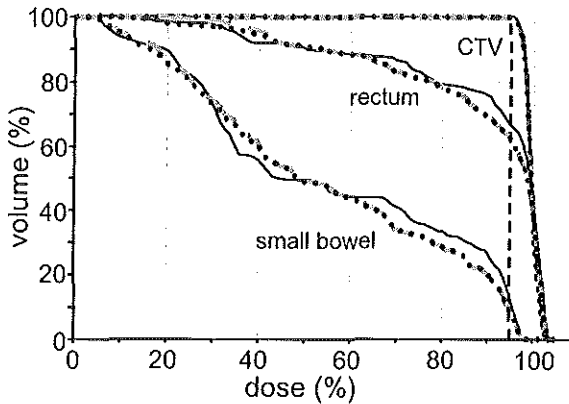


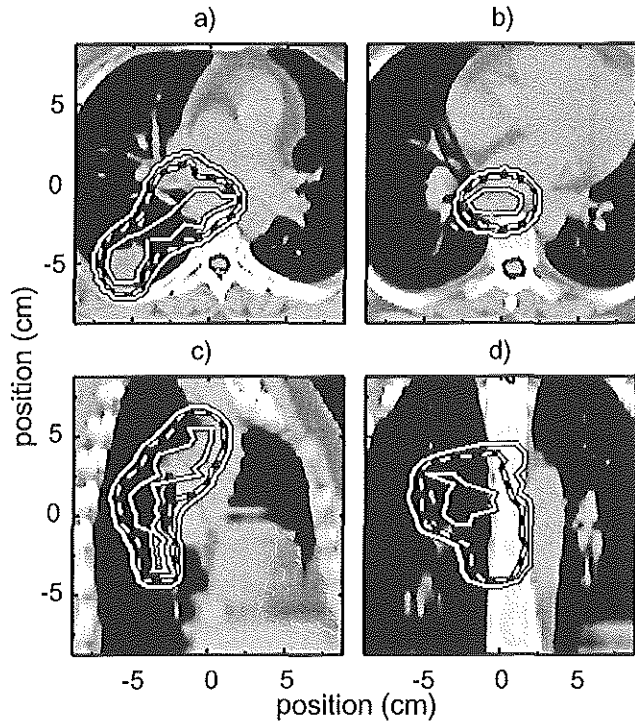
Figure 4-8 Dose distribution verification for the gynecological cancer patient in figure 4-7. DVHs and DPHs for CTV, small bowel, and rectum have been calculated similar to the prostate case of figure 4-6. The effect of the random uncertainties on the rectum and small bowel (dashed grey curve) is again a significant reduction of the high dose volume compared to the original DVH (thin black curve). The DPH curves (dotted) indicate that the CTV is hardly influenced by the systematic or random deviations.

e. Lung cancer case

A last example is a 3-field lung booster plan designed to spare the right lung (figure 4-9). Due to breathing and cardiac motion there is considerable internal tumor movement the magnitude of which has been estimated from previously published values [97]. Values for external set-up deviations are based on the preliminary results of a lung cancer patient positioning study recently conducted in our own institute. The manually outlined CTV is expanded with a 6 - 9 mm margin to cover internal and external systematic deviations. The random deviations require an additional 3 - 5 mm margin for the final PTV and the total margin becomes 10 - 13 mm.

Variations in position of the lungs and the spinal cord are assumed to consist only of set-up deviations. In the DVHs of CTV and left lung the random-deviation-adjusted dose distributions display similar differences with the original as the cervix cancer case (figure 4-10). However, the spinal cord is an exception. Since the beams in the three field plan are positioned (too) close to the spinal cord, there is a strong dose gradient just next to it causing an increase of spinal cord dose in the random-deviation-adjusted plan. To a lesser degree the same holds for the right lung. The DPHs for the critical organs are again practically equal to the DVHs, except for the spinal cord; due to the position of the beams the systematic movements of the spinal cord cause a (slight) increase in average spinal cord volume receiving high dose. The DPH of the CTV is different from the DVHs but the high probability of sufficient dose homogeneity indicates that the PTV and block margins were adequate.

Figure 4-9 Example of the PTV calculation for a lung cancer plan. The geometrical uncertainties are from Table 3-1. The same procedure and line styles as for the prostate case are used (figure 4-5). Two transversal (a,b), a sagittal (c), and a frontal cut (d) through the PTV are shown. The overall CTV-to-PTV margin becomes about 10-13 mm. The critical organs are the two lungs and the spinal cord.



f. Computer performance

The calculation speed depends on the selected method and input. The margin and DPH calculations normally take about 1-2 minutes with the convolution method. Generally the Monte Carlo method is about three to six times slower since a large number (> 1000) of samples have to be taken to obtain sufficient accuracy in the low probability regions. Therefore the Monte-Carlo method is only used for verification in case of questionable results. For both methods the computation time increases linearly with the size of the input and convolution matrices. Since the dose matrices are currently fixed to the standard CadPlan format ($160 \times 112 \times$ number of slices), dose modifications are slower. (In principle only that part of the dose matrix that surrounds the volume of interest needs to be included in the calculations). Besides, almost all elements of the dose matrix are non-zero whereas volume matrices contain a substantial part of zero elements that are ignored in the calculations. The normal time required for dose modifications with the convolution method varies from two (without rotations) to about ten minutes which is a fraction of the time needed for volumetric

dose calculations. Hence the method is sufficiently fast to be used in the iterative planning process.

V. Discussion

a. Margin calculations

The methods proposed in this paper will be particularly useful for designing PTV margins in case of new conformal therapy studies. Based on knowledge (or intelligent guesses) of a set of standard deviations describing all possible geometrical uncertainties of the CTV position, the CP values will give an indication where the

CTV of an individual patient will be positioned over the course of treatment. However, repeated calculations within a specific patient group will normally yield equal margins for all patients independent of the shape of the CTV. For normally distributed deviations and in absence of significant rotational deviations, our choice of isoproability volumes, which is based on the assumption that on average a high percentage of the CTV volume (> 99%) should receive a high dose (> 95%), yields margins of about $2\Sigma + 0.7\sigma$. Consequently, the margins might also be applied directly to the CTV by straightforward CTV expansion algorithms [5,15,106], without having to perform the CP calculations each time.

One difference between rigid margin addition and the CP method might reveal itself at sharp edges. If no smoothing is performed, the former method will normally closely follow all irregularities in the CTV surface so all random deviations in the delineation of the CTV will be present in the PTV as well. The latter method will in itself tend to smooth the surface and can yield a slightly smaller PTV due to rounding of the corners as has been shown in figure 4-3 and figure 4-7d. Another difference

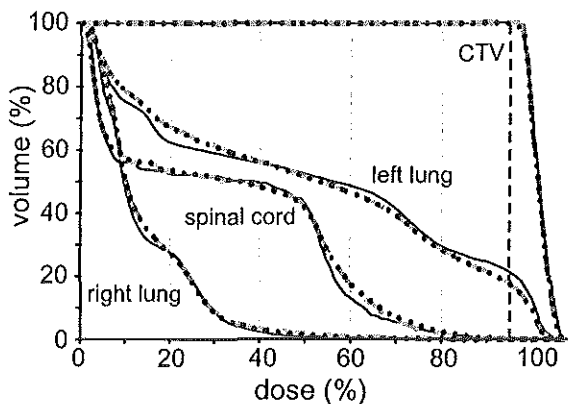


Figure 4-10 DPHs and DVHs of a plan which spares the right lung for the lung cancer patient from figure 4-9. The effect of the random uncertainties (dashed grey curve) on the CTV and left lung is similar to the prostate and cervix case. However, for spinal cord and right lung the effect of random deviations is a slight increase in the high dose volume. The DPH curves (dotted) indicate that the dose distribution in the CTV is influenced by the systematic deviations but the 95% isodose is still adequately placed around the PTV.

will occur at small volumes or near small extensions of a volume. For volumes with diameters less than about 2 SD of the distribution of deviations, a CP value will no longer represent the probability that the volume will be partly outside of it. The actual probability will be larger. Therefore, choosing an iso-probability volume as new PTV will yield too small margins. Rigid margin addition is insensitive to the size of the input volume.

In clinical practice one might prefer a tighter CTV-to-PTV margin near a dose-limiting structure. In the model described in this paper, nearby critical organs are currently ignored in the PTV calculation. However, a critical organ might also be represented by a 3D volume matrix which can then be used to modify the CTV-to-PTV margins locally, as has been described in a previous paper about straightforward margin calculation [106]. The dose probability histograms can of course still be used and the influence of the local margin changes on the average dose volume histogram can immediately be visualized.

The described method assumes that all probability distributions of translations and rotations are mutually independent and of a gaussian nature. The mutual independence is however not always an accurate description of reality; for example, for internal prostate movement a relation between rotations and translations has been found [119]. This might more easily be incorporated in the Monte Carlo method than in the convolution method. Instead of sampling from normal distributions, translations and rotations should be simultaneously obtained from a data base of prostate movements for a large group of patients [74]. This "brute force" method will require a large data base and many samples and will therefore be time consuming. The gaussian nature of the distributions has been verified repeatedly by studies on set-up position verification. At present too few studies have been performed to establish whether this is the case for internal organ movement as well or if differently shaped probability distributions might be more appropriate. The algorithm does however not depend on the type of probability distribution. Instead of using normal distributions for the convolutions, other distributions can be implemented as well. The output of the calculations will still be a 3D matrix with coverage probabilities which will still represent the probability that the CTV lies partly outside the corresponding voxel. Hence the same methods can be applied to obtain the PTV margins.

b. Dose modifications

Dose modifications that account for random deviations cause a shift of high dose to the lower dose regions. Consequently, the critical organs that receive a high dose in the original plan, like the rectum and bladder in the clinical examples, will receive less dose in the modified plan. Furthermore, from figure 4-2 is clear that the average DVH curve for systematic deviations (i.e. the DPH) can also be lower than the original, although the effect is limited for the clinical examples. This implies that the standard DVHs of the planning CT slightly overestimate the dose in those organs. For the critical organs that receive relatively low doses in the planning CT situation, the reverse is true. In the example for the lung cancer patient the organs that have specially been spared (i.e. the spinal cord and the right lung) will on average receive a somewhat higher dose due to the geometrical uncertainties.

A consequence of the application running outside the planning system is that dose inhomogeneity corrections are not included when calculating the dose distribution corrected for random deviations. The effect might be less significant for calculations in the pelvic area but the accuracy of planning in the thorax or neck region will probably be affected. A further simplification of the model is that the position of the beam with respect to the direction of the deviations is of no consequence. In reality the change in dose of a volume moving in the direction of the beam is determined by the inverse square law and the slope of the depth-dose curve, which is not incorporated in the algorithm. The errors will be relatively small [13], but, ideally, dose modifications should be performed for each beam separately which would be a time consuming procedure. In a multiple beam plan the errors are less prominent. Nonetheless, the effect of the set-up deviations might be slightly over estimated.

The application can also be utilized for a check of the delivered dose after the irradiation series have been completed. Once all fractions have been delivered and portal imaging has been applied, systematic and random set-up deviations can be calculated and used as input to the application to evaluate the actually delivered dose distribution. Thus it can be assessed whether the treatment has been performed correctly and if complications or a different local control probability might be expected. The same procedure can also be applied before the end of the treatment series to verify the situation at that moment and possibly alter the course of the treatment, e.g. change the PTV margin [126]. Even the actual set-up deviations for every fraction might be entered separately and the consequences of the treatment on the dose can be computed more precisely.

c. Dose probability histograms

The concept of DPH is especially useful to determine whether the calculated dose distribution guarantees adequate CTV irradiation despite systematical uncertainties. Since the dose has been planned conform the CTV, every variation in CTV position will deteriorate the dose distribution in the CTV. Hence the spread in DVH curves due to systematic deviations will be reflected in the average curve. The mean DVH will therefore directly indicate the probability of CTV underdosage and hence the goodness of the plan in this respect. For critical organs however, positioning deviation in one direction might improve the DVH, movement in the opposite direction worsen the DVH, and the average will be equal to the original. Hence instead of the average DVH for all systematical deviations, the spread of the DVH curves would be more interesting [60,74]. This cannot directly be calculated using DPHs but it is possible to extend the critical organ with a margin for systematical deviations so that an indication of possible dose values in the organ is obtained. This might for instance deteriorate the lung plan because extension of the spinal cord volume might yield a significant probability of higher spinal cord dose than indicated in figure 4-10.

At first sight, there appears to be a discrepancy between figure 4-1 and the DPH calculations in this paper. Figure 4-1 predicts that our choice of the 2.5% isoprobability contour as PTV will for deviations in 3D result in the CTV being partly outside the PTV in at least 28% of all patients. The average DVHs (or DPHs) in the clinical examples indicate however that the probability of underdosage of the CTV (dose < 95%) is at most about a few percent. This is because the extent of CTV volume outside the PTV is small. Using a formula similar to Eq. 5, it can be calculated that the average distance that the CTV border will exceed the PTV border will be about 0.5Σ for those 28% of patients. Since clinical Σ -values range from about 2 to 4 mm, a 1 to 2 mm thick slice of the CTV will be systematically outside the PTV for those patients. This is about equal to the size of one CT pixel and since the 95% isodose volume does normally not enclose the PTV exactly, the probability of underdosage is significantly smaller than the probability of the CTV being outside the PTV.

Since the tightness of the 95% isodose around the PTV will be dependent on the treatment technique used (and on the beam characteristics), the required PTV margins to guarantee a high probability of sufficient dose in the CTV despite systematical deviations will be technique dependent as well. For instance, for conformal techniques

slightly larger PTVs are required than for conventional techniques using rectangular fields to obtain the same DPHs. The same holds for the margin for random deviations. If that margin is based on the shrinkage of the 95% isodose, this will also be technique dependent. For patients groups with standard treatment techniques, the PTV and block margins can be optimized using the DPHs of the dose distribution modified for random deviations. Once the margins are standardized, the iteration process to obtain optimal PTV margins will be superfluous for each patient separately.

VI. Conclusion

A model has been developed which allows for the inclusion of geometrical uncertainties in the radiotherapy planning process. Required parameters are a set of twelve standard deviations describing the various uncertainties. The model calculates PTV margins based on the requirement that on average a large part of the CTV ($> 99\%$) is irradiated with a high dose ($> 95\%$). The size of adequate margins appears to be approximately equal to $2\Sigma+0.7\sigma$. Since rotational deviations are included, the margins can well be anisotropic. Once the patient is planned, the influence of the systematical deviations on the dose distribution in the CTV is determined by the average DVH for all systematic deviations, using so-called dose probability histograms. The influence of random deviations is determined by convolution of the dose distribution with the probability functions. In an iterative process of planning and verification of the CTV coverage, the CTV-to-PTV and block margins can be optimized for each patient separately. For standard planning techniques of specific patient groups, the margins can be standardized and the iterations omitted.

VII. Acknowledgements

The authors wish to thank the Dutch Cancer Society for their financial support (project MVA2 92-86). Furthermore, the discussions with Erik van Dieren, Ben Heijmen, and Arjan Bel have been a great help during the development of the model and the writing of the paper. Finally, the aid of John van Sörnsen de Koste, Gert Korevaar and Sandra Quint with the computer planning was much appreciated.

CHAPTER 5. INTERNAL ORGAN MOTION IN PROSTATE CANCER PATIENTS TREATED IN PRONE AND SUPINE TREATMENT POSITION

J.C. Stroom, P.C.M. Koper, G.A. Korevaar, M. van Os, M. Janssen, H.C.J. de Boer,
P.C. Levendag, B.J.M. Heijmen

Radiother. Oncol. **51**, 237-248, 1999

I. Abstract

Background and Purpose: To compare supine and prone treatment positions for prostate cancer patients with respect to internal prostate motion and the required treatment planning margins. *Materials and Methods:* Fifteen patients were treated in supine and fifteen in prone position. For each patient, a planning CT scan was used for treatment planning. Three repeat CT scans were made in weeks 2, 4, and 6 of the radiotherapy treatment. Only for the planning CT scan, laxation was used to minimize the rectal content. For all patients, the clinical target volume (CTV) consisted of prostate and seminal vesicles. Variations in the position of the CTV relative to the bony anatomy in the four CT-scans of each patient were assessed using 3D chamfer matching. The overall variations were separated into variations in the mean CTV position per patient (i.e. the *systematic* component) and the average “day-to-day” variation (i.e. the *random* component). Required planning margins to account for the systematic and random variations in internal organ position and patient set-up were estimated retrospectively using coverage probability matrices. *Results:* The observed *overall* variation in the internal CTV position was larger for the patients treated in supine position. For the supine and prone treatment positions, the *random* components of the variation along the anterior-posterior axis (i.e. towards the rectum) were 2.4 and 1.5 mm (1 standard deviation, (1 SD)), respectively; the *random* rotations around the left-right axis were 3.0 and 2.9 degrees (1 SD). The *systematic* components of these motions (1 SD) were larger: 2.6 and 3.3 mm, and 3.7 and 5.6 degrees, respectively. The set-up variations were similar for both treatment positions. Despite the smaller overall variations in CTV position for the patients in prone position, the required planning margin is equal for both groups (about 1 cm except for 0.5 cm in lateral

direction) due to the larger impact of the *systematic* variations. However, significant time trends cause a systematic ventral-superior shift of the CTV in supine position only. *Conclusions:* For internal prostate movement, it is important to distinguish systematic from random variations. Compared to patients in supine position, patients in prone position had smaller random but somewhat larger systematic variations in the most important coordinates of the internal CTV position. The estimated planning margins to account for the geometrical uncertainties were therefore similar for the two treatment positions.

II. Introduction

In order to optimally gain from conformal radiotherapy, the planning target volume (PTV [54]) should be as small as possible. Since the PTV consists of the clinical target volume (CTV [54]) plus a margin for geometrical uncertainties in the treatment, these uncertainties, mainly caused by variations in the CTV-position relative to the treatment portals, should be minimized. For prostate cancer patients, deviations of the actual CTV-position from the planned reference position can be separated into errors in the set-up of the patient relative to the isocenter (using markers on the patient's skin), and errors due to variations in the position of the CTV relative to the bony anatomy (i.e. internal organ motion). Reports in the literature indicate that internal organ motion [3,7,9,75,99,119,122] can be of the same magnitude as the set-up variations [14,45,49,101,112]. The difficulty in defining the CTV borders might be considered as another serious cause of geometrical uncertainty in the treatment of prostate cancer patients [24,37,94], but this paper is concerned with the actual CTV movements only.

Patient set-up variations are normally measured by matching the bony structures in portal images with corresponding structures in a digitally reconstructed radiograph or a simulator image. Since the CTV is not visible in portal images, more complicated procedures have to be followed to assess the internal organ motion. A possibility is to implant radio-opaque markers in the CTV so that portal images can still be used [3,7,122]. A disadvantage of this method is that it involves an invasive procedure. Furthermore, the CTV-position is measured indirectly (markers may move within the prostate) and incompletely (only a few markers in the whole prostate and no markers in the seminal vesicles). Recently, Kroonwijk *et al.* [61] have demonstrated that internal prostate motion due to large gas pockets in the rectum of patients can be detected with an electronic portal imaging device (EPID), but this method still needs

quantitative validation. Internal organ motion can also be assessed with repeat CT scans [9,75,99,119]; CTVs are outlined in all scans and manual or automatic matching procedures are applied to determine the prostate positions relative to the bony structures. A drawback of this method is its cumbersomeness in clinical practice; in all reported studies only a few CT scans per patient were made and they were not acquired just prior to a treatment fraction. Therefore, the data could not be used for daily adjustments of the treatment according to the actual position of the CTV.

Recently, Zelefsky *et al.* reported that treatment in prone position reduces dose delivery to the rectum, compared to the supine treatment position [129]. However, their analyses were based on equal PTV margins for both set-up techniques, assuming equal patient set-up uncertainties and internal prostate motion. Most of the studies on internal prostate motion deal with patients treated in supine position [3,7,9,99,119,122]. Only Melian *et al.* [75] have described prostate movement in prone position. Quantitative comparison of the performed studies is often very difficult due to differences in applied protocols to control the rectum and/or bladder filling and due to differences in the applied measurement- and analysis techniques. Moreover, observed internal organ motion is sometimes reported in terms of rotations and translations and sometimes in terms of translations only.

In this paper we report on a systematic investigation based on repeat CT-scans, comparing the prone and the supine treatment position with respect to internal organ motion. Apart from the treatment position, all parameters for acquisition of the CT-scans and for the analyses were kept constant. The variations in internal organ position can be systematic, i.e. the same for each measurement, as well as random, i.e. varying per measurement. Systematic deviations in the internal CTV position, which are due to a non-representative planning CT scan, have a larger impact on the required PTV-margin than random deviations. This is because a serious systematic deviation will cause a shift of the dose distribution with respect to the planned distribution, i.e. the tumor will be underdosed for all fractions of the treatment; random variations will only cause a smearing of the planned dose distribution [102]. Therefore, we have separated the systematic from the random component in the observed internal prostate movements in the CT-scans. Time trends in internal prostate position, e.g. due to radiation induced proctitis and/or cystitis, were also investigated.

III. Materials and methods

a. CT-scans and patient treatment

Thirty T3 prostate cancer patients participated in this study. Fifteen patients were treated in supine position and fifteen in prone position. In supine position, which has been our standard treatment position until this study, only a knee-roll and home-made foot and arm supports were used to position the patient on the treatment table. In prone position a home-made bellyboard in combination with a prone pillow was used. The bellyboard was expected to improve immobilization (especially by minimizing rotational variations), but a positive side effect might be a displacement of the (small) bowel in superior direction and hence a reduction in bowel exposure (not studied in this paper).

For all patients, a planning CT scan was used to design the 3D treatment plan. Following suggestions in the literature [87,109], the patients were asked to take mild laxative suppositories four hours prior to acquisition of the planning CT scan in order to minimize the rectal content. To study the internal CTV motion, three repeat CT scans in treatment position were made in weeks 2, 4, and 6 of the treatment. For all CT-scans the CT pixel size was 2 mm and the slice distance was 5 mm (for most scans) or 3 mm. To avoid large variations in bladder volume, the patients were asked to empty the bladder and to subsequently drink half a liter of water one hour prior to all CT scans and treatment sessions. In all CT-scans, the outlines of the CTV (prostate + seminal vesicles), rectum, and bladder were manually contoured by the radiation oncologist (PK). The length of the delineated rectum was equal to the superior-inferior field length (i.e. the length of the CTV plus margins).

The variability in the outlining of the CTV has been minimized by visual comparison and, if necessary, correction of the outlines in the four CT scans per patient, before the start of the registration procedure. In this way, all CTVs of one patient had similar shapes; possible errors that were made in the delineation were made in all scans of one patient and hence had limited effect on the calculated movements. This is not a realistic situation in clinical practice, but, as mentioned before, the subject of this paper is to calculate the prostate movements; the variability in the CTV delineation is a different subject [24,37,94].

To design the treatment plan, a recently developed algorithm [104,106] was used for a full 3D expansion of the outlined CTV in the planning CT-scan with 1 cm, yielding the planning target volume (PTV). All patients were treated with an isocen-

tric technique using an anterior field and two laterally oblique fields; beam intensity modulation was used to minimize the superior-inferior field length [32]. The patients were treated to a total isocenter dose of 66 Gy, delivered in 2 Gy fractions. For all patients, the minimum PTV dose was 95% of the prescribed isocenter dose; the maximum PTV-dose was always less than 107% [54].

b. Measurement of internal CTV motion

Differences in CTV position relative to the bony anatomy between two CT data sets of a patient (i.e. internal organ movements), were determined by subsequent, 3D chamfer matches of the two CTVs and of the two bony anatomies, followed by a subtraction of the translational and rotational displacements in the bone match from those in the CTV match. For the relatively small rotations that will occur, this method gives a good approximation of the “true” internal CTV movement. Details of the application of chamfer matching for 3D registration of volumes in two different CT data sets have been given elsewhere [119]. Therefore, in this paper the explanation of the method is limited to the following summary that uses the match of two CTVs as an example. In one CT data set, the CTV is represented by a 3D set of contour points while the other data set (the reference) is used to calculate a 3D distance matrix. The voxel values in this matrix represent the distance from the voxel to the nearest CTV outline. Projection of the contour points of the first CTV in this distance matrix and averaging of the distance values under the points, yields the average distance of these points to the CTV contour of the second (reference) scan. This difference indicates the goodness of the match and the similarity of the two matched volumes, and is called the cost function. The contour points are translated and rotated in three dimensions and a simplex search algorithm is applied to find the minimal cost function. The bone matches are similar except that automatically extracted bone edges instead of delineated CTV contours are used. The final result is a set of six parameters, three translations and three rotations, which describe the relative positions of the two CTVs.

In our analyses, the scaling parameters in the chamfer matches were kept constant because the CT pixel size was equal for all scans (2 mm). The three perpendicular rotation axes always intersected in the center-of-mass (CM) of the delineated CTV, both for the bone and the CTV matches.

c. Variations in CTV position

In each CT-scan, the position of the CTV relative to the bony anatomy is described by six parameters: the CM-coordinates along the left-right- (LR), the anterior-posterior- (AP), and the superior-inferior (SI) patient axes, and the rotation angles around these axes. In *Appendix I*, a detailed description is given of the method to accurately determine for each CT-scan of a patient the six coordinates, describing the CTV-position relative to the average CTV-position in the four available scans per patient. The four positions in all 15 patients were pooled to calculate standard deviations describing the *overall* variations (i.e. no separation in systematic and random variations) for the six coordinates (see *Appendix II*).

The same relative CTV-positions were also used to calculate the *random* and the *systematic* components of the observed position variations (see Figure 5-1). For each patient the standard deviations in the six CTV coordinates during the three repeat scans were calculated. For each coordinate, the *random variation* (σ) for a patient group was then determined as the square root of the average of the variances for all patients. Per patient, the difference between prostate position in planning CT and the average position in the three follow-up CTs was calculated as well. The *mean-of-means* (M) was then defined as the mean of the average movement for all patients; the *systematic variation* (Σ) was determined as the standard deviation in these average movements. The internal organ movement for each set-up technique was thus characterized by M -, Σ - and σ -

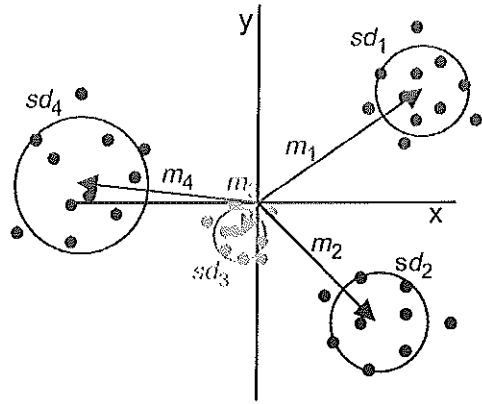


Figure 5-1 Schematic 2D overview of the separation of the variation of CTV coordinates in a group of four (imaginary) patients into a systematic and random component. Indicated are observations (x,y) for several fractions. For each patient i the reference CTV position (i.e. the position in the planning CT) is situated in the origin. The average position in the repeat CT scans are indicated by m_i , and the standard deviation sd_i describes the variation around this average. A patient group is then characterized by the mean of the averages, M , the standard deviation of the averages, Σ , and the square root of the average variance, σ .

values for the three translations and three rotations. A more analytical description of these parameters is given in *Appendix II*.

The difference between supine and prone treatment position was established by testing the equality of the values for M , Σ , σ , and overall variations, using the Student's t-test for the equality of means and a standard deviation test described by Hoel. [47] for the equality of standard deviations. The same tests were used to verify whether M -values were significantly different from zero and whether Σ and σ -values were equal within one group.

d. Time trends and correlations

Without time trends, corrections, or specific differences in patient protocols and geometrical accuracy between CT and accelerator, theoretically M should be zero and Σ should be equal to σ (see *Appendix II*). Therefore, special attention was given to the effect of the rectum laxation, which was given during the planning CT scan only, on the CTV-position. The intention was that minimization of the rectum volume would cause the prostate to be in its most dorsal position [87,109]. The prostate position during acquisition of the planning CT scan would then not be a random sample from the "normal" distribution during treatment, but from a smaller distribution (around a more extreme position). The overall mean motion M would then deviate from zero, but the systematic variation Σ might decrease (and become smaller than the random variation). This might justify significant reduction in PTV margins (see the *PTV margins* section). On the other hand, the radiation treatment might cause a proctitis or cystitis which could reduce variations in bladder and rectum volume, and consequently in prostate position at the end of the treatment. In this case, the random variations might become smaller than the systematic variations. Time trends in CTV-positions were investigated by establishing whether the average positions of the 15 patients in weeks 2, 4, and 6 were significantly different from the planning situation.

In order to assess the influence of bladder and rectum volume changes on the internal prostate position, mutual correlations were determined. Combinations of bladder and rectum changes were also considered. In order to obtain the same dimension for rectum and bladder change as for the CTV translations and in order to obtain optimal correlations, rectum and bladder were represented by a diameter. The rectum volume in those slices that also contained CTV (V_r) was assumed to be cylindrical with length equal to the superior-inferior length (l) of the CTV; conse-

quently the rectum diameter was taken to be $2 \cdot (V_r / (\pi l))^{1/2}$. The bladder volume (V_b) was approximated by a sphere with diameter $2 \cdot (3V_b / (4\pi))^{1/3}$. Correlations between bladder and rectum diameters in the planning CT scan and systematic prostate movements were calculated to investigate whether these diameters can be used to predict the average prostate position during treatment, as suggested by Lebesque *et al.* [66].

e. Patient set-up accuracy

Retrospective calculation of required treatment planning margins to account for geometrical uncertainties also implies knowledge of systematic and random patient set-up errors. For all patients in this study the set-up accuracy was assessed using an EPID. Portal images were regularly acquired for each patient and observed deviations from the intended position, as indicated in a digitized simulator film, were measured. The deviations were used in an off-line set-up correction protocol to minimize the systematic variations [12]. In this protocol the average set-up deviation in several fractions is compared with an action level that shrinks with the square root of the number of measured fractions. When the action level is exceeded, a set-up correction is applied in the following fractions and the protocol is restarted. For the patients in this study, the action level shrank from 8 to 4.6 mm in three fractions. After three successive measurements without corrections, images were acquired weekly; the action level remained 4.6 mm and was applied to the sliding average of the last three measurements. For the three main translations the final set-up accuracy in both groups of fifteen patients was again characterized by a mean-of-means M , a systematic variation Σ , and a random variation σ . (For definitions see previous section and *Appendix II*). From previous experience in our institute, rotations were estimated to be relatively small and are therefore not explicitly considered in the analyses.

f. PTV margins

PTV margins can be determined using coverage probability matrices, which have been introduced in a previous publication [102]. In short, for each patient separately, a 3D coverage probability matrix can be calculated by convolution of the CTV with the distribution of geometrical uncertainties due to internal organ motion and uncertainties in patient set-up. The distributions can either be sampled from actually measured

CTV movements, or normal distributions characterized by standard deviations Σ or σ can be used. Advantage of the former method is that mutual correlations between the different movements are included as well [74]. The voxel values in a coverage probability matrix indicate the probability of the voxel being covered by the CTV (i.e. they vary from 0 to 1). For objects without sharp edges (which is usually the case for CTVs), a voxel value also indicates the probability that the CTV lies outside of that voxel. PTVs are chosen as iso-probability volumes in such a way that on average a large part of the CTV (e.g. > 99%) is adequately covered. Previous research has indicated that adequate iso-probability values are 2.5% for systematic- and 25% for random deviations [102]. In the absence of rotations and with the uncertainties described by normal distributions, this corresponds to a margin equal to about $2\Sigma_{tot} + 0.7\sigma_{tot}$, with Σ_{tot} and σ_{tot} the quadratically summed contributions of translational set-up uncertainty and internal organ motion. This means that the systematic variations are about three times more important than the random variations. In case of significant rotations with non-spherical targets the required margins may become position dependent. The overall mean deviation M is a constant factor (i.e. not an uncertainty) and does not influence the size of the margins. However, in case of M -values significantly different from zero, the calculated PTV should be shifted as a whole accordingly.

IV. Results

a. Overall CTV motion and measurement accuracy

Per treatment position group, 240 CTV movements have been determined (i.e. 16 per patient, see *Appendix I*). There was no significant difference in the chamfer match accuracy between the two groups. For both treatment positions, the average minimal cost function for the bone match was about 1.9 ± 0.3 (1 SD) mm and for the contour match 2.8 ± 0.4 mm. This is adequate considering a pixel size of 2 mm and a slice distance of 3 or 5 mm. The minimal cost function also gives an indication of the similarity in shape of the two matched volumes. The cost function for the bone matches was lower than for the contour matches due to the random irregularities in the manual delineation of the prostate.

As described in *Appendix I*, four separate measurements of the internal prostate position in each CT scan of a patient were used to assess the internal CTV mobility for the two involved patient set-up techniques. For the CTV coordinates along the

Position variation	Supine	Prone
LR translation	0.6 (-1.0 – 1.1)	0.5 (-0.9 – 1.2)
AP translation	<u>2.8</u> (-8.9 – 4.2)	<u>2.1</u> (-6.9 – 4.9)
SI translation	<u>2.8</u> (-6.8 – 7.2)	<u>1.7</u> (-3.6 – 2.6)
Rotation LR-axis	3.4 (-6.8 – 6.2)	3.9 (-10.1 – 6.1)
Rotation AP-axis	0.9 (-2.0 – 1.6)	0.9 (-1.5 – 2.7)
Rotation SI-axis	1.6 (-3.9 – 4.0)	1.3 (-3.0 – 2.8)

Table 5-1 Overall variations in the six coordinates describing the internal CTV position (1 SD) for the supine and prone set-up position in mm and degrees. Standard deviations that are significantly different between the two patient groups are shown underlined ($p < 0.05$). The range of the observed CTV coordinates is indicated between brackets.

of the slice distance being larger than the CT pixel size. The standard deviations describing the overall variations in internal CTV position, as calculated with *equation 3* in *Appendix II*, are presented in *Table 5-1*. Overall internal prostate motion was significantly smaller in prone than supine position for translations in the SI ($p = 0.04$) and AP ($p = 0.0002$) directions. The important rotation around the LR-axis was slightly larger (not significant) in prone position.

b. Correlations

Correlations of CTV movements with rectum and bladder diameter changes are given in *Table 5-2*. Both the correlation of internal CTV displacements with bladder and rectum diameter changes separately, and correlations of CTV motion with the combined effect of changes in the rectum and the bladder are indicated. Mutual correlations between different CTV movements are shown as well. In supine treatment position, the internal prostate position is only affected by rectum diameter changes; correlations with bladder variations are not significant. For patients treated in prone position, bladder and rectum diameter changes correlate with AP CTV translations equally well although the slope for rectum correlations is twice as steep as for bladder correlations; an increase in rectum diameter of e.g. 1 cm, has roughly the same effect on prostate position variation as a 0.5 cm decrease in bladder diameter. Since there is no correlation between rectum and bladder variations, a combination of

main axes and for the rotation angles around these axes, the observed average standard deviations in the four measurements, which also gives an indication of the accuracy of the registration procedure (see *Appendix I*), were about 0.5 mm and 0.9 degrees, respectively. The uncertainty in SI coordinate and lateral rotation angles were the largest because

Observation pair	Supine		Prone	
	r	s	r	s
AP translation/ rectum diameter	-0.76	-0.36	0.51	0.22
SI translation/ rectum diameter	-0.47	0.20	-	-
Rotation LR axis/ rectum diameter	-0.61	-0.34	0.65	0.5
AP translation/ bladder diameter	-	-	-0.51	-0.11
AP translation/ r&b diameter	-0.76	-0.36	0.67	0.19
SI translation/ r&b diameter	0.52	0.20	-	-
Rotation LR-axis/ r&b diameter	-0.65	-0.34	0.71	0.52
AP translation/ rotation LR axis	-	-	0.56	0.57
AP translation/ SI translation	-0.69	-0.76	0.55	0.64

Table 5-2 Significant correlations ($n = 45$, $p < 0.001$) of internal prostate position variations with rectum and bladder diameter changes in supine and prone treatment position. Indicated are the correlation coefficients r and the slopes s (in mm/mm or degrees/mm). The selected combination of rectum and bladder diameters (indicated by "r&b diameter") was that combination that correlated best with the different CTV coordinates.

the two diameter changes actually improves the correlations with AP translations in prone position. The optimal combination was equal to the rectum diameter change minus half the bladder change. Looking at the slopes of the correlations, a 1 mm change in rectum diameter induces an AP prostate movement of about 0.2 (prone) and 0.4 (supine) mm, i.e. diameter changes and prostate displacements are not equal. For both set-up techniques, a correlation was found between AP and SI translations. This implies that the prostate tended to move in an oblique direction. In prone position there was also a strong correlation ($p < 0.001$) between AP translation and rotation around the LR-axis. In supine position this correlation was far less significant ($p = 0.029$, $r = 0.325$).

Rectum and bladder volumes, diameters, and diameter variations are presented in Table 5-3. Both the inter-patient variation and the intra-patient variation are for the rectum similar in both patient groups and are hence not the cause of the observed differences in prostate movement. Since prostate movement is not correlated to bladder diameter in supine position (Table 5-2), the difference between the two set-up techniques in inter-patient bladder diameter variations does in itself not explain the smaller prostate movements in prone position (Table 5-1). There are also differences

in average diameters. The reason for the average rectum diameter being larger in prone position might be explained by the differences in anatomy; in supine position the bladder and prostate weigh down on

organ	Supine				Prone			
	M_{dia}	Σ_{dia}	σ_{dia}	V	M_{dia}	Σ_{dia}	σ_{dia}	V
rectum	35	3	6	123	40	5	5	166
bladder	74	17	9	252	71	11	8	207

Table 5-3 Average rectum and bladder diameters (M_{dia}) and diameter variations in mm for supine and prone patients. The variations have been split into inter-patient variation (Σ_{dia}) and intra-patient variations (σ_{dia}) similar to prostate movements (see equation 5 in Appendix II) except that the mean and standard deviation per patient were taken from the four absolute diameters instead of the three differences with the reference scan (see equation 4 in Appendix II). Mean volumes V (in cc) are also indicated.

the rectum whereas in prone position the rectum may be able to sag more freely. The reason for the difference in average bladder volume between supine and prone position may be explained by the time trends as described in the next section. The average CTV volumes were about 90 cc in both patient groups. The average intra-patient variation was about 4 cc (1 SD) for both groups, i.e. the CTV delineations were sufficiently similar in the different scans of one patient, as was also indicated by the final cost functions of the chamfer matches.

c. Time trends

In Figure 5-2 average organ motions and bladder and rectum variations relative to the planning CT scan are shown as a function of the CT scan number for the 15 supine and 15 prone patients. In *supine* position, there are obvious time trends in rectum diameter and prostate translations. The mean AP position in week 2 and the mean SI positions in weeks 2 and 4 are significantly different ($p < 0.05$) from their respective values during the planning CT scan. Due to the laxation for the planning CT scan, the rectum was relatively empty and the prostate was in a dorsal and inferior position. Since no laxation was applied in subsequent scans, the rectum diameter in weeks 2 and 4 was on average significantly larger ($p < 0.05$). Consequently, the prostate is moved in a superior and ventral direction. By week 6, the average rectum diameter and prostate position returned to the planning CT situation, which may have been caused by a proctitis resulting from the irradiation [87]. The significant ($p < 0.05$) change in the angle around the LR axis in week 6 cannot be correlated with diameter

variations and is as yet not understood. The bladder diameter is never significantly different from its average value.

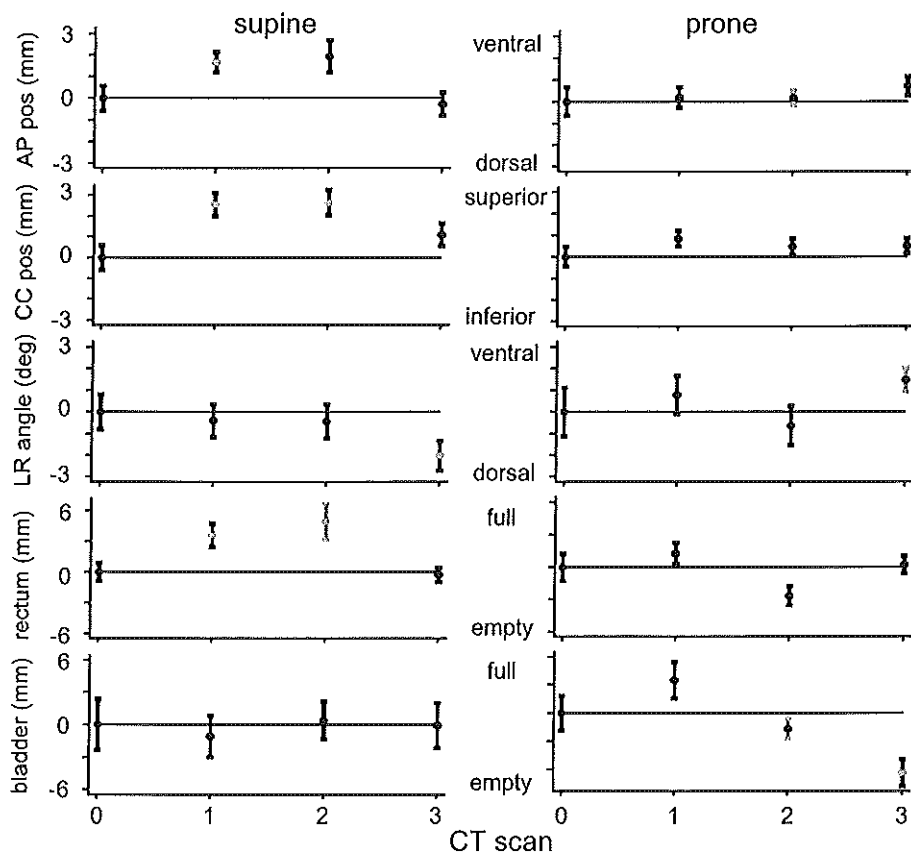


Figure 5-2 Time trends for the average values (of 15 patients) of prostate position and of rectum and bladder diameters, in prone and supine treatment position. Indicated are the average values and standard errors (i.e. $SD/\sqrt{15}$) for the planning CT (scan 0) and the situation in the repeat CT scans (1, 2, and 3). For presentation purposes the averages in week 0 are taken to be zero. If the average values or the standard errors in the repeat CT scans are significantly different from the planning situation ($p < 0.05$), they are shown in gray type. For the rotation around the LR axis, ventral means that the rotation causes the vesicles to move in ventral direction. In supine position a significant change in average prostate position and rectum diameter with time is visible. In prone position there are no significant time trends in prostate location.

In *prone* position, there was no time trend in AP and SI prostate coordinates. The relatively stable prostate position, especially in the first three scans, might be explained by similar but counteractive trends in bladder and rectum diameters in the first three scans (although there is no significant correlation between the two); full bladders, which would push the prostate in dorsal direction, seemed to go hand in hand with full rectums, which would push the prostate in ventral direction. The average angle around the LR axis displays a zigzag behavior that corresponds to rectum diameter variations but they are not significantly different from the planning situation. The trends in rectum and bladder diameter clearly differ from those for supine patients which is possibly explained best by differences in dose delivery to rectum and bladder [129], which in turn might cause differences in the occurrence of proctitis and cystitis. An increased bladder exposure in prone position could also explain the gradual decrease of the bladder diameter in the course of treatment (in week 6 significantly less than in week 0, $p = 0.03$) and hence the smaller average volume as shown in Table 5-3.

d. Systematic and random CTV position variation

The results of the separation of the overall CTV position variations in systematic and random variations are shown in Table 5-4. In contrast to the prone position, the time trends in supine position result in a mean-of-means M that is significantly different from zero for SI translations ($p = 0.02$). The 1.1 mm overall mean shift in ventral direction is not significant. On the other hand, in prone position

Variation	Supine			Prone		
	M	Σ	σ	M	Σ	σ
LR translation	<u>0.4</u>	0.5	0.6	0.1	0.4	0.5
AP translation	-1.1	2.5	<u>2.8</u>	0.4	<u>3.3</u>	<u>1.7</u>
SI translation	<u>2.1</u>	2.7	2.5	0.6	<u>2.2</u>	1.5
rotation LR axis	1.0	3.6	3.3	0.5	<u>5.5</u>	3.4
rotation AP axis	-0.1	0.8	0.9	-0.1	<u>1.1</u>	0.8
rotation SI axis	0.7	1.7	1.5	0.0	0.8	1.4

Table 5-4 CTV coordinate variations split into overall means (M), systematic variations (Σ), and random variations (σ), in mm and degrees, for patients treated in supine and prone position. Overall mean values that are significantly different from zero, systematic variations that are significantly different from the corresponding random variations, and random variations that are significantly different between the two patient groups are shown underlined ($p < 0.05$).

the systematic variations are significantly larger than the corresponding random variations, i.e. the variation of the average position in the follow-up scan with respect to the planning situation is larger than the variation within the follow-up scans. The prostate movement in prone position appears to decrease somewhat in the second half of the treatment, possibly due to inflammations of bladder and rectum. At the moment of the planning CT scan, the variations are larger which is indicated by the error bars in Figure 5-2; in prone position, the standard error of the average values at the planning CT scan are generally larger than the standard errors at the follow-up scans. In supine position they are about equal, so the gain of the laxation might actually be that in supine position the variation at the planning CT scans has been reduced to average values.

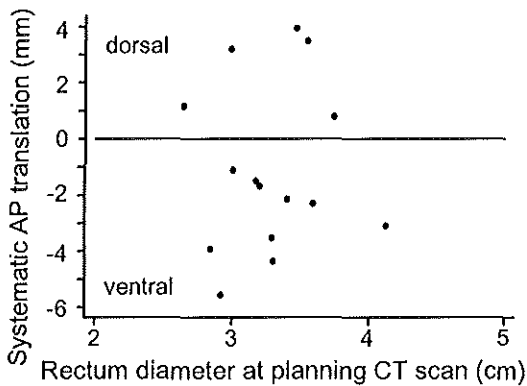


Figure 5-3 Illustration of the effect of the laxative suppositories taken before the planning CT scans only. The average CTV movements in AP direction for the 15 patients treated in supine position are plotted as a function of rectum diameter at the time of the planning CT scan. One would expect only ventral movements because the suppositories are supposed to empty the rectum and cause the CTV to be in a maximum dorsal position. However, 5 of the 15 patients display on average a dorsal translation.

In both treatment positions there was no correlation between absolute rectum and bladder diameters during planning CT scan and subsequent systematic prostate position deviations, i.e. it was not possible to predict the average prostate position during treatment based on the situation during the planning CT scan (see Figure 5-3 for correlations with rectal diameter of the patients treated in supine position). It appeared that there was too much variation between the individual patients, even though *on average* the laxation resulted in a small rectum diameter (see Figure 5-2) and in a mean position of all patients during the planning CT (i.e. M) in cranial-posterior direction from the average

position (see Table 5-4). Figure 5-3 also shows that five out of the fifteen patients had a systematic translation in the repeat CT scans in the dorsal direction despite the use of laxative suppositories.

e. Set-up variation

In Table 5-5 the patient set-up variations for the three main translations are given for the supine and prone treatment positions. The systematic set-up variations are smaller than the systematic internal organ movements, which is partly due to the applied correction protocol. In supine and prone position on average 9 and 10 fractions per patient were analyzed, respectively. The number of set-up corrections was different between the groups: 6 for supine and 20 for prone treatments. The (retrospectively calculated) uncorrected set-up accuracy was clearly worse in prone than in supine position (as reflected by the random variations), which is possibly due to the difference in experience with the two techniques; the supine set-up technique has been in use for many years whereas the prone technique with the bellyboard was first used on the fifteen patients described in this paper. However, the larger number of corrections for

Variation	Supine			Prone		
	M	Σ	σ	M	Σ	σ
LR translation	0.4	<u>1.3</u>	<u>1.6</u>	-0.4	<u>0.8</u>	<u>2.7</u>
AP translation	<u>-1.0</u>	<u>1.5</u>	2.2	-0.1	<u>0.8</u>	2.4
SI translation	<u>-1.0</u>	1.4	<u>1.5</u>	-0.6	<u>0.8</u>	<u>2.4</u>

Table 5-5 Set-up variation data (in mm) for patients treated in supine and prone position. Just as for internal organ motion (Table 5-4), overall mean values that are significantly different from zero, systematic variations that are significantly different from the corresponding random variations, and random variations that are significantly different between the two patient groups are shown underlined ($p < 0.05$). The small systematic variations are due to the use of a set-up correction protocol.

the patients in prone position effectively reduced the systematic deviations such that the final systematic variations were even smaller than in supine position (this is inherent in the protocol). There is no satisfying explanation for the mean-of-means in AP and SI direction in supine position being significantly different from zero.

f. PTV margins

Combination of observed variations for internal organ motion and patient set-up, and application of the $2\Sigma+0.7\sigma$ -rule for the PTV margin [102], yields, for translational deviations only, the margins as shown in Table 5-6. In supine position the whole PTV should be shifted 2 mm in ventral and 1 mm in superior direction to correct for the

direction	Supine	Prone
Left-right	4.0	3.7
Anterior-posterior	8.3	8.8
Superior-inferior	8.2	6.6

Table 5-6 CTV-to-PTV margins (in mm) required for internal organ motion and set-up deviations and ignoring the rotations, for patients treated in supine and prone position.

than in the AP and SI directions, due to the negligible organ motion in the LR direction.

In order to take the significant rotations into account as well, coverage probability calculations have been applied to calculate the margins needed in supine and prone treatment position, for internal organ motions only. The actually measured prostate displacements were used in the calculations, for both the random (45 observations per group) and the systematic deviations (only 15 observations per group). A 2.5% isoprobability level was selected for the systematic variations, and 25% for the random deviations. An indication of the resulting margins is shown in Figure 5-4. Quantitative conclusions should be drawn from this figure with some caution since only 15 observations were used to determine the main part of the margins (systematic variations are 3 times more significant than random variations); the 2.5% isoprobability volume is for 15 measurements actually equal to the enveloping volume of all 15 CTV positions, which gives extreme positions a relatively great weight. Nevertheless, especially in the sagittal slice some differences between supine and prone margins become visible. The supine margin in the SI direction is larger than the prone margin and is also shifted in superior direction. The effect of the rotations is, as expected, larger for the prone margin; at the superior CTV end the margin can become twice as large as at the inferior end. In the transversal slice, the PTV is very close to the CTV in the lateral direction. This is due to the very small variation in lateral direction (see Table 5-4) and the discrete voxel size (2 mm in LR and AP, and 3 mm in SI direction).

mean-of-mean internal organ motions and set-up deviations (the 1 mm AP translation for organ motion was included although it was not significant). Due to the larger impact of the systematic variations, the differences between margins in supine and prone treatment position are small despite the observed differences in random variations. Furthermore, in both positions the margin in LR direction is significantly smaller

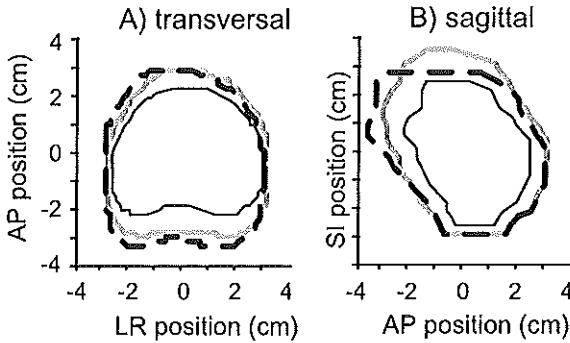


Figure 5-4 CTV (thin solid lines) with PTV margins as determined by coverage probability calculations [22] for the prone (thick dashed lines) and supine (thick gray lines) internal organ motions. Systematic and random variations are included. The 15 systematic motions were the mean CTV positions with respect to the planning situation (as determined from equation 4 in Appendix II), the 45 random variations were the individual positions of the prostate in the repeat CT scans relative to the corresponding planning CT scans. Especially in the sagittal slice, the differences and agreements between the two margins are obvious.

group who conducted the study about (on average) two years *after* the irradiation treatment had been given. The prostate movement might have been less due to smaller rectum variations or due to a radiation-induced fibrosis that could have restricted the prostate movement. The values in the other studies compare reasonably well to our own values as showed in Table 5-1. It should be noticed however, that in Table 5-1 standard deviations of prostate *positions* are given. To obtain the standard deviations of the *movements* (i.e. the differences in position) which are calculated in most other studies [3,7,75,99,122], our values should be multiplied by $\sqrt{2}$. In none of the previously published studies an attempt was made to separate systematic from random prostate motions.

Regarding the supine treatment position, the study most alike our own was performed by van Herk *et al.* [119] analyzing multiple CT data of eleven patients with chamfer matching. In contrast to our study, femurs were excluded in the bone match in order to minimize the cost function and reduce the uncertainty in the match results. But considering that the whole of the pelvic bone is used in the match, misalignment

V. Discussion

a. Comparison with other studies

In most other studies on internal prostate motion [7,75,99,119,122], overall standard deviations of prostate movements in AP and SI directions are in the order of 3 to 4 mm, and in LR direction about 1 mm. Only Althof *et al.* [3], who used implanted ^{125}I seeds and multiple simulator images, appear to have significantly smaller values: standard deviations of 1.1 mm in AP and SI direction.

They were however the only

of the relatively small leg bones is less significant. Furthermore, they used a slightly different cost function for the CTV matches and instead of subtracting the bone match from the CTV match, they acquired the CTV movement by matching the CTVs using the bone match as starting point. They also treated with a full bladder but did nothing to influence the rectum filling. The overall prostate movement, volume variations, and correlations are very similar to our supine data. Our position variation in SI direction was larger than theirs (1.7 mm) which might be due to their smaller CT slice distances (3 mm in the prostate region for all patients), differences in the registration procedure, or to our laxation for the planning CT scan. Their AP position variation (2.7 mm) was similar and the rotational variations (4.0, 1.3, 2.1 degrees around LR, AP and SI axes, respectively) were slightly smaller in our institute which might be due to the data averaging that we performed to decrease the measurement errors (see *Appendix I*).

To our knowledge, only Melian *et al.* have performed a study on internal prostate movement in prone treatment position [75]. They also used multiple CT data and found, for 13 patients, overall standard deviations for translations in LR, AP, and SI directions of 1.2, 4.0 and 3.1 mm respectively. This is larger than our values (even taking into account the $\sqrt{2}$ correction factor). There were however several differences with the study described in this paper: they did not use laxation, they treated some patients with empty bladders, they could not perform automatic 3D matches, they used translational coordinates to determine rotations, and they made one of the three follow-up scans with an artificially expanded rectum. In agreement with our data, they also found correlations between prostate movements and bladder and rectum volume variations.

b. Systematic and random variations, time trends, and margins

Compared to the aforementioned studies, which did not consider time trends, the most remarkable finding of this study were the differences between systematic variations Σ and random variations σ . It appeared that the planning CT situation was not just a random sample of the distribution of situations that occur during the rest of the treatment. In prone position, the prostate position variation at the planning situation was significantly larger than the variation in the course of treatment (see Table 5-4), despite the rectum laxation (if all patients have indeed taken their laxative suppositories, there is no reason to believe that the laxation might actually be the cause of an *increase* of the variation in prone position). Since the uncertainty in prostate position at the planning CT scan determines the systematic variation Σ , which in turn is largely

responsible for the CTV-to-PTV margins, our currently applied margins of 1 cm cannot be decreased. One might even argue that they are too small in the superior region of the CTV (near the vesicles). To get the same coverage there as in the rest of the PTV, the margins should be increased to 1.5 cm or more as indicated in Figure 5-4. There is however some discussion on the relevance of a small underdosage in part of the vesicles (see for instance Pisansky *et al.* [89]).

Another noteworthy result of this study is the significant time trend in CTV position for the patients treated in supine position (see Figure 5-2). Near the end of the treatment the average rectum diameter seems to decrease and return to the (laxated) rectum diameter of the planning CT. The CTV position in AP and SI follow this trend. At the moment, PTV margins are based on measured systematic and random variations. In theory, one could go further and adjust the PTV margins on a weekly basis; the average prostate location changed from ventral to dorsal in the course of treatment and the standard deviations, which are responsible for the size of the margins, changed as well. As with all CT based studies however, the number of measurements per patient in this study is rather low, in our case due the limited availability of the CT scanner for research purposes. If more patients and more CT scans per patient can be measured, the trends, and therefore time-dependent PTV margins, can be determined with a better accuracy.

The small number of CT scans per patient is not fully representative for a prostate treatment of 33 fractions. Therefore only large differences in the measurement data are also statistically significant, like e.g. the difference between systematic and random variations for the internal organ motion in patients treated in prone treatment position (see Table 5-4). Based on the results of this study however, there is no reason to prefer one positioning technique above the other; Table 5-6 shows there is hardly any difference in planning margins for the translational variations. The differences as shown in the more “qualitative” Figure 5-4, which include the rotational variations, also do not clearly favor one technique; in prone position the rotations appear to necessitate a larger margin in posterior direction (near the rectum), whereas in supine position the cranial margin is larger. Therefore, considering the equality of the PTV margins, the decision to treat in prone or supine position might actually be decided by planning studies. Zelefsky *et al.* [129] concluded that prone position was to be preferred over supine position, but since the results may depend on hospital specific issues like protocols for rectum and bladder filling, we are currently conducting our own planning study.

c. Patient data bases and protocols

In both treatment positions, mutual correlations of the different CTV movements make independent margin determination in the different directions less accurate. The measurements showed that the prostate tends to move obliquely from dorsal-inferior to ventral-superior direction, as also observed by van Herk *et al.* [119]. Furthermore, Figure 5-4 indicates that the axis of rotation is not at the center of mass of the prostate but more likely at the inferior apex, as has been reported before [119]. The simple rule for independent margins in LR, AP, and SI direction is then only a first order approximation. Mageras *et al.* [74] suggested generation of a large database of prostate movements, which can be sampled at the time of planning so the expected treatment can be simulated. The question is whether this database could be used universally or if every institute should create its own, considering the complexity of the movement and the dependency on institute specific treatment protocols. Although the overall variations from separate institutes may appear similar, as indicated in a previous section, detailed study of, for instance, systematic and random variations might yield significant differences.

Considering the variation of rectum filling at the planning CT scan (see Figure 5-3), one might ask if the laxative suppositories used in this study were effective enough. Patients were asked to take them four hours before the CT scan but the application and its effect might be too variable for individual patients. To be really sure that the rectum is empty and the prostate at its most dorsal position, other laxation methods like a rectal enema might be a more reliable (but more cumbersome) solution [87]. Furthermore, the time of day on which the patients are treated might be important. Due to the aforementioned limited availability of the CT scanner, all CT scans in this study were made early in the morning. This is however not always representative for the irradiation sessions of prostate cancer patients which can be carried out at all times during the day. Assuming regular bowel movements, particularly in the beginning of the treatment, ideally all treatments, simulations, and acquisitions of the CT scans should be carried out at the same time of day.

d. Conclusion

The more elaborate analysis of our prostate movement data yielded significant differences with previously published studies. Although at first glance the overall prostate movement appeared to be less in prone than in supine position, separation of systematic and random variations showed that this was predominantly because of the smaller random variations. The systematic variations are about equal for both treatment positions. Since systematic variations are largely responsible for the PTV margins, a margin reduction cannot be justified by treating the patient in prone instead of supine position. More measurements should be performed to further confirm this conclusion and obtain more certainty in the observed time trends for patients in supine position.

VI. Appendices

a. Appendix I: Data and error reduction

Assuming that the CTV of a patient is basically a rigid body, its position relative to the bony anatomy is fully described by six coordinates: the CM-coordinates along the AP-, LR-, and the SI axes, and the rotation angles around these axes (the three axes intersect in the CM of the prostate). As explained in the *Methods and materials* section, internal CTV movement was established by subtraction of 3D chamfer match results for bony anatomy from the results of the corresponding CTV match.

Due to (small) differences in delineated CTVs in the different CT-scans of a patient and due to the inability of the applied search algorithm to always find exactly the same optimum match, there is some uncertainty in the results. Moreover, the two CT-data sets in a matching procedure are used in rather different ways; the reference CT-scan is used to calculate a distance transform matrix while the other data set is used to construct a 3D set of contour points (see *Methods and materials* section). In this appendix, a description is given of the method that was used to calculate for each CT scan of a patient the CTV-coordinates relative to the average CTV-coordinates of the patient. With this method the effects of the above mentioned uncertainties can be minimized.

The method is based on the results of 4x4 matches per patient; all CT-scans are subsequently used as the reference scan r and matched with the three other scans and with itself, yielding four sets of CTV displacements, each calculated with a different

CT-scan as the reference scan. Application of Eq. 5-1 given below, yields for each CT scan k of a patient four estimates $p_{av,k}^{(r)}$ (one for each r) of the CTV position relative to the average CTV position. (For convenience, no patient- and CTV coordinate labels are used in the formulas; the formulas are to be applied separately for every patient and for each of the six CTV-coordinates).

$$p_{av,k}^{(r)} = p_{r,k} - p_{r,av} = p_{r,k} - \frac{1}{4} \sum_{r=0}^3 p_{r,k} \quad 5-1$$

with $p_{r,k}$ the position in scan k relative to the reference r (i.e. the result of one bone match for scans r and k subtracted from the corresponding CTV match), and $p_{r,av}$ the average CTV-position relative to the CTV-position in the reference scan r . The four estimates of the CTV-position in scan k relative to the average position are finally averaged

$$p_k = \frac{1}{4} \cdot \sum_{r=0}^3 p_{av,k}^{(r)} \quad 5-2$$

Hence, p_k (or p_k^{ij} if the labels for coordinate i and patient j are denoted as well) is the CTV position for an individual scan k with respect to the average CTV position of that patient (i.e. $\sum_{k=0}^3 p_k = 0$). In this manner, the 16 measured prostate movements per patient are reduced to 4 prostate positions (one for each CT scan).

An estimate of the measurement accuracy is given by the standard deviation of the four measurements, multiplied by a factor $\sqrt{4/3}$ because the four measurements contain the same average and are therefore not fully independent. It should be noted that the effect of uncertainty in CTV delineation is not included in this standard deviation; the same outlines were used for the different matches. The delineation accuracy has been optimized by visual comparison and correction of the CTV outlines in the different scans of one patient, as explained in the *methods and materials* section.

b. Appendix II: Overall, systematic, and random position variations

The coordinates p_k^{ij} , as derived in *Appendix I*, were used to calculate parameters describing the overall CTV position variations and the random and systematic

components. For both patient groups, the *overall* variations in the six CTV-coordinates were quantified using:

$$SD^i = \sqrt{\frac{1}{15} \sum_{j=1}^{15} \frac{1}{3} \sum_{k=0}^3 (p_k^{ij})^2}, \quad 5-3$$

with SD^i the standard deviations for CTV-coordinate i (e.g. the CM-position along one of the axes) for all patients j and all scans k , describing the *overall* variation of this coordinate. Again the normal standard deviation is corrected by a factor $\sqrt{(4/3)}$ because the four measurements of each patient contain the same average.

The CTV position variations p_k^{ij} were also used to calculate, for each patient j and coordinate i , the average deviation m^{ij} of the three repeat CT scans ($k = 1, 2, 3$) with respect to the planning CT scan ($k=0$) and to determine the variation sd^{ij} within the three repeat CT scans:

$$m^{ij} = \frac{1}{3} \sum_{k=1}^3 p_k^{ij} - p_0^{ij} \quad \text{and} \quad sd^{ij} = \sqrt{\frac{1}{2} \sum_{k=1}^3 (p_k^{ij} - p_0^{ij} - m^{ij})^2} \quad 5-4$$

Both patient groups were then characterized by their mean-of-means M , the systematic variation Σ , and the random variation σ for each coordinate i , according to:

$$M^i = \frac{1}{15} \sum_{j=1}^{15} m^{ij}, \quad \Sigma^i = \sqrt{\frac{1}{14} \sum_{j=1}^{15} (m^{ij} - M^i)^2}, \quad \text{and} \quad \sigma^i = \sqrt{\frac{1}{15} \sum_{j=1}^{15} (sd^{ij})^2} \quad 5-5$$

For the random variation σ , the square root of the average of the variances is taken. This value gives a better estimate of the population's distribution than the average standard deviation. In Figure 5-1 the occurrence of systematic and random variations is explained in a graphical manner. Since the systematic deviation per patient (m^{ij}) was determined by only three observations, a relatively large error equal to $sd^{ij}/\sqrt{3}$ was made. This will also manifest itself in the systematic variation Σ , which was therefore corrected according to:

$$\Sigma_{new}^i = \sqrt{(\Sigma_{old}^i)^2 - (\sigma^i/\sqrt{3})^2}. \quad 5-6$$

As a first approximation, one can assume equal distributions of possible prostate positions during planning CT scan and during treatment. If it is then assumed that all patients have about the same variations in prostate position, the prostate position

during the planning CT scan, which will determine the average deviation m , can be considered as just one sample of the distribution of prostate positions during the treatment, which will determine the variation sd . The standard deviation of the average deviations (i.e. Σ) should then be equal to the average of the variations sd (i.e. σ) and M should theoretically be zero.

VII. Acknowledgements

The authors would like to thank the Revolving Fund of the University Hospital Rotterdam for their financial support.

CHAPTER 6. ON-LINE SET-UP CORRECTIONS DURING RADIOTHERAPY OF PATIENTS WITH GYNECOLOGICAL TUMORS

J.C. Stroom, M.J.J. Olofsen-van Acht, S. Quint, M. Seven, M. de Hoog, C.L. Creutzberg, J.C.J. de Boer, A.G. Visser.

Int. J. Radiat. Oncol. Biol. Phys. 46, 499-506, 2000

I. Abstract

Purpose: Positioning of patients with gynecologic tumors for radiotherapy has proven to be relatively inaccurate. To improve the accuracy and reduce the margins from clinical target volume (CTV) to planning target volume (PTV), on-line set-up corrections were investigated. *Methods and Materials:* Anterior-posterior portal images of 14 patients were acquired using the first six monitor units (MU) of each irradiation fraction. The set-up deviation was established by matching three user-defined landmarks in portal and simulator image. If the two-dimensional deviation exceeded 4 mm, the table position was corrected. A second portal image was acquired using 30 MU of the remaining dose. This image was analyzed off-line using a semi-automatic contour match to obtain the final set-up accuracy. To verify the landmark match accuracy, the contour match was retrospectively performed on the six MU images as well. *Results:* The standard deviation (SD) of the distribution of systematic set-up deviations after correction was < 1 mm in left-right and cranio-caudal directions. The average random deviation was < 2 mm in these directions (1 SD). Before correction, all standard deviations were 2 to 3 mm. The landmark match procedure was sufficiently accurate and added on average 3 minutes to the treatment time. The application of on-line corrections justifies a CTV-to-PTV margin reduction to about 5 mm. *Conclusions:* On-line set-up corrections significantly improve the positioning accuracy. The procedure increases treatment time but might be used effectively in combination with off-line corrections.

II. Introduction

a. Geometric uncertainties in radiotherapy

Conformal radiotherapy aims at limiting toxicity of critical organs while maximizing the tumor dose. This goal can be partly achieved by minimizing the treatment field size. The treatment field size is mainly determined by the size of the tumor including subclinical disease and by the margins applied to compensate for geometric uncertainties that occur during radiotherapy. Following the nomenclature proposed by the International Commission on Radiation Units and Measurements (ICRU), the gross tumor volume plus subclinical disease is called clinical target volume (CTV), and the CTV plus safety margins is called planning target volume (PTV) [54]. Minimization of these so-called CTV-to-PTV margins, i.e. restraining internal tumor movement and maximizing patient the set-up accuracy, will therefore benefit conformal radiotherapy.

b. Set-up accuracy of patients with gynecologic tumors

Patients with gynecologic tumors seem somehow more difficult to position accurately on the treatment couch than patients with prostate cancer [14], which is treated in the same pelvic region. Rather large set-up deviations have been reported in the literature [25,77,117]. In recent years, several set-up techniques have been investigated in our institute as well [25,90]. However, they all yielded more or less the same distributions of random (day-to-day) set-up variations; the average standard deviations (σ) were about 3-4 mm in each of the three main directions. Since the simulator film which is used as reference image can be considered as one sample from those distributions, it is plausible that the standard deviation of the distribution of systematic (everyday) set-up deviations for the whole patient group (Σ) initially had similar values [17].

c. Off-line set-up corrections

The only significant improvement of the set-up accuracy was obtained by application of an off-line set-up verification and correction protocol [12,14,17]. The set-up deviations of subsequent fractions are averaged and compared with an action level that decreases with the square root of the number of measurements. If the average deviation exceeds the action level, a table correction will be applied to the following fractions and the protocol is restarted. The procedure stops if a specific number of

measurements is performed without correction. Using such a protocol with about ten measurements per patient, the systematic variations for patients with gynecologic tumors were reduced by a factor two [90], as for patients with prostate cancer [14]. Random variations are not affected by the off-line protocol.

d. CTV-to-PTV margins

In our institute, the CTV-to-PTV margin for patients with gynecologic tumors is mainly determined by the set-up deviations; the internal CTV movement is considered to be relatively small (although this is the subject of an on-going study). Using the off-line protocol, a margin of 1 cm can be applied. This is based on previous research which concluded that the margin should be equal to at least $2\Sigma+0.7\sigma$ to guarantee an adequate tumor dose [102]. Inserting $\Sigma = 2$ mm and $\sigma = 4$ mm in this formula, results in margins of only 7 mm. However, this value is rounded up to 1 cm because of other geometric inaccuracies such as delineation uncertainty and internal organ motion.

e. On-line set-up corrections

To increase the cure rate, we are currently considering to raise the tumor dose for some patients with gynecologic tumors to 60 Gy. In the literature, it has been reported that maximally 30% of the small bowel volume should receive a dose of over 55 Gy [34,81]. With the current CTV-to-PTV margins, it is not always possible to fulfil this criterion for tumor doses higher than 55 Gy. Reduction of margins might be justified if an on-line instead of an off-line set-up protocol is applied. With on-line corrections, the set-up deviation is determined and corrected before the (bulk of the) daily treatment dose is given. Other groups have reported superior set-up accuracies at the cost of increased treatment time [7,30,31,35,39,71,116,117]. In this paper, we will discuss whether on-line set-up corrections are beneficial and clinically feasible in our institute.

III. Methods and materials

a. Treatment planning and immobilization

Fourteen patients with gynecologic tumors were included in the study. The patients were irradiated with a four-field box technique if the CTV could be restricted to the

primary tumor region, the proximal two-third of the vagina, the parametria, and the obturator and iliac lymph nodes. If the CTV included para-aortic lymph nodes, anterior-posterior/posterior-anterior (AP/PA) fields were used. The CTV-to-PTV margin was 1 cm. The AP/PA patients were treated with a source-to-skin distance of 100 cm, whereas the box technique was isocentric. The total dose varied from 46 to 48.6 Gy and the number of fractions from 23 to 27. All patients were treated in supine position at the same accelerator³ with 25 MV photons and a multileaf collimator.

For patient positioning, long lateral, sagittal and transversal laser lines were marked on the patient. The intersection points of these lines were tattooed, together with the caudal field border. A knee roll was used to decrease the pelvic rotations and a homemade foot support further secured foot and leg position. The legs were slightly exorotated to ensure decreased muscle tension in the legs and the buttocks. The arms were positioned above the head by a commercially available arm support⁴. In case of discrepancy between the skin marks in longitudinal direction, the caudal field border tattoo was the decisive parameter for set-up [25,90]. For isocentric treatments, the isocenter-to-table distances were used for table height position. The focus-to-skin distance was measured before each fraction.

b. On-line correction protocol

To determine the deviations in patient set-up, the position of bony structures in AP portal images were compared with corresponding positions in a reference image. The portal images were acquired with a commercially available electronic portal imaging device (EPID)⁵. The technical characteristics of this system were described in previous publications [2,123]. An on-line set-up correction procedure was developed using the high-level script language designed to operate the EPID system automatically. The procedure can be separated in four steps:

1. Before treatment, the operator selects a maximum of three anatomical landmarks in a digitized simulator radiograph (i.e. the reference image), which is displayed on a

³ MM50 Racetrack Microtron, Scanditronix Medical AB, Uppsala, Sweden

⁴ Sinmed BV, Reeuwijk, The Netherlands

⁵ SRI-100, Electa Oncology, Crawley, Great Britain

monitor. For all treatment fractions, these landmarks will reappear automatically in the reference image. Useful landmarks for AP pelvic images are the pubic symphysis and the intersections of horizontal and vertical tangents to the pelvic rim [117], as indicated in Fig. 6-1a.

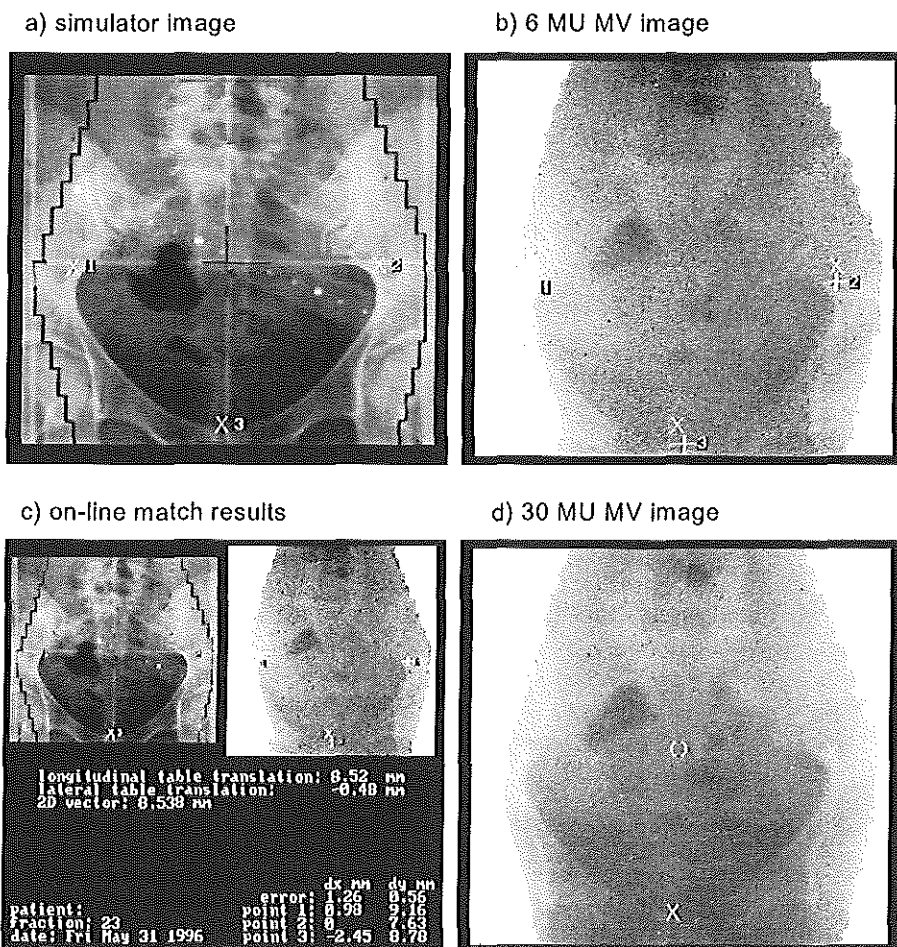


Figure 6-1 The on-line set-up correction procedure. In (a) the digitized simulator image is shown in which 3 reference landmarks must be defined (crosses, x). Then (b) a 6 MU EPID image is obtained in which the same landmarks must be selected (numbered pluses, +). The landmarks are matched (c) and table translations are shown. A correction must be performed if the 2D vector is larger than 4 mm. Finally (d) a 30 MU EPID image is acquired of the final set-up position in which the reference landmarks are shown to verify the correction.

2. The patient is positioned on the treatment couch and a portal image is obtained using the first 6 monitor units (MU) of the treatment dose, after which the irradiation is automatically interrupted. The image quality is improved by automatic adjustment of the display contrast. Landmarks similar to those in the reference image must be defined in the portal image. The image quality of a 6 MU image is usually sufficient to discriminate most of the bony structures, as is shown in Fig. 6-1b; however, in some cases the pubic symphysis can be less pronounced. In case of extreme set-up deviations, the pelvic rim can partially disappear behind the field defining blocks. However, normally at least two landmarks can be indicated to enable image registration.
3. The patient position is determined by calculation of the difference between the center-of-mass of the landmarks in the portal and the reference image. If the two-dimensional (2D) set-up deviation is larger than 4 mm (i.e. about equal to one standard deviation of the expected variations), the patient couch is translated as indicated (Fig. 6-1c). Rotations can generally not be determined and corrected in a fast and reliable manner; in case of rotations, the selected landmarks are matched as well as possible by translations only. Since two landmarks are placed near the top of the pelvic rim and one at the pubic symphysis, the position of the top largely determines the outcome of the match. Once the match has been performed, the set-up position is immediately obtained; a separate field edge match is superfluous because the stiff mechanical structure of the EPID box ensures a reproducible and known isocenter position in the images.
4. With the remaining dose a 30 MU image is made, which is used for off-line determination of the final set-up position (see *contour match* section). To enable instant verification of applied corrections, the 30 MU image is displayed on the monitor with the reference landmarks, which should be in the correct position (Fig. 6-1d).

To be effective, the on-line procedure must be run at each fraction of the treatment. To estimate the extra workload involved with the on-line protocol, the time required for landmark match and table correction was monitored for some patients treated toward the end of the study. At that time, the start-up problems had been solved and the technicians were familiar with the procedure. Since lateral images were available for a limited number of patients and since the largest variations were expected to occur in the cranio-caudal direction [25,90], only AP fields were used for on-line corrections.

c. Contour match

To determine the accuracy of the on-line landmark match, all 6 MU images were retrospectively analyzed by contour matching as well. Contour matching was impossible with the EPID software, but is judged to be more reliable than landmark matching because a larger fraction of the anatomical structure to be matched is actually used in the calculation. To determine the accuracy of the final treatment set-up, the 30 MU images were analyzed with the contour match as well.

The contour match procedure was developed using specialized visualization software⁶. It semi-automatically registers two images, in this case an EPID image with the corresponding digitized simulator radiograph (Fig. 6-2). For both images, the image quality can be improved using display equalization, which *locally* optimizes the display contrast [80]. In both images, the features to be matched must be outlined manually. The contours are subsequently converted to black-and-white binary images, the contours being white on a black background. The cross-correlation function of the two binary images is calculated using Fast Fourier Transforms. The *position* of the maximum of this function gives the translation between the two images. Jones and Boyer [57] used this method to determine the shift between two original megavoltage images directly. Since in our approach binary images are used instead of megavoltage images, the position of the maximum is more sharply defined and less dependent on gray scale variations. However, in case of rotations the delineated structures in the two images may differ in shape, which might cause a (partial) mismatch of the delineated structures if the contours are too thin. Therefore, the line thickness of the contours in the binary images can be increased and is usually about ten pixels (5 – 8 mm). The *value* of the maximum (between 0 and 1) can be considered a correlation coefficient reflecting the adequacy of the match. Values larger than 0.7 normally indicate sufficiently correct matches (accuracy < 1 mm). To obtain an estimate of the in-plane rotations, the rotation with the maximum correlation is determined for a range of rotations around the image center, using the translated images as starting point. The calculation of translations took about 20 seconds on a UNIX workstation⁷, the rotations added another 10 seconds.

⁶ AVS, Advanced Visual Systems, Waltham, MA

⁷ HP715/75, Hewlett Packard, Palo Alto, CA

The structures in the MV images used for matching the AP images are also indicated in Fig. 6-2. The superior part of the pelvic rim is judged to be the best indicator of the target volume position, because it is visible in all images and near the center of the field. The inferior pelvis and symphysis are not included because they

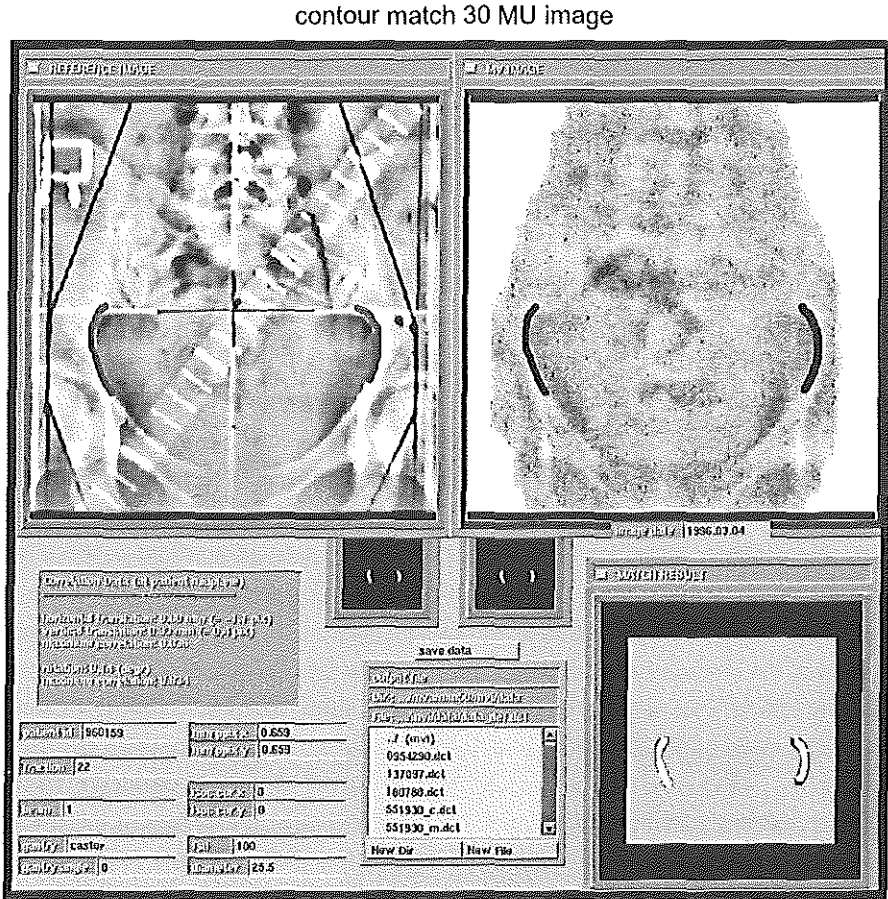


Figure 6-2 Illustration of the developed contour match procedure. In the upper left image the reference image is shown with a manually drawn contour (gray in this black-and-white image). In the upper right image a 30 MU EPID image is shown in which a similar structure is contoured (black). The two small images in the middle depict the binary images that are used for the cross correlation match. The match result is visualized in the lower right image; were the black and gray contour overlap the contours become light gray. Resulting translation values and patient data are shown on the left.

are particularly sensitive to out-of-plane rotations around the lateral axis. The contours thus defined have a center-of-mass similar to that of the landmarks used to determine the on-line corrections. The two match methods will therefore treat (out-of-plane) rotations similarly. To determine the accuracy of the on-line landmark match, all 6 MU images were also analyzed afterwards using contour matching. Contour matching is judged to be more reliable than fiducial landmark matching because a larger fraction of the anatomical structure to be matched is actually used in the calculation. To determine the accuracy of the final treatment set-up, the 30 MU images were analyzed with the contour match as well. For contour matching the images had to be transported to a UNIX workstation and were analyzed off-line. Because of the data transport between EPID PC and Unix system, the contour matching procedure was not used for on-line corrections.

d. Statistical analysis

For each patient i the mean set-up deviation (m_i) and the standard deviation (SD) of the variation around that mean (sd_i) were determined in the left-right and cranio-caudal directions. Next, the mean-of-means M (= MEAN m_i), the variation-of-means Σ (= SD m_i), the mean-of-variations σ (= MEAN sd_i), and the variation-of-variations ν (= SD sd_i) were calculated for both patient groups. M is normally close to zero; there should be no systematic difference between average set-up on the simulator and on the accelerator for a large group of patients. In that case, Σ gives an indication of the size of systematic deviations for the individual patients; therefore, Σ is called the *systematic variation*. Since σ represents an estimate of the average random variation, it is called the *random variation*. Finally, ν indicates the degree of variation in random deviations per patient, i.e. it is a measure of the homogeneity of the mobility in the patient group.

Statistically significant differences of these four variables between the corrected and uncorrected group were investigated using the student's T-test for the mean values and an SD test as described by Hoel [47] for the standard deviations. Furthermore, a possible correlation between (uncorrected) set-up variation and patient diameter (in AP and lateral direction) was investigated. For patients treated with AP/PA fields, patient diameters were only available in the AP direction.

IV. Results

a. On-line set-up correction procedure

The total number of on-line set-up measurements for the 14 patients in the study was 254 (varying from 9 to 23 per patient). In 32 measurements (13%), only two instead of three landmarks could be identified, mostly due to insufficient visibility of the pubic symphysis. In 57% of cases the initial 2D set-up deviation exceeded the 4 mm action level and a correction was applied. Set-up deviations as calculated by the contour match for all patients and all fractions before and after corrections are shown in Fig. 6-3. The 202 measurements for which the contour match results before and after correction were both available are indicated. The mean values per patient are also indicated. Both systematic and random variations are clearly reduced after the corrections. This is confirmed by the results of the statistical analysis as shown in Table 6-1. Systematic variations (Σ) and random variations (σ) which were 2 to 3 mm before corrections significantly decreased ($p < 0.01$) to < 1 mm and < 2 mm (1 SD) after corrections, respectively.

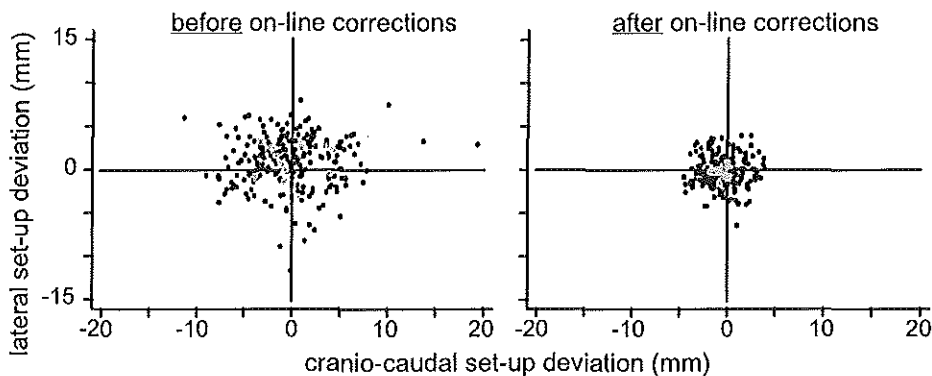


Figure 6-3 Scatter plots of set-up deviations for each fraction before and after the on-line corrections. The gray square dots are the patient means, the black dots the individual measurements for each fraction. The reduction of systematic as well as random set-up position variation after on-line corrections is obvious.

b. Rotations and correlations

The contour match yielded rather small values for in-plane rotations. The overall standard deviations were smaller than 1 degree with extremes less than 4 degrees in all cases. Although there was a relation between the patient diameter in AP direction

and the standard deviations of lateral set-up inaccuracies, the correlations were not significant ($p = 0.09$, $r = 0.47$). Other correlations between diameters and set-up deviations were even less significant.

	M	Σ	σ	ν
Δx (before corrections)	0.9	2.0	2.3	0.7
Δy	-0.2	2.8	3.0	1.3
Δx (after corrections)	-0.2	0.7	1.6	0.5
Δy	-0.5	0.6	1.8	0.3

Table 6-1: The set-up accuracies as determined by the contour match of 14 patients for the pre- and post on-line correction images in left-right (Δx) and cranio-caudal (Δy) direction in mm. For the explanation of M, Σ , σ , and ν see the methods section.

c. Comparison of match methods

For 210 measurements, both the landmark match and the contour match results of the set-up before correction were available. The same technicians (SQ and MS) performed all contour matches, whereas the on-line landmark matches were done by any technician present at the accelerator (under supervision of SQ and MS). Scatter plots of contour match versus landmark match results are shown in Fig. 6-4. The average difference between the two match procedures was 0.3 ± 1.1 mm (1 SD) in the lateral

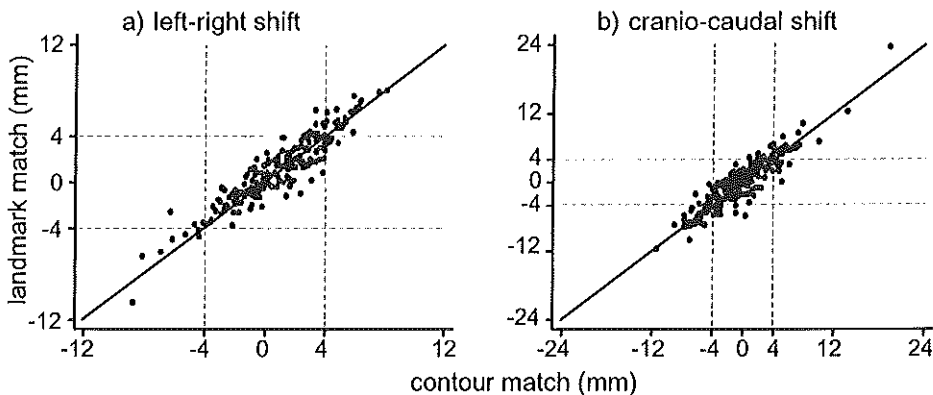


Figure 6-4 Scatter plots of the set-up deviations as measured with the contour match versus the landmark match for left-right (a) and cranio-caudal direction (b). The 4-mm lines are shown to indicate the fractions that have certainly been corrected (the 2D action level was 4 mm). The variation around the ideal one-to-one line immediately indicate that there is some difference between the two match methods.

direction, and 0.4 ± 1.8 mm (1 SD) in the cranio-caudal direction. Both average values are significantly different from zero ($p < 0.01$), which implies that there is a small systematic difference between the two methods; this might be caused by the center-of-mass of the three landmarks, which can be slightly different from that of the contours. The variation in the lateral direction is appropriate, considering that the reproducibility of each method separately is about 0.5 - 1 mm (1 SD). The larger variation in the cranio-caudal direction is probably due to the larger pixel size in that direction (0.8 mm cranio-caudal vs. 0.5 mm lateral at isocenter), and due to the out-of-plane rotations around the left-right axis. Consequently, the match accuracy of the on-line match significantly contributes to the final set-up variation in this direction.

d. Treatment time

The extra treatment time for the on-line procedure per treatment fraction varied from 1-2 minutes if no table translation was required, to 3-5 minutes if a table correction was necessary. Considering a standard treatment time per patient of 10 minutes, this corresponds to an increase in time of 10-20% without and 30-50% with correction. The variation is due to differences in image quality and user experience. The extra treatment time was required for determination of the set-up position (1 min), restart of the accelerator (30 s), and the table correction procedure (2.5 min).

V. Discussion

a. Comparison with previous studies

The measured set-up variation before correction is largest in cranio-caudal direction, which is consistent with previous in-house studies [25,90]. However, particularly the systematic variation in the cranio-caudal direction was already significantly lower ($p = 0.02$) than for the patients in the previously reported mattress study [90], even though set-up technique and accelerator were identical. The average patient obesity was also similar. The extra attention the patients received due to the protocol might already result in better set-up accuracy before correction, especially because only one accelerator and a limited number of technicians were involved in the study. Furthermore, the match technique, e.g. the anatomical structures used for matching, has altered slightly in the course of time. In this study, extra attention has been given to

consequent delineation of the same match structures, which is essential in case of out-of-plane rotations.

Although a significant correlation between patient diameter in AP direction and lateral set-up accuracy has been reported before [117], the low correlation in this study make this diameter a rather weak predictor for set-up accuracy. It is therefore impossible to individualize set-up protocols and PTV margins according to patient diameter.

b. Benefit of on-line set-up correction procedure

As expected, patient set-up was significantly improved using the on-line verification and correction procedure. The 4 mm action level resulted in random variations after correction of 1.5 - 2 mm. Since the systematic variations are reduced to < 1 mm and the margin to cover for geometric variation of the CTV with respect to the beam portals can be approximated by $2\Sigma+0.7\sigma$ [102], a CTV-to-PTV margin for external set-up accuracies of 3 mm will suffice. An even better set-up accuracy can be obtained by decreasing the action level. In principle, the maximum accuracy is limited by the accuracy of matching software and treatment equipment. This will off course yield more corrections and an increase in average treatment time.

Fig. 6-5 shows the dose volume histograms of a patient with a gynecologic tumor planned to a dose of over 60 Gy with

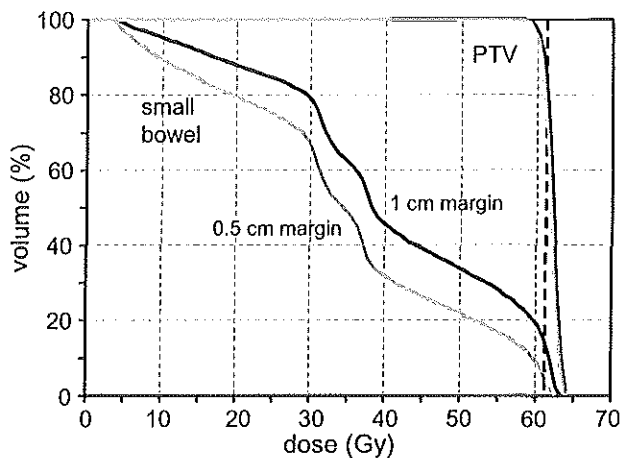


Figure 6-5 Dose volume histograms of a gynecological patient, which show a reduction in small bowel dosage when smaller CTV-to-PTV margins are applied. Until 48.6 Gy the CTV consists of primary tumor region plus elective para-aortic lymph nodes, the boost is given on the primary tumor region only. Use of 5 mm CTV-to-PTV margins (in gray), which is justified if on-line correction are performed, instead of the currently applied 1 cm (in black), reduces the small bowel volume that receives 55 Gy or more to less than 20%.

two different CTV-to-PTV margins: the current clinical margin of 1 cm and a 5 mm margin for on-line corrected patients (the 3 mm is rounded up to include other uncertainties than set-up deviations). With a margin of 5 mm instead of 1 cm, the volume receiving a small bowel dose larger than 55 Gy is reduced from the critical 30% to an acceptable 15%.

c. Extra treatment time

In case of a correction, the extra treatment time was 3 to 5 minutes. During the study, new table settings had to be entered at the treatment console and the patient couch had to be moved accordingly by a technician in the treatment room. However, further automation of the accelerator after the study has enabled fully automatic table corrections within 1 minute. This reduces the overall extra time in case of correction to about 2.5 minutes. Since about half the number of fields had to be corrected, the average extra time per fraction per analyzed field is now about 2 minutes. Because it takes two images to determine the 3D patient set-up, a total of 4 minutes per fraction are maximally needed, which is comparable to most other studies [30,31,39,71,116] and to the routinely used off-line protocol in our institute. Furthermore, elaborate set-up equipment such as mattresses and foot and arm supports also require extra time. One might argue that in most cases the patient set-up technique can be fast and basic as long as on-line corrections can be applied.

d. Recent and future developments

Since we expect that on-line correction of patient set-up (and possibly tumor position) will become an important tool for conformal radiotherapy in the future, we have developed a new portal imaging device especially equipped for on-line applications⁸. The device obtains better quality images with 1 MU than the “old” EPID system with 6 MU. Furthermore, fully automated and fast contour matching will be implemented in the software, which is expected to reduce the total time for on-line corrections to about 1 minute per field. Finally, the image resolution of the new system is significantly improved as well; radioopaque markers can now be visualized, which might be

⁸ Cablon Medical, Leusden, The Netherlands

used to measure and possibly correct the internal CTV position in patients with gynecologic tumors on-line.

e. Combination of off-line and on-line set-up correction protocol

To minimize the current treatment time at the accelerator, a combination of an off-line and on-line protocol is applied for routine patient set-up. Table 1 and previous studies show that the inter-patient variation (v) was rather large for patients with gynecologic tumors. Therefore, initially all patients are treated using the off-line procedure. Only those patients with large random variations, and hence with repeated corrections in the off-line protocol, are entered in the on-line correction protocol. Furthermore, systematic variations can be determined during the course of treatment with the on-line protocol as well; instead of identical corrections each day after 6 MU, table corrections can be applied beforehand (similar to the off-line protocol), which further decreases the treatment time.

VI. Conclusion

The on-line patient set-up correction protocol resulted in a significant improvement of set-up accuracy. This allows for the use of smaller PTVs, which might in turn allow dose escalation while maintaining acceptable complication probabilities for the small bowel. Since we believe that in the future on-line set-up corrections will be used on a more routine basis, the speed and accuracy of the procedure are being improved. Until this has been achieved, a combination of off- and on-line set-up correction protocols will yield optimal set-up accuracy with a minimal workload.

VII. Acknowledgements

The authors wish to acknowledge the Dutch Cancer Society for their financial support which made this research possible (NKB project 92-86).

CHAPTER 7. DETECTION OF INTERNAL ORGAN MOVEMENT IN PROSTATE CANCER PATIENTS USING PORTAL IMAGES

J.C. Stroom, M. Kroonwijk, K.L. Pasma, P.C.M. Koper, E.B. van Dieren, and B.J.M. Heijmen.

Med. Phys. 27, 452-461, 2000

I. Abstract

Previous research has indicated that the appearance of large gas pockets in portal images of prostate cancer patients might imply internal prostate motion. This was verified with simulations based on multiple computed tomography (CT) data for 15 patients treated in supine position. Apart from the planning CT scan, three extra scans were made during treatment. The clinical target volume (CTV) and the rectum were outlined in all scans. Lateral portal images were simulated from the CT data and difference images were calculated for all possible combinations of CT scans; per patient, all scans were used both as reference and repeat scan but gas pockets in the reference scan were removed. Gas pockets in a repeat CT scan then show up as black areas in a difference image. Due to gravity, they normally appear in the ventral part of the rectum. The distances between the ventral edge of a gas pocket in a difference image and the projection of the delineated ventral rectum wall in the reference scan were calculated. These distances were correlated with the “true” rectum wall shifts (determined from direct comparison of the rectum delineations in reference and repeat scan) and with CTV movements determined by three-dimensional chamfer matching. Gas pockets occurred in 23% of cases. Nevertheless, about 50% of rectum wall shifts larger than 5 mm could be detected because they were associated with gas pockets with a large lateral diameter (> 2 cm). Rectum wall shifts with gas pockets in the repeat scan could be accurately detected by the ventral gas pocket edge in the difference images ($r = 0.97$). The shift of the rectum wall as detected from gas pockets also correlated significantly with the anterior-posterior shift of the center-of-mass of the CTV ($r = 0.88$). In conclusion, lateral pelvic images contain more information than the bony structures that are normally used for setup verification. If large gas pockets

appear in those images, a quantitative estimate of the position of prostate and rectum wall can be obtained by determination of the ventral edge of the gas pocket.

II. Introduction

a. Geometrical uncertainties

In order to optimally use the advantages of conformal radiation therapy, the geometrical uncertainties during treatment should be known (to apply adequate safety margins) and minimized where possible (to reduce the size of the safety margins). The geometrical uncertainties consist for a large part of setup errors and internal organ motion. Setup deviations can be derived from portal images acquired during the radiation session. The gray shades in those images reflect the irradiated radiological thicknesses and bony structures are therefore highly visible. Calculation of the position of the bony anatomy relative to the reference situation yields the setup deviation. In the last two decades several electronic portal imaging (EPID) systems have been developed for computerized acquisition and analysis of portal images [2,20,123]. Either off-line [12,14] (before the next treatment session) or on-line [31,105] (while the patient is still on the treatment couch) setup correction protocols can then be used to minimize the setup errors. On-line corrections yield better accuracies than off-line corrections but generally take more time. In recent years, the focus of the research has been shifting toward determination of internal organ movement, especially for prostate cancer patients.

b. Measuring prostate movement

Several methods for measuring internal prostate movement have been reported in the literature. One possibility is to make a number of computed tomography (CT) scans for each patient in the study [29,65,75,103,112,119,128]. In all scans the prostate is delineated, and manual or (semi)automatic registration techniques are used to determine the prostate movement between the different scans. An advantage of this method is that the whole volume is used in the match and that accurate three-dimensional (3D) rotations can be measured. A disadvantage is its cumbersome which at the moment restricts the use of on-line analysis and correction. Some groups are trying to overcome this problem by integrating CT and accelerator [65,72].

Instead of CT, other imaging techniques can be used to visualize the position of the prostate. For instance, ultrasound imaging can be a safe and quick alternative. However, the normal transrectal placement of the ultrasound probe is too uncomfortable to be used for all or many sessions of the radiotherapy treatment. Therefore Troccaz *et al.* decided to place the probe on the belly of the patients at the cost of reduced prostate visibility [113]. They claim however that the image quality is still adequate enough to make on-line corrections of the prostate possible. A clinical study comparing CT and suprapubic ultrasound images has recently been performed with a commercial ultrasound system for prostate localization [64].

A third method to detect internal prostate motion makes use of the aforementioned portal imaging. Since the prostate itself has a similar density as its surroundings, it is not visible in those images. Therefore radio-opaque markers can be implanted in the target volume [7,122]. If the markers can be distinguished in the images, rapid analysis of the prostate position and possible on-line correction can be performed similar to setup corrections. A disadvantage of this invasive procedure is the extra burden for the patient. Furthermore, markers might migrate and since they can only be implanted in the base of the prostate, not all parts of the target volume (like, e.g., the vesicles) can be imaged. Instead of putting radio-opaque markers in the prostate itself, they can also be placed in an urethral catheter [16]. However, side effects of the irradiation inhibit the use of bladder catheters after a few fractions of the irradiation; at the moment this method can only be used for the first few fractions.

c. Indirect detection of prostate movement

Since the prostate is located directly ventral to the rectum, many authors have been able to demonstrate the relation between *rectum volume* and prostate position [29,65, 75,103,112,119]. The correlation coefficients are rather low because other factors like bladder volume are also involved. However, with portal imaging the position of the *ventral rectum wall* might be determined. In routine portal images of pelvic fields, the most visible objects besides bony structures are gas pockets in the rectum. These gas pockets might indicate the position of the ventral rectum wall, which is expected to have a better correlation with the prostate position than the rectum volume. In Fig. 7-1 the rationale behind this correlation is visualized. The beams-eye-view contours of the planned rectum and clinical target volume (CTV) of a prostate cancer patient are superimposed on a lateral portal image that was used for setup verification. The portal image clearly shows a dark spot indicating a gas pocket that extends outside the rec-

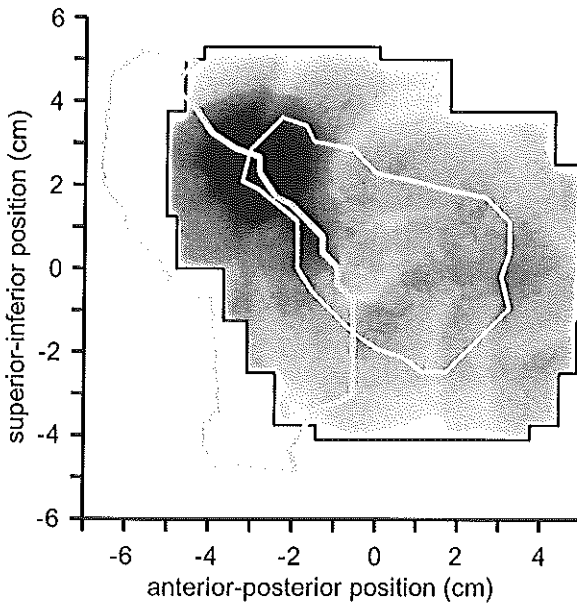


Figure 7-1 The rationale of the use of lateral portal images and naturally occurring gas pockets in the rectum of prostate cancer patients to determine internal rectum and prostate movement relative to the planning CT scan. The beams-eye-view contours of the rectum (thick gray line) and CTV (thin white line) in the planning CT scan of a prostate patient are superimposed on a clinical lateral portal image. The dark spot in the image, indicating a gas pocket, clearly extends outside the delineated rectum. This implies that during treatment the rectum wall, and probably the prostate, were moved in a ventral direction.

tum as delineated in the planning CT scan. This implies that the local rectum wall, and probably the prostate, has moved in a ventral direction. The use of gas pockets to detect internal organ movement would not increase the treatment time because portal images are already routinely acquired for setup verification. Furthermore, it would be a non-invasive technique since rectum gas occurs naturally in prostate cancer patients. Kroonwijk *et al.* already pointed out that gas pockets in portal images can reveal internal organ motion [61]. They did not however specify how this could be used in practice. In this paper, a method for using gas pockets in the rectum for quantitative determination of the rectum wall and prostate position is proposed.

III. Methods and materials

a. Study outline

In order to verify whether gas pockets in clinical portal images can be used to predict the amount of rectum wall and prostate movement, simulations have been performed using previously obtained data of 15 prostate cancer patients of which multiple CT

scans were acquired during treatment [103]. In Fig. 7-2 a schematic outline of the study setup is depicted. First, the four CT data sets per patient were matched and resliced in 3D to remove the setup deviations. Second, portal images for the left lateral beams were simulated from the resliced data sets. In order to automatically detect gas pockets, difference images between two scans were created for all combinations per patient. The gas pocket edges visible in the difference images were subsequently used to estimate the local rectum wall shifts between two scans. Third, the “true” rectum wall shifts between two scans were measured by comparing rectum delineations in reference and repeat CT scan. Corresponding prostate movements were determined from 3D matching. Finally, the rectum wall shifts as determined in the portal images were correlated with the true rectum wall shifts and with the prostate movements.

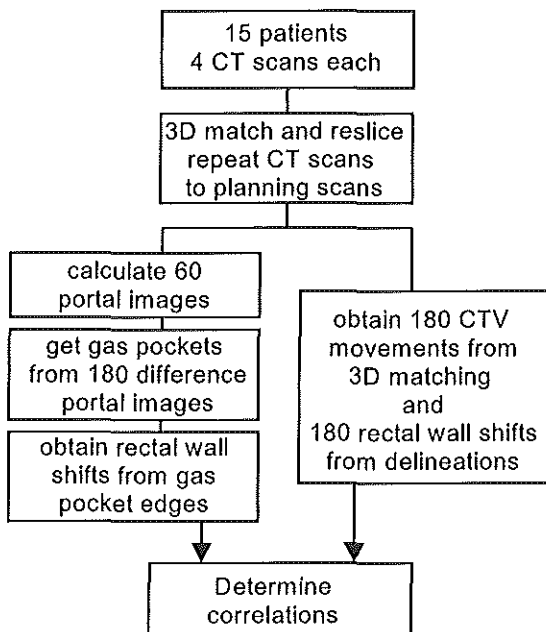


Figure 7-2 Schematic outline of the setup of the study. A multiple CT data set is used to determine the rectum wall shift from gas pockets in simulated portal images. To verify whether this can be used to predict the true rectum wall movement and the prostate movement, the same data set is used to calculate these movements from delineations and by 3D matching, and a correlation analysis is performed. For more detailed information see the section III.

In the following paragraphs, the setup of the study will be explained in more detail.

b. Patient data

In a previous study, the differences in prostate movement between 15 patients treated in supine and 15 in prone position were investigated [103]. The data of the 15 patients

treated in supine position were also used in the current study. For each patient, four CT scans in the supine treatment position were acquired: one planning CT and three repeat CT scans in week two, four, and six of the treatment. Before the planning CT only, mild laxative suppositories were applied to minimize rectum volume. The patients were asked to empty the bladder and subsequently drink half a liter of water before all CT scans (and therapy sessions). In all scans the CTV (i.e., prostate and seminal vesicles), rectum, and bladder were manually contoured by the radiation oncologist. All patients were treated with an isocentric technique using an anterior field and two partly wedged laterally oblique fields; beam intensity modulation was used to minimize the superior-inferior (SI) field length [32]. The patients were treated to a total isocenter dose of 66 Gy, delivered in 2 Gy fractions.

Since we were only interested in the internal organ motion between the different CT scans, the setup differences between the scans of each patient were corrected. 3D chamfer matching was used to match the bony anatomy in the repeat CT scans to their respective planning CT scans. The four CT sets per patient were subsequently aligned to the coordinate system of the planning scan by reslicing of the repeat CT scans. Details of the 3D chamfer matching algorithm and application can be found elsewhere [103,119]. The CT slice distance was 5 mm in most scans and 3 mm in some, the pixel size within the slices was 2 mm in all scans.

c. Radiological thickness images (RTIs)

Portal images for the aligned CT scans were simulated by calculation of radiological thickness images (RTIs). RTIs are a simplified form of digitally reconstructed radiographs, the difference being that a pixel value in a RTI is simply the sum of the electron densities in CT voxels along a ray line. Consequently the unity of the pixel values is easily interpretable: cm radiological thickness. In this study, only the RTIs of the left lateral prostate fields were used because the prostate movements of interest occur predominantly in the sagittal plane; the lateral translation of the prostate is negligible and the rotation around the lateral left-right axis is by far the most significant [29,65,75,103,112,119,128]. The lateral RTIs were obtained for all 60 CT scans with pixel size equal to the CT pixel size (2 mm) at isocenter.

Automatic detection of gas pockets in lateral RTIs appeared to be handicapped by the presence of other pixel gradients in these images due to variation in body contour and due to bony structures. In particular, the femoral heads were frequently in

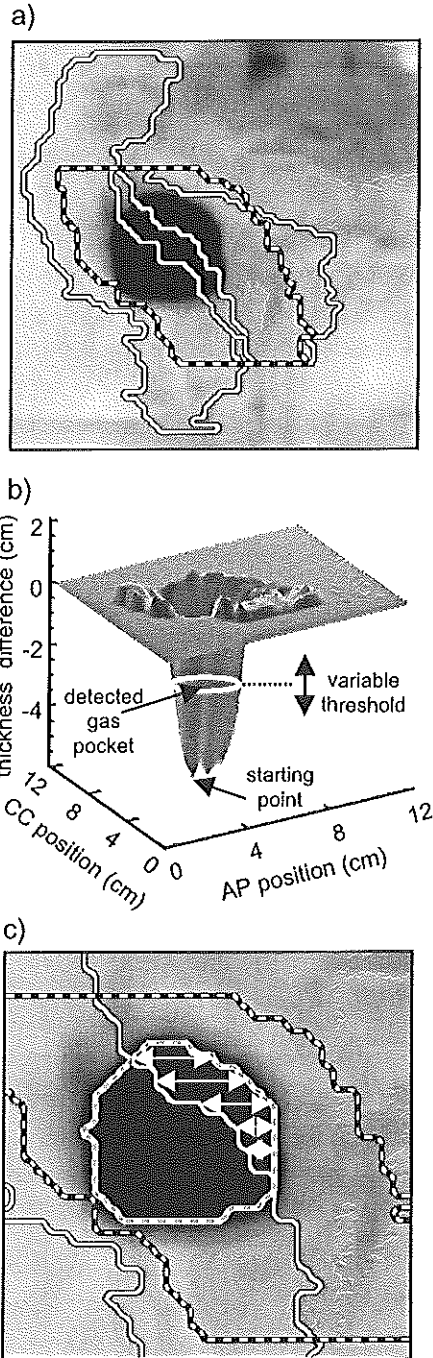
the region where the gas pockets appear. To diminish the effect of these gradients, difference RTIs (dRTIs) were calculated; the pixel values in a reference RTI were subtracted from those in the repeat RTIs. The relatively flat background in the dRTIs made the gas pockets in a repeat CT scan appear as distinctive dark spots. Only the gas pockets in the *repeat* CT scan are useful since they give information about a possible change from the reference situation. To avoid that a gas pocket in the repeat CT scan is neutralized by a similar gas pocket in the reference CT scan, the rectum in the *reference* scan was automatically filled with water-equivalent CT values before calculation of the reference RTI (i.e., gas pockets were removed). In order to study as many internal organ movements as possible, all scans were used both as reference and repeat scan. This yielded 12 dRTIs per patient, i.e., 180 in total. Since every CT scan had two RTIs (one normal and one without gas pockets that was always used as reference), inversion of two CT scans did not automatically yield exactly inverted dRTIs.

d. Rectum wall shift determination using gas pockets in dRTIs

The gas pockets were automatically determined by searching for the dark spots in a specific region in the dRTIs. Since there was some *a priori* knowledge about the location of the gas pockets and because there were some practical restrictions, this region was limited in several ways. All dRTIs were overlaid with the beams eye view (BEV) projections of the corresponding reference prostate and reference rectum. The search region was then composed as follows: (1) The prostate projection was expanded with a two-dimensional (2D) margin of 1.5 cm because that was the usual margin from the CTV to the field borders in our institute. (2) The resulting region was limited in the ventro-dorsal direction because of the known limitations in prostate movement, which is seldom more than 1.5 cm [103]. Therefore, the search region extended maximally 2 cm from the ventral rectum wall projection. (3) In the cranio-caudal direction the search region was limited by the cranial and caudal ends of the prostate; the gas pockets showing up outside that region (i.e. frequently in or near sigmoid or anus) did not have an effect on the prostate motion. An example of the resulting search area is shown in Fig. 7-3a.

Within the search area the minimum pixel value in the dRTI was determined. If the minimum exceeded a certain (thickness) threshold, a gas pocket might have been detected. The extensions of the gas pocket were then determined by searching for all neighboring pixels with values below the threshold, using the position of the

Figure 7-3 Determination of the rectum wall shift in a dRTI. In (a) the construction of the search area (dashed contour) used to find gas pockets in the dRTI from the reference prostate (gray contour) and rectum (white contour) BEV projections is indicated. The search area is limited to the cranio-caudal length of the prostate, and extends 1.5 cm from the dorsal prostate edge and 2.0 cm from the ventral rectum edge. In (b) the gas pocket detection in the same dRTI is illustrated. If the maximum radiological thickness difference in the search area exceeds a user-defined threshold, the position of that maximum is used to start the search for connecting pixel values that also exceed the threshold. In (c) the automatically detected gas pocket is indicated by the lightly dashed contour. The rectum wall shift is estimated as the average AP shift along the cranio-caudal length of the gas pocket, as indicated by the arrows.



minimum as a starting point (see Fig. 7-3b). Hence a selected threshold can be considered as the minimal required lateral dimension of a gas pocket. If the gas pocket in the dRTI was positioned in the outermost cranio-caudal centimeter of the search area and if its size was smaller than about 0.5 cm^2 , the pocket was discarded because there was a high probability that it was an artifact resulting from e.g. an imperfect alignment of bony structures. The applied radiological thickness threshold was varied to find an optimum value; too small thresholds resulted in picking

up too many artifacts in the dRTIs, too large values resulted in the miss of genuine gas pockets. In Fig. 7-3c the detected gas pocket edge, using a threshold of 2 cm, is depicted.

Also indicated in Fig. 7-3c is the method to estimate the local rectum wall shift from the detected gas pocket. Due to gravity, the gas pockets normally appear in the ventral part of the rectum for patients treated in supine position. The ventral edge of the detected gas pocket was therefore expected to correlate with the position of the ventral rectum wall in the repeat CT scan. Consequently, the local rectum wall shift was obtained by calculation of the anterior-posterior (AP) position of the ventral gas pocket wall with respect to the rectum wall position in the reference CT, as is indicated by its BEV projection. To get as much information as possible, average shifts along the horizontal pixel lines in the cranio-caudal reach of the gas pocket were calculated (see Fig. 7-3c). Only the shifts in AP direction were considered because that was the clinically most relevant direction.

e. Rectum wall shift validation

To validate whether the local rectum wall shifts as measured from gas pocket edges in dRTIs, they were correlated with the “true” local rectum wall shifts. The true local rectum wall shifts could be determined from the position of the rectum projection in the repeat CT scan relative to the rectum projection in the reference CT scan. Again the shifts were averaged over all horizontal pixel lines in the cranio-caudal extent of the gas pocket. Correlation coefficients, statistical significance, and the slope of the fit were determined for the relation between rectum wall shifts estimated from gas pocket edges in dRTIs and true rectum wall shifts.

Since all 12 possible dRTIs per patient were used in the correlation, it might seem that some data are counted double, which would falsely improve the statistical significance. However, the dRTIs are determined from subtraction of two images, and since the reference image (A') in this subtraction is different from the original (A) because the gas pockets have been removed, the subtraction image $A-B'$ is not directly correlated to $B-A'$. Similarly, $C-A'$ is not a simple combination of $C-B'$ and $B-A'$. The reference image is only equal to the repeat image when there are no gas pockets in the rectum but in that case they are not counted in the correlation anyway.

f. Prostate shift prediction

Since the prostate normally rests on the rectum and is at the base actually physically connected to it, a measured shift of the ventral rectum edge could well be a predictor of prostate shifts. Therefore the rectum wall shifts derived from gas pockets in dRTIs were also correlated with the AP translations of the center-of-mass (c.m.) of the CTV that were determined in a previous study with chamfer matches [103]. In short, differences in CTV position relative to the bony anatomy between two (not aligned) CT data sets of a patient, were determined by subsequent, 3D chamfer matches of the two CTVs and of the two bony anatomies, followed by a subtraction of the translational and rotational displacements in the bone match from those in the CTV match. Each scan was used as a reference to calculate the prostate position in the three other scans of a patient, which yielded a total of 180 3D prostate translations and rotations, identical to the number of dRTIs. Correlations of the rectum wall shift with the other significant prostate movements (i.e., c.m. translations in cranio-caudal direction and rotations around the lateral axis) and with combinations of those movements were also

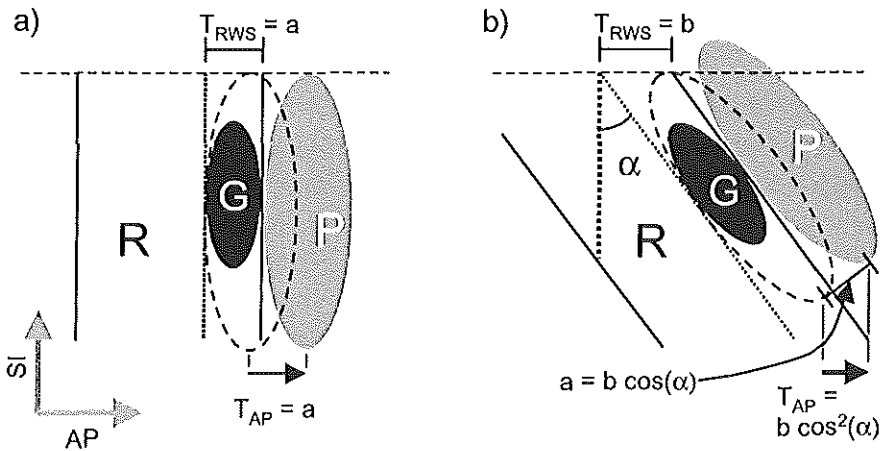


Figure 7-4 A geometrical correction factor for transforming detected rectum wall shifts in AP direction (T_{RWS}) into prostate c.m. shifts in the AP direction (T_{AP}). Schematic illustrations of rectum (R), gas pocket (G), and prostate (P) are depicted in a situation without (a) and with correction (b). Dotted and dashed lines indicate the reference rectum and prostate, respectively; solid lines represent the repeat situation. Since it is assumed that the prostate is physically connected to the rectum, a correction equal to $\cos^2(\alpha)$ is needed if there is an angle (α) between rectum wall and the vertical S axis.

investigated. Since they yielded far less significant results, they are not considered any further in this paper.

In order to use the estimated rectum wall shifts as a predictor for AP prostate c.m. movements, two corrections were applied. First, gas pocket edges never exactly coincide with the *outer* rectum wall edges since the rectum wall itself is not taken into account. Moreover, the choice of the threshold also influenced the exact position where the gas pocket edge was detected; higher threshold values resulted in smaller detected gas pocket cross sections, with ventral gas pocket edges that moved in dorsal direction (see the slope of the gas pocket in Fig. 7-3b). Therefore the differences between gas pocket edges in the dRTI and true rectum edges in the repeat scans were averaged for all data for a specific threshold, and a threshold-dependent correction was applied on the estimated rectum wall shift. Second, in case of an angle α between the reference rectum wall and the SI axis, the rectum wall shift as derived from gas pockets was multiplied by a factor $\cos^2(\alpha)$ to predict the AP shift of the prostate c.m. (see Fig. 7-4). Angles larger than 45° were found, yielding correction factors smaller than 0.5.

g. Efficacy of the method

An obvious drawback of the described method to determine prostate shifts is that it relies on naturally occurring gas pockets; there may be rectum wall and prostate shifts from the reference position without a noticeable gas pocket in the dRTI (i.e., false negatives). The efficacy of the method was therefore investigated by answering the following questions. (1) How often did gas pockets occur? For all 60 scans a sagittal CT reconstruction through the rectum and the center of the prostate was calculated. The number of potentially useful CT scans (of the 60 scans present) was determined by automatic and visual inspection of the presence of gas pockets in the relevant part of the rectum. (2) How many of the occurring gas pockets were actually detected with the described method? Each occurring gas pocket should have been measured in three dRTIs because each repeat scan was combined with three different reference scans. (3) How many and what type of prostate movements could be detected by the method? This was the main question because ultimately the method should detect organ movements. If there is no significant change from the reference situation, there is no need for detection. Therefore, the percentage of prostate movements that was detected by the gas pockets was determined as a function of the size and direction of the prostate translation.

IV. Results

a. Example

In Fig. 7-5 an example of a significant prostate shift between two CT scans of the same patient, due to the appearance of a gas pocket, and its effect on the RTIs is demonstrated. In this figure six images are shown, two normal RTIs (a and b), two RTIs without gas pockets that are used as reference (c and d), and the two dRTIs of these images (e and f). Furthermore the BEV projection of the respective prostates and

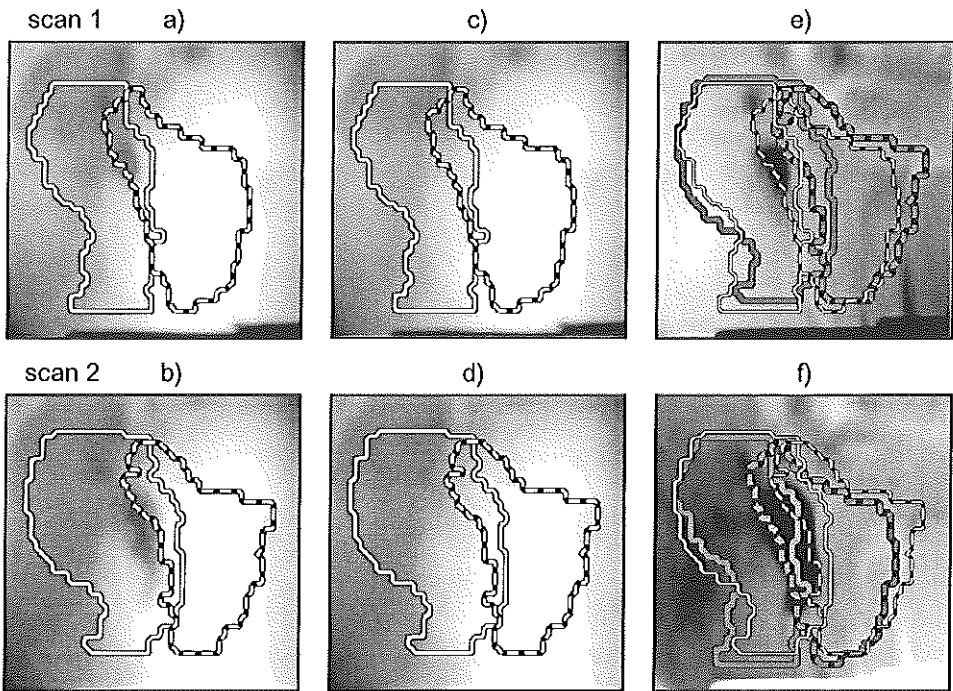


Figure 7-5 Demonstration of the correlation of ventral rectum wall shift, gas pocket appearance, and prostate movement, as measured in radiological thickness images obtained from multiple CT data. For two CT scans, the normal RTIs (a, b), the reference RTIs with the gas pockets removed (c, d), and the dRTIs are indicated. Figure (e) is the difference between (a) and (d), figure (f) is the difference between (b) and (c). BEV projections of rectums are indicated by solid lines, prostates by dashed lines. In the dRTIs the reference organs are indicated by thick gray lines, the repeat organs by thin white lines. There is a good correlation between gas pocket wall, rectum wall and prostate position for both the ventral and the dorsal shift.

rectums are indicated. In scan 2 the rectum is clearly larger than in scan 1. In the difference image with *scan 1 as reference and scan 2 as repeat scan* (f), a rather large gas pocket is visible, the ventral edge of which corresponds nicely to the rectum wall in scan 2. Hence the edge of the gas pocket gives in this case a good estimate of the position of the rectum wall. Moreover, comparing the two prostate projections yields a clear ventral shift of the prostate which in turn corresponds to the rectum wall shift. In the difference image with *scan 2 as reference and scan 1 as repeat scan* (e), a small gas pocket can be discerned. The edge of this pocket also aligns nicely with the corresponding repeat rectum edge of scan 1. So even though the rectum wall and the prostate have moved dorsally, it could be detected by a gas pocket. This example also shows why the gas pockets are removed for calculation of the reference RTIs; if the large gas pocket in scan 2 had not been removed, the small gas pocket from scan 1 would not have been detected in the dRTI.

Also visible in the difference images (e and f) are some black and white shadows that indicate the legs. Although the bony structures in the two CT images were aligned before the generation of the RTIs, it is impossible to align every bone if the legs have moved with respect to the pelvic rim. Hence there are some black areas that might be mistaken for gas pockets if a too low threshold has been selected.

b. Local rectum wall shift

In Fig. 7-6 it is verified whether the relation between the gas pocket edge and rectum wall is always as straightforward as appeared from the example shown in Fig. 7-5. The rectum wall shift as de-

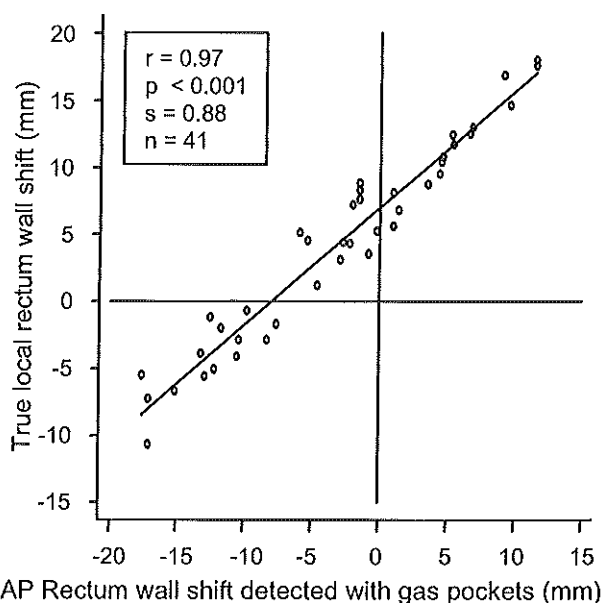


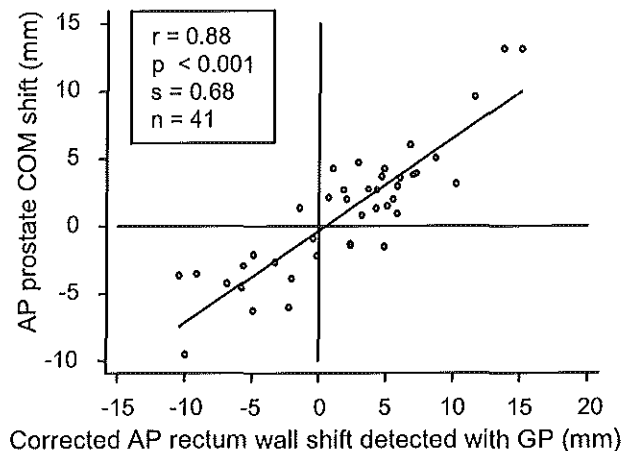
Figure 7-6 The correlation between true local rectum wall shifts and rectum wall shifts detected using gas pockets in dRTIs. Ventral shifts are positive and dorsal shifts negative.

rived from gas pockets in dRTIs is plotted against the true rectum wall shift (see section III.e). The thickness threshold that was used for gas pocket detection was equal to the optimal value of 2 cm. Lower values generated too many false positive gas pockets (i.e., artifacts), which were mostly due to imperfect alignment of the bony structures. Another reason for the occurrence of false positives is that the smaller gas pockets are not always positioned at the ventral border of the rectum but can be found anywhere in the rectum. Threshold values larger than 2 cm reduced the number of detected gas pockets, i.e., increased the number of false negatives, and hence decreased the efficacy of the method. Fig. 7-6 shows an excellent correlation between true and estimated rectum wall shift, $r = 0.97$. This implies that if a gas pocket is detected in a lateral portal image, one is able to predict the position of the local rectum wall with great certainty. The offset of the straight fit from zero is due to the fact that the gas pocket edge is always more dorsal than the true rectum wall due to the thickness of the wall itself and due to the threshold that is used to detect the gas pocket (see section III.f). For a 2 cm threshold, the combination of these two factors yields an offset of about 7.5 mm. The slope of the fit (0.88) is somewhat smaller than the expected value of 1. The number of data points is 41 out of a possible 180, which will be discussed in section III.d.

c. AP prostate center-of-mass movements

The remaining question is whether a rectum wall shift that has been detected with a gas pocket can also predict prostate c.m. movements. In Fig. 7-7 the measured AP

Figure 7-7 The correlation between AP movements of the c.m. of the prostate, as measured with 3D chamfer matching, and rectum wall shifts detected from gas pockets in the dRTIs. The applied rectum wall shifts were corrected for the slope of the rectum wall near the gas pockets and the threshold-dependent distance between the true rectum wall and the gas pocket edge.



rectum wall shifts (with threshold equal to 2 cm) that were corrected for offsets and tilted rectum walls (see section III.f), are plotted versus the corresponding AP translations of the c.m. of the prostate that were measured with 3D chamfer matching. The correlation coefficient of 0.88 is highly significant, the slope of the fit equals 0.68. One possible explanation for the correlation and the slope not being equal to 1 is that the translation of the prostate *center of mass* has been plotted against a local rectum wall shift, and for instance prostatic rotations have not been taken into account. Furthermore, especially near the cranial part of the prostate (where most gas pockets are observed), there can be a relatively wide separation between prostate and rectum, i.e., the rectum may shift locally without moving the prostate with it. This can cause an overestimation of the expected prostate translations and consequently a decrease of the slope in Fig. 7-7. The offset of the linear fit through the data points actually becomes zero, which implies that the threshold dependent correction was adequate.

d. Efficacy of the method

As shown in Figs. 7-6 and 7-7, the number of internal organ motions detected by gas pockets was 41, i.e., 23% from a possible total of 180 internal motions. At maximum, 51 rectum wall shifts might have been detected because visual inspection indicated that 17 of the 60 CT scans contained a gas pocket in the relevant part of the rectum, and each gas pocket should be visible in 3 dRTIs. This implies that the method found 80% of the occurring gas pockets. In Fig. 7-8 the percentage of detected AP prostate movements is plotted as a function of the minimal size of the movement (i.e., data with absolute prostate translations smaller than the minimum are discarded). If all 180 prostate shifts are considered, the previously mentioned 23 percent can be detected. With increasing minimum AP shift, the detection probability increases to about 50%. When only the ventral prostate shifts are considered, 40% (4 of 10) larger than 5 mm was accompanied by a detected gas pocket, and all shifts (3) larger than 7 mm were detected. This trend is due to the fact that large ventral shifts imply a large increase in rectum volume which are more likely to be accompanied by gas pockets. For the same reason, dorsal prostate movements are far less likely to be detected (although they can, see the example in Fig. 7-5). This also explains the asymmetrical shape of Fig. 7-7.

In clinical practice one might be particularly interested in ventral shifts because those imply movement of the rectum, which is the most critical structure for prostate treatments, into the treatment field. In our institute, the ventral shifts dominate because

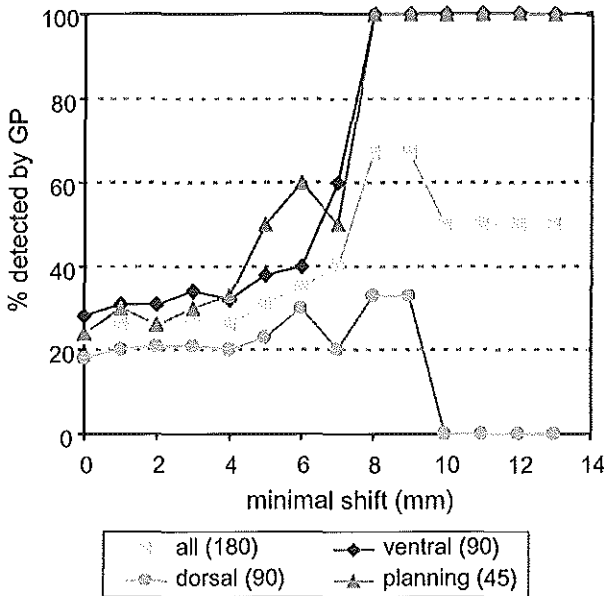


Figure 7-8 Effectiveness of the method described in this paper. The percentage of prostate movements actually detectable by gas pockets is plotted as a function of the minimum AP prostate translation, considering 1) all data, 2) only those data with shifts in the ventral direction, 3) only those data with shifts in dorsal direction, and 4) only those data with the original planning CT as reference. For the latter (clinical) category, about 50% of translations larger than 5 mm was detected.

versa. Pasma *et al.* have indicated that RTIs can be derived from portal images obtained with a charge-coupled device camera based fluoroscopic EPID [84,86]. In short, a transmission image can be obtained from the ratio of a portal image acquired with the patient in the beam and a portal image acquired without the patient in the beam. The raw EPID images are only corrected for the nonlinear response of the system [85]. The radiological thicknesses are then determined from the primary component of the transmission, which is obtained by correcting the transmission image for scatter from the patient onto the EPID.

The clinical images will generally be noisier than the simulated RTIs used in this study, which might make the smaller gas pockets invisible. Furthermore, small

rectum laxation is used before acquisition of the planning CT scan. The detection probability for the 45 shifts with respect to the clinical planning CTs only, confirm this: 50% (3 of 6) of shifts larger than or equal to 5 mm is detected.

V. Discussion

a. Clinical portal images

In order to use clinically acquired portal images to quantify internal organ movement, the “repeat” portal image as acquired with e.g. an EPID should be comparable to the reference image as acquired from the CT data. This implies that the clinical portal dose image should be converted to a reference RTI, or vice

artifacts due to e.g. misalignment of bony structures might occur more frequently in clinical images since matching of bony structures will normally be done in 2D, instead of 3D as in this study. If too many artifacts appear, the threshold for gas pocket detection might have to be increased. This would decrease the number of detected gas pockets, but the largest and most significant ones would still be caught.

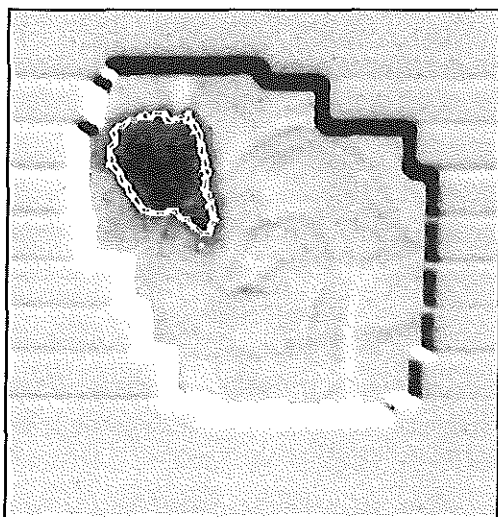


Figure 7-9 Simulation of a dRTI by subtraction of two clinical portal images. A reference portal image without significant gas pockets has been subtracted from the portal image that was shown in Fig. 6-1. The difference image makes the edge of the gas pocket more pronounced, which enables accurate automatic detection of the edge of the gas pocket (dashed line). The bony structures of the images were matched before the subtraction (as is demonstrated by the black and white edges at the field borders), to be able to focus on the internal organ motion only.

Fig. 7-9 shows that the basic principle of the method, determination of a rectum wall in a difference image of two portal images, also works for clinical megavoltage images. The gas pocket clearly shows up as a dark spot in an overall relatively flat difference image which enables automatic detection. This indication is further supported by clinical portal images that were available for 9 of the 15 patients in this study. The 2 patients who showed the most variation in the clinical images due to appearance and disappearance of gas pockets, also had on average the largest gas pocket size in the CT data, and vice versa.

b. Clinical application of the method

The main result of this study is that the position of ventral gas pocket edges as observed in dRTIs (i.e., portal images) with respect to the reference rectum edge, correlates highly significantly with rectum wall shifts (Fig. 7-6) and AP prostate movements (Fig. 7-7). An important advantage of the proposed method for internal organ motion detection over other methods is that it is noninvasive and no extra work

during treatment is required; portal images are already routinely made for setup verification in our institute. In clinical practice, the method seems mainly useful for *on-line* corrections of internal organ positions. In this case the images are acquired using only a small fraction of the total irradiation, which is subsequently interrupted, and the setup deviation is determined by matching the bony structures in the portal image with the reference image. The portal image is then aligned with the reference image and a dRTI is calculated after conversion of the portal dose image into a RTI (see section *V.a*). If a rectum wall shift from the reference situation is found in the dRTI, two different strategies may be followed before the rest of the fraction is given.

The first strategy is aimed at sparing the rectum. Especially the local rectum wall position can be predicted accurately with the described method (see Fig. 7-6). At some (boost) stage of the prostate treatment, sparing of the rectum volume might get a higher priority than adequate irradiation of the tumor [130]. Hence, in case the ventral gas pocket wall in the dRTI indicates that a significant part of the rectum wall has moved into the treatment field, a correction of the table position or the lateral treatment field can be applied so that the rectum wall is better shielded. If the fields are shaped with multileaf collimators, improved local shielding of the rectum might be obtained by moving only some of the leaves.

The second strategy primarily aims at an accurate irradiation of the prostate. If a rectum wall shift is observed, the fit in Fig. 7-7 can be used to determine the probable prostate movement. The isocenter of the lateral beams can then be moved accordingly before the rest of the fraction dose is applied. The prostate position is less accurately predicted than the rectum wall position, but if action is undertaken only in case of larger prostate shifts (e.g., > 5 mm), the benefits will be greater than the damages. Even if only a limited percentage of prostate movements is correctable (i.e., accompanied by gas pockets), the size of the safety margins and treatment portals might be decreased. For instance, the overall standard deviation of the AP prostate c.m. movements for the 45 shifts from the planning CT scans in this study was 3.8 mm. If the detected gas pockets would have been used to correct the prostate position (in 11 cases), this standard deviation would reduce to 2.8 mm. If we assume the planning margin equal to about 2 times this overall standard deviation [102] (and if we neglect other sources of uncertainties), a significant margin reduction of 2 mm would be justified.

c. Possible improvement and future developments

Half of the AP translations of the CTV from the planning CT scan situation larger than or equal to 5 mm were detected with the described method (Fig. 7-8). The laxation before the planning CT scan causes the rectum to be on average relatively empty, so larger shifts will occur if the rectum is full in the repeat situation. Because gas pockets are more likely to be found in fuller rectums, laxation results in a relatively high detection probability of large shifts. In theory there is ample room to improve the detection probability but different treatment protocols or patient instructions which might establish this seem not so realistic. For instance, possible injection of air in the rectum before the irradiation session will seriously complicate the otherwise so simple and quick method. Furthermore it can probably only be considered for a prostate boost at the beginning of the treatment [16], because radiation-induced proctitis may hamper it at the end.

To increase correction accuracy, the correlation of rectum wall shifts with prostate translations might be improved. To try this, additional information from the dRTIs, like size, position, and the extreme pixel values in the gas pockets in dRTIs, was added to the regression analysis but it appeared that at least three variables were needed to really improve the correlation, which prevents a clear physical understanding of what is going on. Alternatively, from sagittal CT reconstructions the gap between prostate and rectum in the cranial part of the prostate in the reference situation can be measured (see section *IV.c*). In the BEV projections of rectum and prostate this is normally not visible because of the frequent overlap of the prostate and rectum. If such a gap exists, a rectum movement in the ventral direction might have a reduced effect on the prostate which may be corrected for. This correction can not however be applied for the inverse (dorsal) rectum wall motions because in clinical practice it seems not possible to predict from one planning CT scan if a gap between rectum and prostate will develop or not.

Before preparing a possible clinical introduction of the method, available clinical portal images will be checked for gas pockets to verify whether they appear as frequent as in the 60 CT scans used in this study (28%). There might for instance be time trends in the gas pocket formation which were not detectable in the limited amount of data points available in this CT based study. Treatment fractions from which multiple portal images have been acquired can be used to determine the likelihood of intratreatment motion. Furthermore, a clinical test of the method should be done by comparing CTV movement as measured by gas pockets with CTV

movement as measured from the same images using radio-opaque markers. Such a study is currently being performed.

d. Conclusion

A quick and noninvasive method has been proposed for determination of internal organ motion in prostate cancer patients with an EPID. A study based on multiple CT data indicated that gas pockets in normal portal images (i.e., without radio-opaque markers, etc.) might be used to detect the ventral rectum wall and the prostate c.m. position. Since not all portal images display gas pockets not all movements can be detected, but the method is especially sensitive for the larger movements; half of the AP shifts larger than or equal to 5 mm and all shifts larger than 7 mm were detected. The accuracy of the method to quantify the AP movement of the prostate and especially the local rectum wall is more than adequate. Hence clinical portal images which were until now only used for setup correction, might also be used to correct field shapes for internal organ motions.

VI. Acknowledgments

The authors wish to thank the revolving fund of the University Hospital Rotterdam and the Dutch Cancer Society (project no. 98-1681) for their financial support. Gert Korevaar, Marjolein van Os, and Marjolein Janssen are gratefully acknowledged for their work in the acquisition and preparation of the CT scans, and Hans de Boer for discussing the subject and for his help in the preparation of some of the figures.

CHAPTER 8. GENERAL DISCUSSION

I. ICRU 50 volumes

This thesis deals with the determination and minimization of safety margins for geometrical inaccuracies that occur during radiotherapy of cancer patients. With the rapidly increasing technological possibilities to closely shape the high dose volume to the tumor, and the increasing interest in dose escalation, taking into account the geometrical uncertainties has become crucial. The International Commission on Radiation Units and Measurements recognized this by publication of ICRU report 50 in which volumes are defined which should be used in the planning of a radiation treatment [54]. The first volume is the gross tumor volume (GTV), which contains the palpable and/or visible tumor. Around the GTV, a margin should be taken for invisible microscopic extension of the tumor, yielding the clinical target volume (CTV). Finally, extra margins should be applied to account for geometrical uncertainties during treatment, yielding a planning target volume (PTV), which should be planned with the prescribed tumor dose in order to ensure an adequate dose coverage of the CTV.

II. Automatic 3D expansion of the CTV to generate a PTV

The ICRU 50 report did however not explain *how* a given margin can be constructed around a 3D volume. In clinical practice, anatomical structures of interest in the 3D CT data sets have always been delineated manually and slice-by-slice. However, to manually draw a 3D margin around an already existing 3D volume is an impossible task. Therefore an algorithm have been developed to perform this task accurately and generally within minutes (see Chapter 2). The algorithm is now used routinely in our institute and implemented in at least one commercial planning system (CadPlan, Varian-Dosetek). Almost simultaneously another group published a different method for 3D margin calculations [15], followed by another algorithm one year later [10]. An algorithm published earlier performed automatic multi-2D margin calculations [5]; slice-by-slice a 2D margin was applied, ignoring the third dimension (perpendicular to the slices), and simulating manual 2D extension of a 3D volume. That the multi-2D approach can lead to serious errors has been shown in Chapter 3; tumor control

probabilities can decrease with 15%. Similar results were found in a comparable study published in the same year [59]. Nevertheless, still not all planning systems are equipped with an algorithm for automatic margin calculation in three dimensions.

III. Calculation and verification of 3D margins based on patient data

How large the CTV-to-PTV margins must actually be was another issue untouched by the ICRU report. To answer this question the typical geometrical uncertainties associated with certain irradiation treatments should be known (see Chapter 5). Therefore many hospitals have investigated the external set-up variations for various tumor sites [11,14,18,22,23,25,26,27,30,31,35,36,39,44,46,50,51,53,78,91,96,101,108,121]. Lately, internal organ movements have also been examined, especially for prostate cancer patients [3,7,9,75,97,99,119,122]. However, complete geometrical uncertainty data of other tumor sites than the prostate (and lung) tumors are rare and should be still acquired. The question is also whether data from different institutes can be shared or if each institute must determine their own database due to large inter-institute differences in patient treatment (see Chapter 5.V.c).

Most of the geometrical uncertainties are reported as standard deviations. Different strategies are applied to obtain margin sizes from these standard deviations. In Chapter 4 such a strategy has been developed by investigation of the effect of geometrical uncertainties on the dose in the CTV for each individual patient. This resulted in margin sizes equal to about 2 times the systematic deviation plus 0.7 times the random deviation, i.e., systematic “every-day” deviations are far more important than random “day-to-day” deviations. Many authors do not really make this distinction. Furthermore, the margins are often based on the probability of the CTV lying outside the PTV (see Fig. 4-1), which ignores the effect of the uncertainties on the dose distribution in the CTV. Consequently they arrive at different margins [4,56,111]. One group that does recognize the difference between systematic and random deviations has recently come to similar recommendations for margin sizes as described in this thesis [118]. They developed a model that calculates PTV-margins based on so-called dose population histograms, which are comparable to the dose probability histograms described in Chapter 4. However, their model is still purely theoretical since it can only be applied for spherically symmetrical CTVs (which implies also that rotations are not taken into account) and with perfectly homogeneous dose distributions.

The dose probability histograms as presented in Chapter 4, show the average dose volume histogram of the CTV of a particular patient for all possible systematic deviations that can occur in the patient group. To include random deviations the dose distribution as calculated by the planning system is convolved with the appropriate uncertainty distributions. An adequate irradiation is only obtained when the final dose probability histogram shows a high uniformity of the CTV dose; i.e., on average a high percentage of the CTV volume (e.g. > 99%) must receive a high dose (e.g. > 95%). There are also groups which calculate the average treatment situation simply by monte-carlo simulations, i.e., multiple sampling from all possible CTV movements using a large data base of measured set-up deviations and internal organ movements [60,73,74]. The advantage is that motion of critical organs and the mutual dependency of different movements can more easily be taken into account. However, monte-carlo simulations are more time consuming than the more analytical solutions (like in Chapter 4), which makes them rather tedious to use in clinical practice. Furthermore, the authors did not present simple margin prescriptions based on their simulations.

IV. Internal Target Volume (ITV)

The ICRU has not yet addressed the two problems mentioned in the previous two paragraphs. However, in a new report that is presented as supplement to ICRU 50, the ICRU 50 nomenclature has been extended with the introduction of the *internal target volume* (ITV) to separate set-up errors from internal organ motion [55]. This concept has originally been proposed by the Nordic Association of Clinical Physicists (NACP) [1]. In their report, the ITV is equal to the CTV plus margins for internal organ motions and delineation uncertainty. The effect of patient and beam set-up deviations is overcome by use of a *Setup Margin*; for each separate beam, margins should be added in the beams-eye-view to ensure that the prescribed dose is delivered to the ITV. The reason of the NACP to distinguish between organ motion and set-up deviation is that two kinds of reference points are used in clinical practice: *External Reference Points* (skin markings, etc.) for patient set-up and *Internal Reference Points* (bony structures) for determination of internal organ motion. Another advantage of the ITV would be its closer resemblance to the CTV, i.e., the planned ITV dose gives a better indication of the CTV dose than the planned PTV dose. However, there are some remarks to be made about the use of an ITV as proposed by the NACP.

First, the practical implementation is not fully clear. The use of Setup Margins for variations in the *beam set-up*, due to uncertainty in field shape for instance,

appears a logical idea. However, the largest setup variations are due to 3D *patient set-up* deviations, especially since the beam setup is almost fully automated in these days. It seems rather cumbersome to adjust the 2D field sizes for 3D motions, instead of applying a 3D margin around the CTV. In order to obtain applicable (simple) Setup Margin sizes, the set-up deviations must be perpendicular to the beams. Since the deviations are usually measured in the three main orthogonal directions, coordinate transformations would be required when gantry angles differ from 0° or 90° . This is not always trivial in case of oblique beams, and even more so when the deviations also contain (out of plane) rotations. According to the NACP, the size of the Setup Margins should ideally be determined iteratively, in such a way that the cumulative dose distribution, i.e., corrected for set-up deviations, still encloses the ITV with the prescribed isodose. (The dose distribution in the ITV only makes sense when the distribution has been corrected for the deviations). This might be accomplished similar to how margins for random uncertainties are calculated in Chapter 4 and by Bel *et al.* [13]; the dose distribution is convolved with the distribution of uncertainties, and the shrinking of the prescribed isodose volume determines the required margin.

Second, there is no need to separate internal organ motions and set up variations completely. If the treatment room coordinate system is taken as the reference, one can consider both geometrical variations as movements of the tumor within the fixed dose distribution delivered by the accelerator in the 3D space. Apart from the second order approximations mentioned in Chapter 4.V.b, the effect of set-up errors on the tumor dose equals the effect of internal organ motions with the same standard deviation. Since the two types of variations are generally independent, their respective standard deviations should be added in quadrature to determine the overall deviations (and hence the margin). If they are added linearly, as suggested by the NACP, the final margin will become too large. The NACP claims that the extra margin is needed to “ensure a save patient set-up using the *external reference points*”. But, although *external* reference points are normally used for set-up, both organ motion and set up movements are analyzed with respect to the same *internal* reference points, i.e., bony structures, so that quadratic summation of the standard deviations seems legitimate.

Third, of major concern in the NACP proposal (and also in the new ICRU report) is that no distinction is made between systematic and random deviations. In Chapter 4 was shown that this distinction is crucial for margin calculations. In the NACP report is suggested that systematic deviations should be corrected by portal imaging, but this is generally only possible for set-up deviations. Furthermore, unless on-line every-day corrections are applied (which will also reduce random deviations), there will always

be some residual systematic deviation left. The NACP also suggests to add the standard deviations of systematic and random deviations in quadrature. As an example, they mention a margin to account for internal organ motion equal to about 0.6 times this total standard deviation. The multiplication factor (0.6) is approximately equal to what was found to be adequate for random deviations (see Chapter 4 and Bel *et al.* [13]), but it is too small to account for systematic deviations, which require a multiplication factor of about 2 (see Chapter 4).

As pointed out before, an advantage of the ITV over the PTV is that the ITV dose is closer to the real CTV dose than the PTV dose because the set-up deviations are accounted for in the expected cumulative dose distribution. This makes it a better predictor of the treatment outcome. However, the effects of internal organ motion and systematic deviations are not yet included. To get a full picture of the expected CTV dose, it might be better to use the dose probability histograms (DPHs) of the CTV as recommended in Chapter 4; the effect of all types of uncertainties on the dose distribution in the CTV is visualized in one graph. If the DPHs are used to adjust the treatment fields iteratively, the PTV becomes just a tool to guide the treatment planner in defining correct field sizes, but the dose in the PTV itself becomes superfluous; the DPHs of the CTV will then be used for prescribing, recording, and reporting radiation treatments. With the clinical introduction of automatic inverse treatment planning, one might even leave out the PTV completely; instead of optimizing the dose distribution in the PTV, the *random-deviation-corrected* dose (i.e., convolved with the distribution of random deviations) in the *coverage probability volume of the CTV for systematic deviations* could be optimized. In this manner, the effects of all geometrical uncertainties might be incorporated during the optimization. This is subject of further study.

V. On-line corrections

The logical solution to avoid complicated margin calculation is to reduce the geometrical uncertainties to negligible values. The obvious way to achieve that is by on-line corrections, i.e., by correcting the tumor position each day before the full irradiation dose is given. For set-up variations, the use of electronic portal imaging for this purpose has been investigated several times, as is described in Chapter 6 and in previous publications [7,30,31,35,39,71,116,117]. The accuracy that can be obtained by this method is in principle limited by the accuracy of the measurements and the corrections, which depends highly on the mechanical accuracy of the accelerator, treatment table, and EPID. The predominant obstacle for routine clinical application is

still the extra time that is required to measure and correct the patient set-up on-line. In our institute, on-line corrections are at the moment only applied when the random set-up variations of a patient appear too large for meaningful application of the off-line correction protocol (see Chapter 6). For these patients, only variations larger than a specific threshold are corrected, which seriously reduces the amount of corrections (and hence extra treatment time), whilst maintaining a very high accuracy (see Chapter 6).

Online correction of internal organ motions is more complicated because the tumor is normally not visible in the portal images that are obtained using the treatment beam. In 0 a method to infer the prostate position from the gas pockets that are visible in routine portal images is presented. The method may be quick and simple but the final accuracy will be limited because internal organ motion is not always accompanied by gas pockets. Clinical studies are needed to evaluate the use of this method. At the cost of an extra burden for the patient, radio-opaque markers can be implanted in the tumor to increase the visibility of the prostate [7,16,122]. Other imaging modalities like ultrasound [64,113] or CT [65,72] may also be applied. Ultrasound has the advantage of being quick and easy to apply, whereas CT scans display a better image quality, but at the moment these techniques are still in the experimental phase. However, development of accurate and easy-to-use tools for on-line detection and correction of tumor position would lead to significant reductions in safety margins with new possibilities for dose escalation.

VI. Future directions

Apart from further improvement of on-line correction procedures, some other hot-topics concerning geometrical uncertainties in radiotherapy are the following: measurement and correction of rotations, the measurement and minimization of intra-treatment variations, the incorporation of biological models and critical organ motion to determine treatment margins, and the accurate delineation of the target volumes. Some discussion on these issues is supplied in the next sections

a. Rotations

For patients treated in the pelvic area, rotational variations in internal tumor position can be up to 20° , see Chapter 5 and van Herk *et al.* [119]. The external set-up of

patients with head and neck tumors can be rotated up to 10° with respect to the reference position [40]. The measurement of rotational set-up deviations in portal images can normally only be performed within the plane of the portal image. If serious out-of-plane rotations occur, the bony structures will project differently in the portal image and will not match with the reference image anymore. Only sophisticated software can provide the 3D rotations from 2D portal images, and at least 2 portal images are required to match them with the 3D CT data sets [41]. Internal rotations have up till now mainly been measured in patients with prostate cancer. Since the principal rotation axis appears to be perpendicular to the sagittal plane, in principle one sagittal image through the prostate is sufficient to establish the rotation. Once the typical rotations are known, they can be used to determine the CTV-to-PTV margin (see Chapter 4). It gets more complicated when parts of the CTV can rotate with respect to each other. For gynecological tumors, the primary tumor region that is located within the pelvic bone can rotate with respect to the elective lymph nodes that lie along the spinal cord. In that case one might have to split the CTV in two, determine separate margins for both parts, and combine the resulting volume into one PTV.

Instead of applying safety margins, one might try to correct for rotational variations, either on-line or off-line. It is however more difficult to handle rotations than translations, which are corrected by shifting the treatment table. In-plane rotations are also relatively easy to correct; if the rotation axis is in the same direction as the beam axis, the rotation can be corrected by rotating the collimator if one is careful to use the same rotation axis in the correction as in the measurement. Normally however, multiple beams are used from different directions. In theory, all possible tumor rotations can be covered by combinations of rotations of collimator, gantry and treatment table. In practice, this can imply unacceptable changes in treatment geometry. Consequently, a table has been developed which can tilt and roll within a range of $\pm 4^\circ$ [48]. The range may be too small in some cases, but larger rotations of the table might cause a change in the patient anatomy (or worse). Therefore, the general solution is to correct rotations by translations, aligning especially those structures with the highest priority (often close to the isocenter). The residual rotational variation must then be included in the PTV margins (see Chapter 4).

b. Intra-treatment variations

Another subject currently under investigation is the minimization of the effect of intra-treatment variations, i.e., tumor movement during one radiation session. Although this

can in principle be considered as a random variation (if the reference position is equal to the average intra-treatment position), which contributes relatively little to the PTV margin (see Chapter 4), the amplitudes for internal organ motion due to breathing can be over a centimeter [8]. Furthermore, combination of intra-treatment motion of the target with intra-treatment variation of the field shape, as happens with dynamic multi leaf collimation, can yield serious over- and underdosages [127]. Therefore, especially for treatment of tumors in the upper torso new equipment is being developed to account for this movement, either by automatically turning the accelerator on and off at specific moments in the normal breathing cycle [62], or by artificially controlling the breathing cycle during treatment by interrupting the air supply [124]. The former method is still in the experimental phase and the latter method seems quite a burden for the patient. It is therefore not clear whether these techniques will be routinely used in the future. Although the treatments in the thorax region are most likely to display significant intra-treatment motion, recently MR imaging has been used to demonstrate prostate movement during one treatment [83]. Because control of the tumor position seems not possible for the prostate as for lung tumors, the intra-treatment motion will remain even in case of on-line tumor position correction, and should be included in the PTV margins as being random variations.

c. Biological modelling

The criteria that were used in the margin calculation procedure described in Chapter 4, were based on geometrical considerations; the field sizes should be such that on average a sufficiently homogeneous dose is delivered to the CTV. However, the clinical value of a treatment might be scored better using biological models that try to predict the tumor control probability (TCP) and normal tissue complication probabilities (NTCP) from the calculated dose distributions in tumor and critical organs, respectively. In theory, margin calculation could be based on TCP and NTCP as well. The problem with these parameters is however that they are not yet reliable enough. Especially for the NTCP, more clinical studies are needed to justify their use. In inverse radiotherapy treatment planning a similar discussion is going on. There is much controversy about whether radiobiological models can already be used or if the optimization should still be based on dose and volume criteria only [19,21].

If the CTV-to-PTV margin that yields an optimal radiobiological effect is to be calculated, a combination of TCP and NTCPs must be optimized. This poses the question of how the probability of tumor control should be compared to the probab-

ity of serious complications. To some extent, this comparison will always be arbitrary but there seems to be some consensus about a quantity called P^+ which unites the TCP and NTCPs for all critical organs in a simple manner [21]. When determining margins, the position variation of the critical organs should ideally be taken into account as well. However, critical organs like bladder and rectum can, apart from moving around, also vary significantly in shape. Several groups have started to develop models to describe these variations [74,125].

d. Delineation uncertainty reduction

Concerning reduction of uncertainties in radiotherapy, probably the largest progress to be made is in accurate determination of the CTV borders. Due to the insufficient visibility in the diagnostic images of these borders (and especially the microscopic spread), there can be significant variation in delineation. This uncertainty has not been addressed in this thesis so far because it is somewhat different from organ motion or set-up deviation; there is uncertainty in *size* instead of *position* of the CTV. Furthermore, the delineation accuracy can be very anisotropic due to variations in surrounding tissues. However, since tumor delineation is performed only during planning, possible errors are systematic (i.e., influencing all treatment fractions) and should not be ignored. Variances in delineation might therefore somehow be added to the variances of the systematic set-up deviations and organ motions [1]. Nevertheless, at the moment few people explicitly include these uncertainties when establishing margins.

CT is the standard imaging modality used to obtain 3D patient data for radiation treatment planning. CT has the advantage that Hounsfield units of the CT are easily converted into electron densities, which are required for adequate dose calculation. Unfortunately, not all tumors are clearly visible in these images because the tumor can have similar electron densities as its surroundings; for instance, it can be very hard to distinguish the border between bladder and prostate in CT images. Many investigations have been performed to determine the variability in tumor delineation, especially for prostate cancer. Local differences between physicians or between the same physician at different times can exceed 1 cm [24,37,68,100,115,131].

To increase the delineation accuracy many groups have investigated the use of other image modalities like MRI, SPECT or ultrasound to find the real tumor borders [6,33,58,76,92,93]. Since these images are not suitable for treatment planning

(because direct information about electron densities is lacking), delineations in the images should be transferred to CT images to be able to continue the planning. This has stimulated a whole new field of 3D matching of images of different modalities [58,88,110,120]. But, whatever modality is used, there will always be some inter-physician variability. To avoid this, software should be generated to contour the different organs automatically. This would also reduce the time that is required for planning considerably, but until now the only contours that can be drawn automatically are around high contrast organs like bones or patient skin.

REFERENCES

1. P. Aaltonen, A. Brahme, I. Lax, S. Levernes, I. Naslund, J.B. Reitan, and I. Turesson, "Specification of dose delivery in radiation therapy. Recommendation by the Nordic Association of Clinical Physics (NACP)," *Acta Oncol.* **36** (Suppl 10), 1-32 (1997).
2. V.G. Althof, J.C. de Boer, H. Huizenga, J.C. Stroom, A.G. Visser, and B.N. Swanenburg, "Physical characteristics of a commercial electronic portal imaging device," *Med. Phys.* **23**, 1845-1855 (1996).
3. V.G. Althof, C.J. Hoekstra, and H.J. te Loo, "Variation in prostate position relative to adjacent bony anatomy," *Int. J. Radiat. Oncol. Biol. Phys.* **34**, 709-715 (1996).
4. J.A. Antolak and I.I. Rosen, "Planning target volumes for radiotherapy: how much margin is needed?" *Int. J. Radiat. Oncol. Biol. Phys.* **44**, 1165-1170 (1999).
5. M. Austin-Seymour, I. Kalet, J. McDonald, S. Kromhout-Schiro, J. Jacky, S. Hummel, and J. Unger, "Three dimensional planning target volumes: a model and a software tool," *Int. J. Radiat. Oncol. Biol. Phys.* **33**, 1073-1080 (1995).
6. K.R. Badiozamani, K. Wallner, W. Cavanagh, and J. Blasko, "Comparability of CT-based and TRUS-based prostate volumes," *Int. J. Radiat. Oncol. Biol. Phys.* **43**, 375-378 (1999).
7. J.M. Balter, H.M. Sandler, K. Lam, R.L. Bree, A.S. Lichter, and R.K. Ten Haken, "Measurement of prostate movement over the course of routine radiotherapy using implanted markers," *Int. J. Radiat. Oncol. Biol. Phys.* **31**, 113-118 (1995).
8. J.M. Balter, R.K. Ten Haken, T.S. Lawrence, K.L. Lam, and J.M. Robertson, "Uncertainties in CT-based radiation therapy treatment planning associated with patient breathing," *Int. J. Radiat. Oncol. Biol. Phys.* **36**, 167-174 (1996).
9. C.J. Beard, P. Kijewski, M. Bussiere, R. Gelman, D. Gladstone, K. Shaffer, M. Plunkett, P. Castello, and C.N. Coleman, "Analysis of prostate and seminal vesicle motion: implications for treatment planning," *Int. J. Radiat. Oncol. Biol. Phys.* **34**, 451-458 (1996).
10. J.L. Bedford and G.S. Shentall, "A digital method for computing target margins in radiotherapy," *Med. Phys.* **25**, 224-231 (1998).
11. A. Bel, R. Keus, R.E. Vijlbrief, and J.V. Lebesque, "Setup deviations in wedged pair irradiation of parotid gland and tonsillar tumors, measured with an electronic portal imaging device," *Radiother. Oncol.* **37**, 153-159 (1995).
12. A. Bel, M. van Herk, H. Bartelink, and J.V. Lebesque, "A verification procedure to improve patient set-up accuracy using portal images," *Radiother. Oncol.* **29**, 253-260 (1993).
13. A. Bel, M. van Herk, and J.V. Lebesque, "Target margins for random geometrical treatment uncertainties in conformal radiotherapy," *Med. Phys.* **23**, 1537-1545 (1996).

14. A. Bel, P.H. Vos, P.T. Rodrigus, C.L. Creutzberg, A.G. Visser, J.C. Stroom, and J.V. Lebesque, "High-precision prostate cancer irradiation by clinical application of an offline patient setup verification procedure, using portal imaging," *Int. J. Radiat. Oncol. Biol. Phys.* **35**, 321-332 (1996).
15. R. Belshi, D. Pontvert, J.C. Rosenwald, and G. Gaboriaud, "Automatic three-dimensional expansion of structures applied to determination of the clinical target volume in conformal radiotherapy," *Int. J. Radiat. Oncol. Biol. Phys.* **37**, 689-696 (1997).
16. P. Bergstrom, P.O. Lofroth, and A. Widmark, "High-precision conformal radiotherapy (HPCRT) of prostate cancer- a new technique for exact positioning of the prostate at the time of treatment," *Int. J. Radiat. Oncol. Biol. Phys.* **42**, 305-311 (1998).
17. J. Bijhold, J.V. Lebesque, A.A. Hart, and R.E. Vijlbrief, "Maximizing setup accuracy using portal images as applied to a conformal boost technique for prostatic cancer," *Radiother. Oncol.* **24**, 261-271 (1992).
18. R. Bissett, K. Leszczynski, S. Loose, S. Boyko, and P. Dunscombe, "Quantitative vs. subjective portal verification using digital portal images," *Int. J. Radiat. Oncol. Biol. Phys.* **34**, 489-495 (1996).
19. T. Bortfeld, "Optimized planning using physical objectives and constraints," *Semin. Radiat. Oncol.* **9**, 20-34 (1999).
20. A.L. Boyer, L. Antonuk, A. Fenster, M. van Herk, H. Meertens, P. Munro, L.E. Reinstein, and J. Wong, "A review of electronic portal imaging devices (EPIDs)," *Med. Phys.* **19**, 1-16 (1992).
21. A. Brahme, "Optimized radiation therapy based on radiobiological objectives," *Semin. Radiat. Oncol.* **9**, 35-47 (1999).
22. R.W. Byhardt, J.D. Cox, A. Hornburg, and G. Liermann, "Weekly localization films and detection of field placement errors," *Int. J. Radiat. Oncol. Biol. Phys.* **4**, 881-887 (1978).
23. D.L. Carter, L.B. Marks, and G.C. Bentel, "Impact of setup variability on incidental lung irradiation during tangential breast treatment," *Int. J. Radiat. Oncol. Biol. Phys.* **38**, 109-115 (1997).
24. L.F. Cazzaniga, M.A. Marinoni, A. Bossi, E. Bianchi, E. Cagna, D. Cosentino, L. Scandolaro, M. Valli, and M. Frigerio, "Interphysician variability in defining the planning target volume in the irradiation of prostate and seminal vesicles," *Radiother. Oncol.* **47**, 293-296 (1998).
25. C.L. Creutzberg, V.G. Althof, M.D. de Hoog, A.G. Visser, H. Huizenga, A. Wijnmaalen, and P.C. Levendag, "A quality control study of the accuracy of patient positioning in irradiation of pelvic fields," *Int. J. Radiat. Oncol. Biol. Phys.* **34**, 697-708 (1996).
26. C.L. Creutzberg, V.G. Althof, H. Huizenga, A.G. Visser, and P.C. Levendag, "Quality assurance using portal imaging: the accuracy of patient positioning in irradiation of breast cancer," *Int. J. Radiat. Oncol. Biol. Phys.* **25**, 529-539 (1993).

27. C.L. Creutzberg, A.G. Visser, P.M. De Porre, J.H. Meerwaldt, V.G. Althof, and P.C. Levendag, "Accuracy of patient positioning in mantle field irradiation," *Radiother. Oncol.* **23**, 257-264 (1992).
28. J.M. Crook, Y. Raymond, D. Salhani, H. Yang, and B. Esche, "Prostate motion during standard radiotherapy as assessed by fiducial markers," *Radiother. Oncol.* **37**, 35-42 (1995).
29. L.A. Dawson, K. Mah, E. Franssen, and G. Morton, "Target position variability throughout prostate radiotherapy," *Int. J. Radiat. Oncol. Biol. Phys.* **42**, 1155-1161 (1998).
30. W. De Neve, F. Van den Heuvel, M. Coghe, D. Verellen, M. De Beukeleer, A. Roelstraete, P. De Roover, L. Thon, and G. Storme, "Interactive use of on-line portal imaging in pelvic radiation," *Int. J. Radiat. Oncol. Biol. Phys.* **25**, 517-524 (1993).
31. W. De Neve, F. Van den Heuvel, M. De Beukeleer, M. Coghe, L. Thon, P. De Roover, M. Van Lancker, and G. Storme, "Routine clinical on-line portal imaging followed by immediate field adjustment using a tele-controlled patient couch," *Radiother. Oncol.* **24**, 45-54 (1992).
32. M.L. Dirkx, B.J. Heijmen, G.A. Korevaar, M.J. van Os, J.C. Stroom, P.C. Koper, and P.C. Levendag, "Field margin reduction using intensity-modulated x-ray beams formed with a multileaf collimator," *Int. J. Radiat. Oncol. Biol. Phys.* **38**, 1123-1129 (1997).
33. D.F. Dubois, B.R. Prestidge, L.A. Hotchkiss, J.J. Prete, and W.S. Bice, Jr., "Intraobserver and interobserver variability of MR imaging- and CT-derived prostate volumes after transperineal interstitial permanent prostate brachytherapy," *Radiology* **207**, 785-789 (1998).
34. B. Emami, J. Lyman, A. Brown, L. Coia, M. Goitein, J.E. Munzenrider, B. Shank, L.J. Solin, and M. Wesson, "Tolerance of normal tissue to therapeutic irradiation," *Int. J. Radiat. Oncol. Biol. Phys.* **21**, 109-122 (1991).
35. A. Ezz, P. Munro, A.T. Porter, J. Battista, D.A. Jaffray, A. Fenster, and S. Osborne, "Daily monitoring and correction of radiation field placement using a video-based portal imaging system: a pilot study," *Int. J. Radiat. Oncol. Biol. Phys.* **22**, 159-165 (1992).
36. D.A. Fein, K.P. McGee, T.E. Schultheiss, B.L. Fowble, and G.E. Hanks, "Intra- and interfractional reproducibility of tangential breast fields: a prospective on-line portal imaging study," *Int. J. Radiat. Oncol. Biol. Phys.* **34**, 733-740 (1996).
37. C. Fiorino, M. Reni, A. Bolognesi, G.M. Cattaneo, and R. Calandrino, "Intra- and inter-observer variability in contouring prostate and seminal vesicles: implications for conformal treatment planning," *Radiother. Oncol.* **47**, 285-292 (1998).
38. E. Fontenla, C.A. Pelizzari, and G.T. Chen, "Implications of 3-dimensional target shape and motion in aperture design," *Med. Phys.* **23**, 1431-1441 (1996).
39. J. Gildersleve, D.P. Deamaley, P.M. Evans, M. Law, C. Rawlings, and W. Swindell, "A randomised trial of patient repositioning during radiotherapy using a megavoltage imaging system," *Radiother. Oncol.* **31**, 161-168 (1994).
40. K.G. Gilhuijs, K. Drukker, A. Touw, P.J. van de Ven, and M. van Herk, "Interactive three dimensional inspection of patient setup in radiation therapy using digital portal

- images and computed tomography data," *Int. J. Radiat. Oncol. Biol. Phys.* **34**, 873-885 (1996).
41. K.G. Gilhuijs, P.J. van de Ven, and M. van Herk, "Automatic three-dimensional inspection of patient setup in radiation therapy using portal images, simulator images, and computed tomography data," *Med. Phys.* **23**, 389-399 (1996).
42. M. Goitein, "Nonstandard deviations," *Med. Phys.* **10**, 709-711 (1983).
43. M. Goitein, "Calculation of the uncertainty in the dose delivered during radiation therapy," *Med. Phys.* **12**, 608-612 (1985).
44. S.E. Griffiths and R.G. Pearcey, "The daily reproducibility of large, complex-shaped radiotherapy fields to the thorax and neck," *Clin. Radiol.* **37**, 39-41 (1986).
45. J. Hanley, M.A. Lumley, G.S. Mageras, J. Sun, M.J. Zelefsky, S.A. Leibel, Z. Fuks, and G.J. Kutcher, "Measurement of patient positioning errors in three-dimensional conformal radiotherapy of the prostate," *Int. J. Radiat. Oncol. Biol. Phys.* **37**, 435-444 (1997).
46. C.F. Hess, R.D. Kortmann, R. Jany, A. Hamberger, and M. Bamberg, "Accuracy of field alignment in radiotherapy of head and neck cancer utilizing individualized face mask immobilization: a retrospective analysis of clinical practice," *Radiother. Oncol.* **34**, 69-72 (1995).
47. P.G. Hoel, *Introduction to Mathematical Statistics*, 279-300, John Wiley & Sons, New York (1984).
48. D.C. Hornick, D.W. Litzenberg, K.L. Lam, J.M. Balter, J. Hetrick, and R.K. Ten Haken, "A tilt and roll device for automated correction of rotational setup errors," *Med. Phys.* **25**, 1739-1740 (1998).
49. R.A. Huddart, A. Nahum, A. Neal, M. McLean, D.P. Dearnaley, M. Law, J. Dyer, and D. Tait, "Accuracy of pelvic radiotherapy: prospective analysis of 90 patients in a randomised trial of blocked versus standard radiotherapy," *Radiother. Oncol.* **39**, 19-29 (1996).
50. H. Huizenga, P.C. Levendag, P.M. De Porre, and A.G. Visser, "Accuracy in radiation field alignment in head and neck cancer: a prospective study," *Radiother. Oncol.* **11**, 181-187 (1988).
51. M. Hulshof, L. Vanuytsel, W. Van den Bogaert, and E. van der Schueren, "Localization errors in mantle-field irradiation for Hodgkin's disease," *Int. J. Radiat. Oncol. Biol. Phys.* **17**, 679-683 (1989).
52. M.A. Hunt, T.E. Shultheiss, G. Desobry, and G.E. Hanks, "Convolving set-up uncertainties with dose distributions (Abstr.)," *Med. Phys.* **20**, 929 (1993).
53. M.A. Hunt, G.J. Kutcher, C. Burman, D. Fass, L. Harrison, S. Leibel, and Z. Fuks, "The effect of setup uncertainties on the treatment of nasopharynx cancer," *Int. J. Radiat. Oncol. Biol. Phys.* **27**, 437-447 (1993).
54. International Commission on Radiation Units and Measurements. *ICRU report 50: Prescribing, recording, and reporting photon beam therapy*, p.23, ICRU Publications, Bethesda MD (1993).

-
55. International Commission on Radiation Units and Measurements. *ICRU Report 62: Prescribing, recording, and reporting photon beam therapy (Supplement to ICRU Report 50)*, p.23, Bethesda, MD (1999).
56. D. Jones, M.D. Hafermann, J.W. Rieke, and S.S. Vermeulen, "An estimate of the margin required when defining blocks around the prostate," *Br. J. Radiol.* **68**, 740-746 (1995).
57. S.M. Jones and A.L. Boyer, "Investigation of an FFT-based correlation technique for verification of radiation treatment setup," *Med. Phys.* **18**, 1116-1125 (1991).
58. K. Kagawa, W.R. Lee, T.E. Schultheiss, M.A. Hunt, A.H. Shaer, and G.E. Hanks, "Initial clinical assessment of CT-MRI image fusion software in localization of the prostate for 3D conformal radiation therapy," *Int. J. Radiat. Oncol. Biol. Phys.* **38**, 319-325 (1997).
59. V.S. Khoo, J.L. Bedford, S. Webb, and D.P. Dearnaley, "Comparison of 2D and 3D algorithms for adding a margin to the gross tumor volume in the conformal radiotherapy planning of prostate cancer," *Int. J. Radiat. Oncol. Biol. Phys.* **42**, 673-679 (1998).
60. J.H. Killoran, H.M. Kooy, D.J. Gladstone, F.J. Welte, and C.J. Beard, "A numerical simulation of organ motion and daily setup uncertainties: implications for radiation therapy," *Int. J. Radiat. Oncol. Biol. Phys.* **37**, 213-221 (1997).
61. M. Kroonwijk, K.L. Pasma, S. Quint, P.C. Koper, A.G. Visser, and B.J. Heijmen, "In vivo dosimetry for prostate cancer patients using an electronic portal imaging device (EPID); demonstration of internal organ motion," *Radiother. Oncol.* **49**, 125-132 (1998).
62. H.D. Kubo and B.C. Hill, "Respiration gated radiotherapy treatment: a technical study," *Phys. Med. Biol.* **41**, 83-91 (1996).
63. G.J. Kutcher, G.S. Mageras, and S.A. Leibel, "Control, correction, and modeling of setup errors and organ motion," *Semin. Radiat. Oncol.* **5**, 134-145 (1995).
64. J. Lattanzi, S. McNeeley, W. Pinover, E. Horwitz, I. Das, T.E. Schultheiss, and G.E. Hanks, "A comparison of daily CT localization to a daily ultrasound-based system in prostate cancer," *Int. J. Radiat. Oncol. Biol. Phys.* **43**, 719-725 (1999).
65. J. Lattanzi, S. McNeely, A. Hanlon, I. Das, T.E. Schultheiss, and G.E. Hanks, "Daily CT localization for correcting portal errors in the treatment of prostate cancer," *Int. J. Radiat. Oncol. Biol. Phys.* **41**, 1079-1086 (1998).
66. J.V. Lebesque, A.M. Bruce, A.P. Kroes, A. Touw, R.T. Shouman, and M. van Herk, "Variation in volumes, dose-volume histograms, and estimated normal tissue complication probabilities of rectum and bladder during conformal radiotherapy of T3 prostate cancer," *Int. J. Radiat. Oncol. Biol. Phys.* **33**, 1109-1119 (1995).
67. J. Leong, "Implementation of random positioning error in computerised radiation treatment planning systems as a result of fractionation," *Phys. Med. Biol.* **32**, 327-334 (1987).
68. G. Leunens, J. Menten, C. Weltens, J. Verstraete, and E. van der Schueren, "Quality assessment of medical decision making in radiation oncology: variability in target volume delineation for brain tumours," *Radiother. Oncol.* **29**, 169-175 (1993).

69. B.K. Lind, P. Kallman, B. Sundelin, and A. Brahme, "Optimal radiation beam profiles considering uncertainties in beam patient alignment," *Acta Oncol.* **32**, 331-342 (1993).
70. T. LoSasso, C.S. Chui, G.J. Kutcher, S.A. Leibel, Z. Fuks, and C.C. Ling, "The use of a multi-leaf collimator for conformal radiotherapy of carcinomas of the prostate and nasopharynx," *Int. J. Radiat. Oncol. Biol. Phys.* **25**, 161-170 (1993).
71. K. Luchka and S. Shalev, "Pelvic irradiation of the obese patient: a treatment strategy involving megavoltage simulation and intratreatment setup corrections," *Med. Phys.* **23**, 1897-1902 (1996).
72. T.R. Mackie, T. Holmes, S. Swerdloff, P. Reckwerdt, J.O. Deasy, J. Yang, B. Paliwal, and T. Kinsella, "Tomotherapy: a new concept for the delivery of dynamic conformal radiotherapy," *Med. Phys.* **20**, 1709-1719 (1993).
73. G.S. Mageras, Z. Fuks, S.A. Leibel, C.C. Ling, M.J. Zelefsky, H.M. Kooy, M. van Herk, and G.J. Kutcher, "Computerized design of target margins for treatment uncertainties in conformal radiotherapy," *Int. J. Radiat. Oncol. Biol. Phys.* **43**, 437-445 (1999).
74. G.S. Mageras, G.J. Kutcher, S.A. Leibel, M.J. Zelefsky, E. Melian, R. Mohan, and Z. Fuks, "A method of incorporating organ motion uncertainties into three-dimensional conformal treatment plans," *Int. J. Radiat. Oncol. Biol. Phys.* **35**, 333-342 (1996).
75. E. Melian, G.S. Mageras, Z. Fuks, S.A. Leibel, A. Niehaus, H. Lorant, M. Zelefsky, B. Baldwin, and G.J. Kutcher, "Variation in prostate position quantitation and implications for three-dimensional conformal treatment planning," *Int. J. Radiat. Oncol. Biol. Phys.* **38**, 73-81 (1997).
76. M. Milosevic, S. Voruganti, R. Blend, H. Alasti, P. Warde, M. McLean, P. Catton, C. Catton, and M. Gospodarowicz, "Magnetic resonance imaging (MRI) for localization of the prostatic apex: comparison to computed tomography (CT) and urethrography," *Radiother. Oncol.* **47**, 277-284 (1998).
77. C. Mitine, E. van Eyken, Ph. Nickers, B. Delcoigne, M. Hoornaert, and M. Beauduin, "Pelvic irradiation: influence of technique of set-up on the accuracy of field alignment (Abstr.)," *Radiother. Oncol.* **32** (Suppl. 1), S146 (1994).
78. C. Mitine, A. Dutreix, and E. van der Schueren, "Tangential breast irradiation: influence of technique of set-up on transfer errors and reproducibility," *Radiother. Oncol.* **22**, 308-310 (1991).
79. S.M. Morrill, M. Langer, and R.G. Lane, "Real-time couch compensation for intra-treatment organ motion: theoretical advantages (Abstr.)," *Med. Phys.* **23**, 1083 (1996).
80. J. Moseley and P. Munro, "Display equalization: a new display method for portal images," *Med. Phys.* **20**, 99-102 (1993).
81. J.E. Munzenrider, A.P. Brown, J.C. Chu, L.R. Coia, K.P. Doppke, B. Emami, G.J. Kutcher, R. Mohan, J.A. Purdy, and B. Shank, "Numerical scoring of treatment plans," *Int. J. Radiat. Oncol. Biol. Phys.* **21**, 147-163 (1991).
82. I. Nassi and B. Shneiderman. *Flowchart techniques for structured programming*, p.23, SIGPLAN Notices (ACM), New York (1973).

83. A.R. Padhani, V.S. Khoo, J. Suckling, J.E. Husband, M.O. Leach, and D.P. Dearnaley, "Evaluating the effect of rectal distension and rectal movement on prostate gland position using cine MRI," *Int. J. Radiat. Oncol. Biol. Phys.* **44**, 525-533 (1999).
84. K.L. Pasma, B.J. Heijmen, M. Kroonwijk, and A.G. Visser, "Portal dose image (PDI) prediction for dosimetric treatment verification in radiotherapy. I. An algorithm for open beams," *Med. Phys.* **25**, 830-840 (1998).
85. K.L. Pasma, M. Kroonwijk, J.C. de Boer, A.G. Visser, and B.J. Heijmen, "Accurate portal dose measurement with a fluoroscopic electronic portal imaging device (EPID) for open and wedged beams and dynamic multileaf collimation," *Phys. Med. Biol.* **43**, 2047-2060 (1998).
86. K.L. Pasma, M. Kroonwijk, E.B. van Dieren, A.G. Visser, and B.J. Heijmen, "Verification of compensator thicknesses using a fluoroscopic electronic portal imaging device," *Med. Phys.* **26**, 1524-1529 (1999).
87. B. Pickett, M. Roach, L. Verhey, P. Horine, C. Malfatti, C. Akazawa, D. Dea, B. Varad, C. Rathbun, and T.L. Phillips, "The value of nonuniform margins for six-field conformal irradiation of localized prostate cancer," *Int. J. Radiat. Oncol. Biol. Phys.* **32**, 211-218 (1995).
88. U. Pietrzyk, K. Herholz, G. Fink, A. Jacobs, R. Mielke, I. Slansky, M. Wurker, and W.D. Heiss, "An interactive technique for three-dimensional image registration: validation for PET, SPECT, MRI and CT brain studies," *J. Nucl. Med.* **35**, 2011-2018 (1994).
89. T.M. Pisansky, M.L. Blute, V.J. Suman, D.G. Bostwick, J.D. Earle, and H. Zincke, "Correlation of pretherapy prostate cancer characteristics with seminal vesicle invasion in radical prostatectomy specimens," *Int. J. Radiat. Oncol. Biol. Phys.* **36**, 585-591 (1996).
90. S. Quint, M. Seven, M. de Hoog, M. Olofsen, and C. Creutzberg, "Positioning gynecological patients for conformal radiotherapy using vacuum mattresses (Abstr.)", 4th Int. Workshop on Electronic Portal Imaging, Amsterdam, The Netherlands (1996).
91. I. Rabinowitz, J. Broomberg, M. Goitein, K. McCarthy, and J. Leong, "Accuracy of radiation field alignment in clinical practice," *Int. J. Radiat. Oncol. Biol. Phys.* **11**, 1857-1867 (1985).
92. C. Rasch, I. Barillot, P. Remeijer, A. Touw, M. van Herk, and J.V. Lebesque, "Definition of the prostate in CT and MRI: a multi-observer study," *Int. J. Radiat. Oncol. Biol. Phys.* **43**, 57-66 (1999).
93. M. Roach, P. Faillace-Akazawa, C. Malfatti, J. Holland, and H. Hricak, "Prostate volumes defined by magnetic resonance imaging and computerized tomographic scans for three-dimensional conformal radiotherapy," *Int. J. Radiat. Oncol. Biol. Phys.* **35**, 1011-1018 (1996).
94. M. Roach, B. Pickett, S.A. Rosenthal, L. Verhey, and T.L. Phillips, "Defining treatment margins for six field conformal irradiation of localized prostate cancer," *Int. J. Radiat. Oncol. Biol. Phys.* **28**, 267-275 (1994).

95. J.C. Roeske, J.D. Forman, C.F. Mesina, T. He, C.A. Pelizzari, E. Fontenla, S. Vijayakumar, and G.T. Chen, "Evaluation of changes in the size and location of the prostate, seminal vesicles, bladder, and rectum during a course of external beam radiation therapy," *Int. J. Radiat. Oncol. Biol. Phys.* **33**, 1321-1329 (1995).
96. S.A. Rosenthal, M. Roach, B.J. Goldsmith, E.C. Doggett, B. Pickett, H.S. Yuo, E.M. Soffen, R.L. Stern, and J.K. Ryu, "Immobilization improves the reproducibility of patient positioning during six-field conformal radiation therapy for prostate carcinoma," *Int. J. Radiat. Oncol. Biol. Phys.* **27**, 921-926 (1993).
97. C.S. Ross, D.H. Hussey, E.C. Pennington, W. Stanford, and J.F. Doornbos, "Analysis of movement of intrathoracic neoplasms using ultrafast computerized tomography," *Int. J. Radiat. Oncol. Biol. Phys.* **18**, 671-677 (1990).
98. V. Rudat, M. Flentje, D. Oetzel, M. Menke, W. Schlegel, and M. Wannenmacher, "Influence of the positioning error on 3D conformal dose distributions during fractionated radiotherapy," *Radiother. Oncol.* **33**, 56-63 (1994).
99. V. Rudat, P. Schraube, D. Oetzel, D. Zierhut, M. Flentje, and M. Wannenmacher, "Combined error of patient positioning variability and prostate motion uncertainty in 3D conformal radiotherapy of localized prostate cancer," *Int. J. Radiat. Oncol. Biol. Phys.* **35**, 1027-1034 (1996).
100. S. Senan, J. van Sornsens de Koste, M. Samson, H. Tankink, P. Jansen, P.J. Nowak, A.D. Krol, P. Schmitz, and F.J. Lagerwaard, "Evaluation of a target contouring protocol for 3D conformal radiotherapy in non-small cell lung cancer [In Process Citation]," *Radiother. Oncol.* **53**, 247-255 (1999).
101. P.Y. Song, M. Washington, F. Vaida, R. Hamilton, D. Spelbring, B. Wyman, J. Harrison, G.T. Chen, and S. Vijayakumar, "A comparison of four patient immobilization devices in the treatment of prostate cancer patients with three dimensional conformal radiotherapy," *Int. J. Radiat. Oncol. Biol. Phys.* **34**, 213-219 (1996).
102. J.C. Stroom, H.C. de Boer, H. Huizenga, and A.G. Visser, "Inclusion of geometrical uncertainties in radiotherapy treatment planning by means of coverage probability," *Int. J. Radiat. Oncol. Biol. Phys.* **43**, 905-919 (1999).
103. J.C. Stroom, P.C. Koper, G.A. Korevaar, M. van Os, M. Janssen, H.C. de Boer, P.C. Levendag, and B.J. Heijmen, "Internal organ motion in prostate cancer patients treated in prone and supine treatment position," *Radiother. Oncol.* **51**, 237-248 (1999).
104. J.C. Stroom, G.A. Korevaar, P.C. Koper, A.G. Visser, and B.J. Heijmen, "Multiple two-dimensional versus three-dimensional PTV definition in treatment planning for conformal radiotherapy," *Radiother. Oncol.* **47**, 297-302 (1998).
105. J.C. Stroom, M.J. Olofsen-van Acht, S. Quint, M. Seven, M. de Hoog, C.L. Creutzberg, H.C. de Boer, and A.G. Visser, "On-line set-up corrections during radiotherapy of patients with gynecologic tumors," *Int. J. Radiat. Oncol. Biol. Phys.* **2000**, Jan. 15;46(2):499-506. **46**, 499-506 (2000).
106. J.C. Stroom and P.R. Storchi, "Automatic calculation of three-dimensional margins around treatment volumes in radiotherapy planning," *Phys. Med. Biol.* **42**, 745-755 (1997).

107. J.C. Stroom, A.G. Visser, J.C.J. de Boer and H. Huizenga, *Proceedings of the XIth International Conference on the Use of Computers in Radiation Therapy*, A.R. Hounsell, J.M. Wilkinson and P.C. Williams (eds), 264-265, North Western Medical Physics Department, Christie Hospital, Manchester (1994).
108. B.W. Taylor, Jr., N.P. Mendenhall, and R.R. Million, "Reproducibility of mantle irradiation with daily imaging films," *Int. J. Radiat. Oncol. Biol. Phys.* **19**, 149-151 (1990).
109. R.K. Ten Haken, J.D. Forman, D.K. Heimburger, A. Gerhardsson, D.L. McShan, C. Perez-Tamayo, S.L. Schoepfel, and A.S. Lichter, "Treatment planning issues related to prostate movement in response to differential filling of the rectum and bladder," *Int. J. Radiat. Oncol. Biol. Phys.* **20**, 1317-1324 (1991).
110. R.K. Ten Haken, A.F. Thornton, Jr., H.M. Sandler, M.L. LaVigne, D.J. Quint, B.A. Fraass, M.L. Kessler, and D.L. McShan, "A quantitative assessment of the addition of MRI to CT-based, 3- D treatment planning of brain tumors," *Radiother. Oncol.* **25**, 121-133 (1992).
111. A. Tinger, J.M. Michalski, W.R. Bosch, R.K. Valicenti, D.A. Low, and R.J. Myerson, "An analysis of intratreatment and intertreatment displacements in pelvic radiotherapy using electronic portal imaging," *Int. J. Radiat. Oncol. Biol. Phys.* **34**, 683-690 (1996).
112. A. Tinger, J.M. Michalski, A. Cheng, D.A. Low, R. Zhu, W.R. Bosch, J.A. Purdy, and C.A. Perez, "A critical evaluation of the planning target volume for 3-D conformal radiotherapy of prostate cancer," *Int. J. Radiat. Oncol. Biol. Phys.* **42**, 213-221 (1998).
113. J. Troccaz, Y. Menguy, M. Bolla, P. Cinquin, P. Vassal, N. Laieb, L. Desbat, A. Dusserre, and S. Dal Soglio, "Conformal external radiotherapy of prostatic carcinoma: requirements and experimental results," *Radiother. Oncol.* **29**, 176-183 (1993).
114. M.M. Urie, M. Goitein, K. Doppke, J.G. Kutcher, T. LoSasso, R. Mohan, J.E. Munzenrider, M. Sontag, and J.W. Wong, "The role of uncertainty analysis in treatment planning," *Int. J. Radiat. Oncol. Biol. Phys.* **21**, 91-107 (1991).
115. R.K. Valicenti, J.W. Sweet, W.W. Hauck, R.S. Hudes, T. Lee, A.P. Dicker, F.M. Waterman, P.R. Anne, B.W. Corn, and J.M. Galvin, "Variation of clinical target volume definition in three- dimensional conformal radiation therapy for prostate cancer," *Int. J. Radiat. Oncol. Biol. Phys.* **44**, 931-935 (1999).
116. J. Van de Steene, F. Van den Heuvel, A. Bel, D. Verellen, J. De Mey, M. Noppen, M. De Beukeleer, and G. Storme, "Electronic portal imaging with on-line correction of setup error in thoracic irradiation: clinical evaluation," *Int. J. Radiat. Oncol. Biol. Phys.* **40**, 967-976 (1998).
117. F. Van den Heuvel, W. De Neve, D. Verellen, M. Coghe, V. Coen, and G. Storme, "Clinical implementation of an objective computer-aided protocol for intervention in intra-treatment correction using electronic portal imaging," *Radiother. Oncol.* **35**, 232-239 (1995).
118. M. van Herk, P. Remcijs, C. Rasch, and J.V. Lebesque, "The probability of correct target dosage - dose population histograms for deriving treatment margins in radiotherapy," *Int. J. Radiat. Oncol. Biol. Phys.* **In Press**, (2000).

119. M. van Herk, A. Bruce, A.P. Kroes, T. Shouman, A. Touw, and J.V. Lebesque, "Quantification of organ motion during conformal radiotherapy of the prostate by three dimensional image registration," *Int. J. Radiat. Oncol. Biol. Phys.* **33**, 1311-1320 (1995).
120. M. van Herk and H.M. Kooy, "Automatic three-dimensional correlation of CT-CT, CT-MRI, and CT- SPECT using chamfer matching," *Med. Phys.* **21**, 1163-1178 (1994).
121. G. van Tienhoven, J.H. Lanson, D. Crabeels, S. Heukelom, and B.J. Mijnheer, "Accuracy in tangential breast treatment set-up: a portal imaging study," *Radiother. Oncol.* **22**, 317-322 (1991).
122. E. Vigneault, J. Pouliot, J. Laverdiere, J. Roy, and M. Dorion, "Electronic portal imaging device detection of radioopaque markers for the evaluation of prostate position during megavoltage irradiation: a clinical study," *Int. J. Radiat. Oncol. Biol. Phys.* **37**, 205-212 (1997).
123. A.G. Visser, H. Huizenga, V.G. Althof, and B.N. Swanenburg, "Performance of a prototype fluoroscopic radiotherapy imaging system," *Int. J. Radiat. Oncol. Biol. Phys.* **18**, 43-50 (1990).
124. J.W. Wong, M.B. Sharpe, D.A. Jaffray, V.R. Kini, J.M. Robertson, J.S. Stromberg, and A.A. Martinez, "The use of active breathing control (ABC) to reduce margin for breathing motion," *Int. J. Radiat. Oncol. Biol. Phys.* **44**, 911-919 (1999).
125. D. Yan, D.A. Jaffray, and J.W. Wong, "A model to accumulate fractionated dose in a deforming organ," *Int. J. Radiat. Oncol. Biol. Phys.* **44**, 665-675 (1999).
126. D. Yan, F. Vicini, J. Wong, and A. Martinez, "Adaptive radiation therapy," *Phys. Med. Biol.* **42**, 123-132 (1997).
127. C.X. Yu, D.A. Jaffray, and J.W. Wong, "The effects of intra-fraction organ motion on the delivery of dynamic intensity modulation," *Phys. Med. Biol.* **43**, 91-104 (1998).
128. M.J. Zelefsky, D. Crean, G.S. Mageras, O. Lyass, L. Happersett, C.C. Ling, S.A. Leibel, Z. Fuks, S. Bull, H.M. Kooy, M. van Herk, and G.J. Kutcher, "Quantification and predictors of prostate position variability in 50 patients evaluated with multiple CT scans during conformal radiotherapy," *Radiother. Oncol.* **50**, 225-234 (1999).
129. M.J. Zelefsky, L. Happersett, S.A. Leibel, C.M. Burman, L. Schwartz, A.P. Dicker, G.J. Kutcher, and Z. Fuks, "The effect of treatment positioning on normal tissue dose in patients with prostate cancer treated with three-dimensional conformal radiotherapy," *Int. J. Radiat. Oncol. Biol. Phys.* **37**, 13-19 (1997).
130. M.J. Zelefsky, S.A. Leibel, P.B. Gaudin, G.J. Kutcher, N.E. Fleshner, E.S. Venkatramen, V.E. Reuter, W.R. Fair, C.C. Ling, and Z. Fuks, "Dose escalation with three-dimensional conformal radiation therapy affects the outcome in prostate cancer," *Int. J. Radiat. Oncol. Biol. Phys.* **41**, 491-500 (1998).
131. S.M. Zhou, G.C. Bentel, C.G. Lee, and M.S. Anscher, "Differences in gross target volumes on contrast vs. noncontrast CT scans utilized for conformal radiation therapy treatment planning for prostate carcinoma," *Int. J. Radiat. Oncol. Biol. Phys.* **42**, 73-78 (1998).

LIST OF PUBLICATIONS

J.C. Stroom and P.R. Storchi, "Automatic calculation of three-dimensional margins around treatment volumes in radiotherapy planning," *Phys. Med. Biol.* **42**, 745-755 (1997).

J.C. Stroom, G.A. Korevaar, P.C. Koper, A.G. Visser, and B.J. Heijmen, "Multiple two-dimensional versus three-dimensional PTV definition in treatment planning for conformal radiotherapy," *Radiother. Oncol.* **47**, 297-302 (1998).

J.C. Stroom, J.C.J. de Boer, H. Huizenga, and A.G. Visser, "Inclusion of geometrical uncertainties in radiotherapy treatment planning by means of coverage probability," *Int. J. Radiat. Oncol. Biol. Phys.* **43**, 905-919 (1999).

J.C. Stroom, P.C. Koper, G.A. Korevaar, M. van Os, M. Janssen, P.C. Levendag, and B.J.M. Heijmen, "Internal organ motion in prostate cancer patients treated in prone and supine position," *Radiother. Oncol.* **51**, 237-248 (1999).

J.C. Stroom, M.J.J. Olofsen-van Acht, S. Quint, M. Seven, M. de Hoog, C.L. Creutzberg, J.C.J. de Boer, and A.G. Visser, "On-line set-up corrections during radiotherapy of patients with gynecological tumors," *Int. J. Radiat. Oncol. Biol. Phys.* **46**, 499-506, (2000).

J.C. Stroom, M. Kroonwijk, K.L. Pasma, P.C. Koper, E.B. van Dieren, and B.J.M. Heijmen, "Detection of internal organ movement in prostate cancer patients using portal images," *Med. Phys.* **27**, 452-461, (2000).

V.G. Althof, J.C. de Boer, H. Huizenga, J.C. Stroom, A.G. Visser, and B.N. Swanenburg, "Physical characteristics of a commercial electronic portal imaging device," *Med. Phys.* **23**, 1845-1855 (1996).

A. Bel, P.H. Vos, P.T. Rodrigues, C.L. Creutzberg, A.G. Visser, J.C. Stroom, and J.V. Lebesque, "High-precision prostate cancer irradiation by clinical application of an offline patient setup verification procedure, using portal imaging," *Int. J. Radiat. Oncol. Biol. Phys.* **35**, 321-332 (1996).

M.L. Dirkx, B.J. Heijmen, G.A. Korevaar, M.J. van Os, J.C. Stroom, P.C. Koper, and P.C. Levendag, "Field margin reduction using intensity-modulated x-ray beams

formed with a multileaf collimator," *Int. J. Radiat. Oncol. Biol. Phys.* **38**, 1123-1129 (1997).

P.C. Koper, J.C. Stroom, W.L. van Putten, G.A. Korevaar, B.J. Heijmen, A. Wijnmaalen, P.P. Jansen, P.E. Hanssens, C. Griep, A.D. Krol, M.J. Samson, and P.C. Levendag, "Acute morbidity reduction using 3DCRT for prostate carcinoma: a randomized study," *Int. J. Radiat. Oncol. Biol. Phys.* **43**, 727-734 (1999).

C. Rasch, P. Remeijer, P.C. Koper, G.J. Meijer, J.C. Stroom, M. van Herk, J.V. Lebesque, "Comparison of prostate cancer treatment in two institutions: a quality control study," *Int. J. Radiat. Oncol. Biol. Phys.* **45**, 1055-1062, (1999).

SAMENVATTING

Inleiding

De behandeling van kankerpatiënten met radiotherapie is er op gericht de tumor te vernietigen door middel van ioniserende straling. Bij externe radiotherapie wordt de straling meestal gegenereerd door een lineaire versneller. De patiënt wordt op de behandeltafel in de versnellerruimte gelegd en de stralenbundel uit de versneller wordt op de tumor gericht. Meestal wordt er vanuit meerdere richtingen gestraald om de schade aan het normale weefsel (dat altijd meebestraald wordt) zoveel mogelijk te beperken. Radiotherapie is het effectiefst wanneer de totale dosis in meerdere fracties wordt gegeven; het normale weefsel kan tussen de fracties beter herstellen dan het tumor weefsel. Een vereiste is dan dat de tumor zich elke fractie op dezelfde geplande (referentie) positie ten opzichte van de bestralingsbundels bevindt. Maar hoewel er veel aandacht wordt besteed aan het betrouwbaar positioneren van de patiënt, zijn geometrische variaties onvermijdelijk. Deze variaties kunnen opgesplitst worden in "systematische" and "random" variaties. Systematische variaties geven aan hoe de gemiddelde afwijking van de referentie positie varieert van patiënt tot patiënt, terwijl random variaties een indicatie geven van de van-dag-tot-dag verschillen in de patiënt positionering.

Uit praktische overwegingen vindt er ook vaak een opsplitsing plaats tussen externe positioneringsonzekerheden en interne orgaan bewegingen. Onzekerheden in positionering zijn variaties in de positie van de patiënt ten opzichte van de stralenbundels. Deze worden normaal gesproken gemeten met (elektronische) afbeeldingsapparatuur, waarmee, net als bij een normale röntgenfoto, een doorlichtingsbeeld van de bestraling kan worden gemaakt (niet alle straling wordt in de patiënt geabsorbeerd). De botstructuren die in deze beelden zichtbaar zijn, kunnen dan vergeleken worden met de geplande referentie situatie. Orgaan bewegingen zijn de bewegingen van de tumor ten opzichte van de bot structuren. Het is minder eenvoudig om deze bewegingen te meten omdat de tumor zelf meestal niet zichtbaar is in de doorlichtingsbeelden, maar verschillende methoden om dit te ondervangen zijn in ontwikkeling. Om te voorkomen dat de tumor gemist wordt tijdens de bestraling als gevolg van deze onzekerheden, worden er tijdens het plannen van de behandeling normaliter veiligheidsmarges rond de tumor aangehouden.

De planning gebeurt vaak met behulp van een computer waarmee een behandeling gesimuleerd kan worden. De drie-dimensionale (3D) patiënt anatomie is meestal beschikbaar in de vorm van een serie 2D computed tomography (CT) coupes. Hierop kunnen tumor en kritieke organen aangegeven worden. De planner bepaald dan welke stralenbundels er gebruikt gaan worden, en met een computeralgoritme wordt de verwachte dosis in tumor en kritieke organen uitgerekend. Vaak worden dosis volume histogrammen (DVH) gebruikt ter verificatie van een bestralingsplan. Een DVH geeft aan welk deel van een bepaald orgaan een bepaalde dosis krijgt.

Sinds 1993 wordt het te bestralen tumorgebied met (eventueel) microscopische uitbreiding vaak het CTV (clinical target volume) genoemd. Het CTV met veiligheidsmarges voor geometrische onzekerheden is het PTV (planning target volume). De gekozen bundelconfiguratie in een plan moet dan zodanig zijn dat de dosis in het PTV voldoende is (met maximale sparing van gezonde weefsels). In dit proefschrift zijn manieren onderzocht om PTV-marges te berekenen en minimaliseren.

Automatische 3D expansie van een CTV tot een PTV

In hoofdstuk 2 wordt beschreven hoe een PTV-marge van gegeven grootte automatisch kan worden berekend. Het CTV is een 3D volume, dat door de radiotherapeut wordt ingetekend in een serie 2D CT-coupes van de patiënt. Omdat de geometrische afwijkingen in elke richting kunnen optreden, zijn de benodigde veiligheidsmarges ook 3D. In de praktijk is gebleken dat het onmogelijk is om een 3D marge met de hand in 2D CT coupes in te tekenen. Daarom is een algoritme ontwikkeld om de vorm van het drie dimensionale PTV te berekenen. De input van het algoritme is het CTV en de gewenste marge in de drie orthogonale hoofdrichtingen. De CTV contouren die zijn ingetekend in de CT-coupes, worden gebruikt om een volume in een 3D rekenmatrix te creëren; volume elementen (voxels) binnen het CTV hebben waarde 1, voxels erbuiten waarde 0. Elk CTV voxel wordt dan uitgebreid met een ellipsoïde met diameters gelijk aan de gewenste marges in de drie richtingen. Uit dit 3D PTV volume worden vervolgens weer 2D contouren berekend die worden teruggezet in de CT coupes voor verdere planning van de behandeling. Deze automatische methode verhoogt de snelheid en nauwkeurigheid van de PTV intekening enorm.

In hoofdstuk 3 wordt het klinische voordeel van automatische 3D marge berekening bestudeerd. Omdat handmatige intekening van 3D marges onmogelijk is, werd (en wordt) in veel praktische gevallen de derde dimensie (loodrecht op de CT coupes) gewoon genegeerd. 2D marges worden dan coupe voor coupe, en alleen

binnen de coupes, bepaald. Voor 10 patiënten met prostaatkanker zijn de fouten gekwantificeerd die zo worden gemaakt. Afhankelijk van de vorm van het CTV, bleek dat de 2D marges op sommige plaatsen meer dan een centimeter kleiner waren dan de 3D uitgerekende marges. Dit kon leiden tot serieuze onderdosering van de tumor en tot een verlaging van de verwachte waarschijnlijkheid van tumor controle met 15%.

Berekening en verificatie van PTV-marges aan de hand van patiënt data

Een meer complete methode van marge berekening wordt voorgesteld in hoofdstuk 4. De methode maakt gebruik van kennis van gemeten systematische en random variaties voor relevante patiënt categorieën. De CTV matrix (zie vorige sectie) wordt geconvolveerd met de distributies van deze variaties in translaties en rotaties. Dit levert zogenaamde “bedekkingwaarschijnlijkheidsmatrices” op met voxelwaardes tussen 0 en 1. De voxelwaardes geven de kans aan dat het voxel door het CTV wordt bedekt. Iso-waarschijnlijkheid volumes worden dan gekozen als PTV zodanig dat het CTV een adequate dosis krijgt. Dit kan worden gecontroleerd door dezelfde bedekkingwaarschijnlijkheidsmatrix te gebruiken voor snelle en analytische berekening van het gemiddelde DVH van het CTV voor alle mogelijke systematische afwijkingen. Het effect van random variaties op de CTV dosis kan worden bepaald door de geplande dosis eerst te convolveren met de betreffende distributies. Tezamen levert dit een compleet beeld op van het effect van alle variaties op de dosis in het CTV. Het blijkt dat de systematische variaties ongeveer drie maal zwaardere consequenties hebben voor de CTV dosis dan de random variaties.

In het vijfde hoofdstuk wordt het in het hierboven beschreven model gebruikt voor patiënten met prostaat kanker. Voor deze patiënten is de interne tumor beweging significant omdat de tumor tussen de blaas en het rectum in ligt, die beide aanzienlijk in volume kunnen variëren. Het doel was om te bepalen of er verschillen in PTV-marges zijn wanneer de patiënten in rug of in buikligging worden bestraald. Hiervoor zijn van een groep van 30 patiënten met prostaatkanker 4 CT scans gemaakt gedurende de bestralingsperiode van 7 weken. 15 patiënten zijn behandeld in rugligging en 15 in buikligging. De bewegingen van de ingetekende prostaten zijn verkregen door middel van automatische vergelijking van de 3D positie. De positioneringsonzekerheden zijn gemeten met behulp van een elektronisch afbeeldingsapparaat. Hoewel de buikligging in eerste instantie voordelig leek (d.w.z. minder geometrische onzekerheden), bleek na scheiding van systematische en random variaties dat de vereiste PTV-marges ongeveer gelijk zijn.

On-line corrigeren van geometrische onnauwkeurigheden.

In het zesde hoofdstuk is de efficiëntie van het *on-line* corrigeren van positioneringsfouten bestudeerd. Bij *on-line* correcties worden de positioneringsfouten gemeten met doorlichtingsbeelden die gemaakt zijn met slechts een klein gedeelte van de dagelijkse bestralingdosis. De bestraling wordt onderbroken en de afwijking wordt gemeten. Voordat de rest van de bestraling wordt gegeven, kan een fout in de positie worden gecorrigeerd. De methode is getest voor 14 patiënten met gynaecologische tumoren. Deze patiënten vertonen relatief grote positioneringsfouten, zelfs wanneer een *off-line* correctieprotocol toegepast wordt. *Off-line* correcties hebben tot doel de systematische variaties te reduceren door de gemiddelde positioneringsfout te bepalen voor de eerste paar fracties, en vervolgens de rest van de fracties hiervoor te corrigeren. Het blijkt dat een aantal minuten extra behandelingstijd nodig is voor het uitvoeren van een *on-line* correctie. Dit resulteerde echter wel in bijna verwaarloosbaar kleine positioneringsfouten wat een significante verkleining van de PTV marges rechtvaardigt. Voorlopig wordt echter een combinatie van *off-line* en *on-line* correctie protocollen gebruikt totdat *on-line* correcties sneller uitgevoerd kunnen worden. In eerste instantie worden alle patiënten met het *off-line* protocol behandeld. Pas wanneer het *off-line* protocol slechte resultaten geeft, wordt overgegaan op *on-line* correcties.

In hoofdstuk 7 is de haalbaarheid van het detecteren van interne orgaan beweging met "normale" doorlichtingsbeelden van de bestraling onderzocht voor patiënten met prostaatkanker. De veronderstelling is dat gas in het rectum, dat in de beelden net zo goed zichtbaar is als botstructuren, gebruikt kan worden om de ventrale rectum wand te bepalen. Omdat de prostaat op het rectum ligt voor patiënten in rugligging, zou mogelijk ook de prostaat positie hieruit afgeleid kunnen worden. De CT data van de 15 in rugligging behandelde patiënten uit hoofdstuk 5 zijn gebruikt om dit te verifiëren. De doorlichtingsbeelden zijn gesimuleerd door berekening van digitale reconstructies van de CT data. De verplaatsingen van de ventrale rectumwand, zoals automatisch gemeten aan de hand van rectumgas in de beelden, zijn gecorreleerd met de werkelijke rectumwand verplaatsingen (gemeten met behulp van de ingetekende rectum contouren) en met de prostaatbewegingen (zie hoofdstuk 5). De correlatie coëfficiënt was in beide gevallen zeer significant. Een nadeel van de methode is dat er niet altijd gas in het rectum zit zodat niet alle prostaatbewegingen gedetecteerd kunnen worden. Maar zelfs wanneer wordt aangenomen dat alleen de zichtbare prostaat verplaatsingen voor de groep van 15 patiënten in deze studie worden gecorrigeerd, kan de PTV-marge met ongeveer 2 mm worden verkleind.

NAWOORD

OK dan, eindelijk weer tijd voor enkele wat persoonlijkere noten. Voor the making of het boekje gaat bovenal mijn dank uit naar alle collega's die mijn tijd op de afdeling klinische fysica van de Daniel zo aangenaam maken en hebben gemaakt. Het feit dat ik al acht jaar zonder eigenlijk een trein te missen tussen Amsterdam en Rotterdam op-en-neer aan het reizen ben, geeft al aan dat het met de werksfeer wel goed zit. Na een avondje uit (of werken natuurlijk) met de collega's hoefde ik nooit lang te zoeken naar een goedkope (een gebakje slechts) en comfortabele slaappleats: vooral Jack, ErikL, en Kasper heb ik zodoende aardig kunnen vetmesten.

Gezamenlijk congresbezoek werd ook eigenlijk standaard verlengd met minimaal een paar dagen vakantie. Zo heb ik ondermeer met Maarten en ErikK een heel stuk gezien van respectievelijk de zuidoostelijke VS en Schotland. Ook de doorgaans waterige survival-weekendjes met de afdeling waren een groot succes. Over mijn kamergenoten in de afgelopen jaren eveneens niets dan lof: de momenten die ik samen met onder andere Marjan, Hans, Kasper, Marco en ErikD heb doorgebracht waren van een grote gezelligheid. Dat geeft me trouwens ook de gelegenheid om mijn toekomstig kamergenoot te bedanken: Robert, ideaal dat je twee maanden voor mij bent gaan promoveren. Dat heeft me een hoop werk bespaard.

De goede sfeer is absoluut een eerste voorwaarde voor het tot stand komen van dit boekje geweest. De tweede voorwaarde is natuurlijk de hulp die ik heb gehad. En dan wil ik naast alle coauteurs in ieder geval even de projectleiders Andries, Henk, en Ben noemen, die mij op sympathieke wijze goed aan de gang hebben gekregen. Ik vraag mij wel eens af of zij wel eens hebben getwijfeld aan mijn promotie (ik in ieder geval meerdere malen) maar uiteindelijk lijkt het toch zover te komen. En verder natuurlijk Hans, die ons MVA-clubje precies op het juiste moment kwam versterken. Het is wat mij betreft geen toeval dat ik eigenlijk pas sinds die tijd echt ben opgeschoten met het onderzoek.

Een groot voordeel van het fysisch-klinisch onderzoek vind ik toch wel dat het zo dicht bij de praktijk staat. Ideeën en ontwikkelde software werden vaak meteen getest en in gebruik genomen door de klinici. Het contact met de laboranten, en met name Marjan, SandraQ, Marjolein, John, Gert, en Merik, is wat mij betreft altijd bijzonder fijn en leerzaam geweest. Hetzelfde geldt voor de samenwerking met de

betrokken radiotherapeuten waaronder Carien, PeterK en Manouk. Van de meer ondersteunende afdelingen wil ik verder met name de secretaresses, de audiovisuele dienst, de bibliotheek, de automatisering en natuurlijk het personeelsrestaurant hartelijk bedanken voor de perfecte en snelle service die altijd geleverd werd.

En verder toch maar even op de zaken vooruitlopend, voor de afronding van het geheel ben ik vanzelfsprekend ook dank verschuldigd aan de "kleine" promotiecommissie onder voorzitterschap van Peter Levendag. Ook de overige leden van de "grote" promotiecommissie, die niet voorin vermeld staan, wil ik even noemen: Anders Brahme, Wilfried De Neve, Ben Mijnheer, en Roland Kanaar: thanks for the trouble of reading the thesis and appearing at the promotion.

De oplettende lezer vraagt zich na al deze positieve geluiden misschien af waarom ik in de afgelopen acht jaar eigenlijk nog niet verhuisd ben naar het Rotterdamse. Naast dat ik Amsterdam als stad toch echt een tikkie gezelliger vind dan Rotterdam, komt dat voornamelijk doordat ik een aantal dierbare personen bij mij in de buurt heb zitten. En nu ik toch bezig ben, grijp ik meteen de gelegenheid aan om mijn waardering voor hen even op papier te zetten. Om te beginnen de gabbers van AMVJ, hetzelfde geldt eigenlijk voor hen als voor de collega's: met name de gezelligheid brengt mij er toch altijd toe om zelfs in regen, sneeuw en storm altijd mijn balletje (en pedalen) te gaan trappen. Vier vrienden met wie ik niet toevallig minimaal een AMVJ verleden deel moet ik er zeker even uitlichten: Henkie, Otje, Maus en Causio, het spijt me bijzonder dat ik slechts twee van jullie als paranimf heb kunnen kiezen. Weet in ieder geval de tijd die ik regelmatig met jullie doorbreng altijd een buitengewoon genoegen is.

Het moge kortom duidelijk zijn dat ik het goed naar mijn zin heb. Echter, de voornaamste reden dat ik tot op heden absoluut niet mag klagen is toch wel omdat ik zoon van mijn ouders, broer van mijn broertje, en vriend van mijn vriendinnetje ben.

CURRICULUM VITAE

De auteur werd geboren in de ochtend van 1 februari 1967 in Amsterdam. Daar groeide hij op en bezocht hij de kleuterschool, lagere school, en middelbare school. In 1985 haalde hij zijn gymnasium diploma aan het St. Ignatius gymnasium. Vervolgens studeerde hij natuurkunde aan de Universiteit van Amsterdam, wat resulteerde in een propedeutisch examen in 1986. Het doctoraal examen werd gehaald in 1991, na stage te hebben gelopen bij het FOM instituut voor Atoom- en Molecuul Fysica. Het stageonderzoek was gericht op het modelleren en doormeten van poly-kristallijne zonnecellen. Aan het eind van zijn studenten tijd realiseerde de auteur zich dat er nog meer te doen was aan de universiteit, wat resulteerde in het volgen van de bijvakken Spaans, Russisch en Milieukunde. Na een korte periode van werkloosheid ging hij begin 1992 aan de slag bij de Daniel den Hoed Kliniek in Rotterdam. De eerste vier jaren werden gevuld met onderzoek naar het gebruik van het in-huis ontwikkelde megavolt afbeeldingsapparaat. Daarna volgde drie jaar onderzoek naar de optimale bestraling van patiënten met prostaatkanker. Deze twee projecten hebben uiteindelijk geresulteerd in het proefschrift wat hier voor u ligt. Op dit moment is de auteur bezig met een derde project in de Daniel den Hoed Kliniek, met als doel het bestuderen van de voordelen van het bestralen met hoog-energetische elektronen naast fotonen. Ook volgt hij een opleiding tot klinisch fysicus. De auteur woont nog steeds in Amsterdam en gaat met de trein en de fiets naar zijn werk. Hij heeft uitgerekend dat het totaal aantal afgelegde woon-werk kilometers overeenkomt met ongeveer 8 maal een rondje aardbol (waarvan een half op de fiets).

